Injurious Compression Induced Apoptosis in Articular Cartilage

by

Andreas Markus Loening

Submitted to the Department of Electrical Engineering and Computer Science
in partial fulfillment of the requirements for the degree of

Master of Engineering in Electrical Engineering and Computer Science

at the

MASSACHUSETTS INSTITUTE OF TECHNOLOGY

February 1999

Author . . . . . .
Department of Electrical Engineering and Computer Science
December 21, 1998

Certified by . . . . . .
Alan J. Grodzinsky
Professor of Electrical, Mechanical, and Bioengineering
Thesis Supervisor

Accepted by . . . . . .
Arthur C. Smith
Chairman, Department Committee on Graduate Students

Injurious Compression Induced Apoptosis in Articular Cartilage

by

Andreas Markus Loening

Submitted to the Department of Electrical Engineering and Computer Science
on December 21, 1998, in partial fulfillment of the
requirements for the degree of
Master of Engineering in Electrical Engineering and Computer Science

Abstract

Increased numbers of apoptotic cells have been identified in OA cartilage, and it has been suggested that apoptosis may play an important role in the pathogenesis of OA. Autoradiography studies of injuriously compressed normal cartilage tissue have shown subpopulations of cells exhibiting little or no matrix turnover and condensed nuclei suggestive of apoptotic cell death. The objectives of this thesis were to determine if mechanical loading could induce apoptosis in non-arthritic cartilage *in vitro*, and to compare any mechanically induced apoptosis with other markers of tissue injury. Bovine cartilage was subjected to unconfined compression-release cycles producing peak stresses of 0-20 MPa. Tissue was stained via TUNEL for apoptotic nuclei and via ethidium bromide/fluorescein diacetate for viability. Additionally, wet weight changes, sulfated glycosaminoglycan (sGAG) loss, and nitric oxide (NO) release were measured. Compression of explants to just 4.5 MPa peak applied stress produced a significant increase in the number of nuclei staining positive for apoptosis via TUNEL. A dose dependent response was seen, with $\sim$50% of chondrocytes staining positive for apoptosis following a 20 MPa compression. Changes in cell viability corresponded closely with those of the TUNEL assay. Wet weight changes and sGAG loss also increased in a dose-dependent manner and were indicative of collagen network damage from the injury. NO release increased for only the most severely compressed condition (20 MPa). In summary, mechanical injury of articular cartilage tissue was found to induce chondrocytic apoptosis. Additionally, this effect was observable at injury levels (4.5 MPa) below what was needed to induce detectable effects in wet weight (13 MPa), sGAG release(6 MPa), and viability (10 MPa). This suggests that programmed cell death may be one of the earliest events in response to injury of articular cartilage and could hypothetically lead to subsequent tissue degeneration due to tissue hypocellularity. An alternative interpretation is that the *in vitro* mechanical injury could be more representative of fibrillated tissue and be interpreted as evidence of apoptosis as a secondary effect of fibrillation, perhaps relevant to the OA process.

Thesis Supervisor: Alan J. Grodzinsky
Title: Professor of Electrical, Mechanical, and Bioengineering

Acknowledgments

I'd like to begin by thanking Al. I've truly appreciated him as an advisor. He's given me the opportunity to start off on something sort of new and the freedom to figure things out on my own. When I wandered into his office two and a half years ago, looking for what began as a UROP, he started talking to me like I already had the job. I never got around to saying "no thank you" and I'm glad I didn't.

I'd like to thank Mike Lark, Mark Nuttall (two l's), Alison Badger, and Ian James. They formed the SmithKline contingent that guided much of this research and they provided more then their fair share of valuable insight and knowledge. I'm especially grateful to Ian James, who got to do the "phun" (that's fun with a "ph") grundge work of infinite sectioning and TUNEL of the cartilage disks. Without Ian, there would be no thesis.

Marc Levenston did the greater portion of the biomechanical work that is in appendix: C. He also taught me first hand what it takes to be a good scientist. I'm sincerely glad falling asleep while Marc was talking in my initial interview didn't reflect badly enough on me to deny me the UROP. Stephanie Soohoo helped in running some of the experiments that became appendix: C and kept me entertained. Han-Hwa helped an immeasurable amount with a failed attempt at using agarose gel electrophoresis (appendix: D). Additionally, she taught me almost everything I know about cell-culture and cell isolation and kept the lab running smoothly. Deb Zamble provided the cisplatin treated cells that provided the only positive laddering on agarose gels (appendix: D). Rusty Sammon was my roommate and project partner for 6.344 and is partially responsible for what became appendix: B.

Thanks to Vicki, who has served as the chief listener of my complaints, accusations, and irrelevant bitching over the past year and a half, a role that no one in this world would envy, trust me. She also proof-read my thesis, giving her the distinction of being the only person who will ever read my thesis cover to cover. Cyndi tried doing some histology on some of my samples and made "the super corer" for which every calf person in this lab is supremely indebted. She's been a great office mate and advisor, and I can't thank her enough for getting me into kayaking.

Thanks to Linda, who made me feel at home with my own tendency toward potty mouth. She also babied me by keeping the FedEx system a black-box abstraction to my eyes. Eliot saved me a load of work by incorporating my little hardware feedback circuit into the main incustat hardware himself (and doing a great job of it). He also built the machine that my thesis is based upon and kept a watchful eye on my ORS abstract as it headed out the door.

Paula gave me advice, encouragement, wisdom, and again, encouragement. She's been a great source of friendship and conned me into learning scuba diving (yeah, 45°F water, warm, if you break in your wet suit) Steve gave me advice on my thesis and kept me entertained on long, boring nights as we both struggled with moving thought to expression. Bodo provided convincing evidence of what it really means to be a German. Additionally, Emo, Parth, Moonsoo, Fen, Bryant, Jeff, and JT all provided the vibrant background that keeps this lab alive.

Thanks to Andrea Pomrehn, Mike Marino, and Tomas Perez for randomly timed intellec-

tual conversations on biology that made me interested enough in the subject to “bend to the darkside” and get my feet wet (and drown in it too).

I’d of course like to thank my parents for reasons to numerous to list.

Finally, thanks to Aaron McCabe, who helped in making my undergraduate years tolerable and initially got me interested in bioengineering. 5.12 6.001, 6.002, 6.003, 6.004, 6.011, 6.012, 6.013, 6.023 6.041, 6.121, 6.241, 6.302, 6.344, 8.01, 8.02, and 18.04.... that’s a lot of shared pain.

Further Acknowledgements

You guys are electrical engineers, why don’t you design something with socially redeeming value? - Chris Benton, on the topic of television.

No matter what you engineer, people will find a way to put porn and commercials on it. -Rusty Sammon, on the topic of socially redeeming engineering.

Yeah, but you can get a job - Aaron McCabe, on why EE is better then Bio.

Yeah, I could finite element model your body, but it’s not going to get me layed - Anonymous, on the merits of finite eliminate modeling.

Calibration of the incustat is a symphonic blend of engineering handwaiving and total bullshit - Me, on my first attempt at a description of calibrating the incustat.

Garbage people help people too, they take away our crap. The world would suck if we didn’t have garbage people. - Paula Ragan, on why all professions are important.

Funding Funding for this work was provided by SmithKline Beecham Pharmaceuticals and NIH grant AR33236.

Contents

1 Introduction and Background **13**

1.1 Articular Cartilage . . . 14

1.1.1 Molecular Composition . . . 15

1.1.2 Cellular Structure . . . 15

1.2 Osteoarthritis . . . 16

1.3 Chondrocyte Response to Mechanical Loading . . . 18

1.4 Processes for Cell Death . . . 18

1.4.1 Necrosis . . . 19

1.4.2 Apoptosis . . . 19

1.4.2.1 Causative Agents . . . 20

1.4.2.2 Signal Transduction . . . 21

1.4.2.2.1 CD95 . . . 23

1.4.2.2.2 TNF . . . 23

1.4.2.2.3 Other Signaling Proteins . . . 24

1.4.2.3 Mitochondrial Roles . . . 24

1.4.2.4 Caspases . . . 25

1.4.2.5 Other Apoptosis Associated Proteins . . . 27

1.4.2.6 Cellular Effects . . . 28

1.4.2.6.1 Phosphatidylserine Translocation . . . 28

1.4.2.6.2 Chromosomal DNA Cleavage . . . 28

1.4.2.6.3 Apoptotic Body Formation . . . 31

1.5 Thesis Objectives . . . 32

2 Materials and Methods **33**

2.1 Materials . . . 33

2.2 Methods . . . 34

2.2.1 Tissue Protocols . . . 34

2.2.1.1 Tissue Harvesting . . . 34

2.2.1.2 Feeding . . . 35

2.2.2 Injurious Compression Protocols . . . 35

2.2.3 Biochemical Assays . . . 37
2.2.3.1 Wet Weight Measurements . . . 37
2.2.3.2 Sulfated GAG Assay . . . 37
2.2.3.3 NO Assay . . . 37
2.2.3.4 Apoptosis Assays . . . 38
2.2.3.5 Red/Green Fluorescence Cell Viability Assay . . . 38
2.3 Statistics . . . 39

3 Results of Injurious Compression on Articular Cartilage 41
3.1 Effects on Cellular Viability . . . 41
3.1.1 Apoptotic Response . . . 41
3.1.1.1 Induction of Apoptosis . . . 41
3.1.1.2 Effects of Apoptosis Inhibitors . . . 44
3.1.1.3 Effects of Apoptosis Inducing Cytokines . . . 45
3.1.2 General Viability Changes . . . 46
3.1.2.1 Results of Cell Viability Assay . . . 46
3.2 Effects on Tissue Properties . . . 49
3.2.1 Biochemical Changes . . . 49
3.2.1.1 Wet Weight . . . 49
3.2.1.2 Sulfated GAG Loss . . . 49
3.2.1.3 Nitric Oxide Release . . . 54

4 Discussion and Conclusion 59
4.1 Apoptosis Findings . . . 59
4.2 Viability Findings . . . 60
4.3 Changes in Biochemical Properties . . . 61
4.4 Conclusions . . . 62
4.5 Future Experiments . . . 63

A The Incustat and its Controller 65
A.1 Introduction . . . 65
A.2 Non-linearities . . . 66
A.3 Feedback Compensation . . . 67
A.4 Software Issues . . . 69
A.5 Calibration Procedures . . . 72

B Quantitative Analysis of Ethidium Bromide and Fluorescein Diacetate Stained Cartilage Tissue Sections 75
B.1 Introduction . . . 75
B.2 Methods . . . 78

B.3 Image Processing & Results . . . 79
B.4 Conclusion . . . 85

C Biomechanical Characterization of Loaded Disks **93**
C.1 Introduction . . . 93
C.2 Methods . . . 93
C.3 Results . . . 94
C.3.1 Equilibrium Moduli . . . 94
C.3.2 Dynamic Stiffness . . . 97
C.3.3 Other Measurements . . . 97
C.4 Conclusion . . . 97

D Preliminary Results: Other Assays for Apoptosis **103**
D.1 Flow Cytometry of TUNEL stained cells . . . 103
D.1.1 Introduction . . . 103
D.1.2 Materials and Methods . . . 104
D.1.2.1 Tissue Harvesting . . . 104
D.1.2.2 Culture . . . 105
D.1.2.3 Cell Isolation . . . 105
D.1.2.4 Red/Green Cell Viability Assay . . . 105
D.1.2.5 Paraformaldehyde/Ethanol Fixation of Cells . . . 106
D.1.2.6 TUNEL Staining of Fixed Cells . . . 106
D.1.3 Results and Discussion . . . 107
D.2 Flow Cytometry of PI stained cells . . . 108
D.2.1 Introduction . . . 108
D.2.2 Materials and Methods . . . 108
D.2.2.1 Ethanol Fixation of Cells . . . 109
D.2.2.2 Nuclear Content Measurements . . . 109
D.2.2.3 Results and Discussion . . . 109
D.3 Agarose Gel Electrophoresis of Apoptotic DNA . . . 110
D.3.1 Introduction . . . 110
D.3.2 Materials and Methods . . . 110
D.3.2.1 Harvest, Culture, and Compression . . . 110
D.3.2.2 DNA Isolation . . . 110
D.3.3 Results and Discussion . . . 111

Bibliography **113**

List of Figures

1-1 Drawing of the Extracellular Matrix of Articular Cartilage 16
1-2 Diagram of Apoptosis Pathways 22
1-3 Diagram of the Nucleosomes 29
1-4 Diagram of Agarose Gel Laddering 30

2-1 Explant Diagram 34
2-2 Injurious Compression Protocol 36

3-1 Examples of TUNEL Stained Tissue 42
3-2 Apoptosis in Injured Tissue, Dose Response 43
3-3 Apoptosis in Injured Tissue, Lower Limit 44
3-4 Apoptosis in Injured Tissue, Inhibitor Response 45
3-5 Examples of Vital Dye Stained Tissue 47
3-6 Viability in Injured Tissue, Dose Response 48
3-7 Viability in Injured Tissue, Kinetics 48
3-8 Increases in Tissue Wet Weight 50
3-9 Tissue Wet Weight Rates 51
3-10 Sulfated-GAG Cumulative Release, Time Course 52
3-11 Sulfated-GAG Release Rate, Time Course 53
3-12 Cumulative Sulfated-GAG Loss, Dose Response 54
3-13 Cumulative Sulfated-GAG Loss, Apoptosis Inhibitor Effects 55
3-14 Cumulative Nitric Oxide Release, Dose Response 56
3-15 Cumulative Nitric Oxide Release, Apoptosis Inhibitor Effects 56
3-16 Cytokine Induced NO Release 57

A-1 Static compression chamber 66
A-2 Incustat - Closeup 67
A-3 Incustat - Schematic 68
A-4 Incustat Hardware Feedback Diagram 69
A-5 Incustat Hardware Feedback Schematic 70
A-6 Incustat 71

A-7 Strain versus Peak Stress 73

B-1 Spectra of intercalated Ethidium Bromide 76
B-2 Spectra of Fluorescein 77
B-3 Components of the Original Image 80
B-4 Components of the Transformed Image 83
B-5 Low-pass Filters for Unsharp Filtering 84
B-6 Filtering and Thresholding of Fluorescein Component 86
B-7 Filtering and Thresholding of EtBr Component 87
B-8 Binary EtBr and Fluorescein Components 88
B-9 Erosion and Dilation Filters 89
B-10 Enhanced Image 90
B-11 Two Further Examples 92

C-1 Equilibrium Moduli for Different Peak Loads 95
C-2 Normalized Equilibrium Moduli for Different Peak Loads 96
C-3 Dynamic Stiffness for Different Peak Loads 98
C-4 Normalized Confined Dynamic Stiffness for Different Peak Loads 99
C-5 Normalized Unconfined Dynamic Stiffness for Different Peak Loads 100

D-1 Agarose Gel of Apoptotic DNA 112

List of Tables

3.1 Effects of Apoptosis Inducing Cytokines 46

Chapter 1

Introduction and Background

Osteoarthritis (OA) is a debilitating disease of articular cartilage that causes pain and decreased mobility in millions of people. One form of OA, secondary osteoarthritis, is commonly associated with mechanical injury of articulating joints [19, 54], such as car accidents and falls from height, and is presumably related to degenerative changes in the cartilage following such trauma. Currently, little is known about what occurs following an injury, such as the cartilage's response to injury and the cause of further degenerate changes within the cartilage.

Cellular apoptosis, or programmed cell death, is normally a physiological process involved in development, immune response, and removal of potentially carcinogenic and damaged cells. In cartilage, apoptosis occurs during development, as evidenced by the apoptosis of hyaline cartilage chondrocytes during endochondral ossification [31]. Aberrant apoptosis, however, can be pathogenic and has been observed in diseases such as Alzheimer's [18] and in neuronal cell death following spinal cord injury [22]. Recent findings of apoptotic chondrocytes in human osteoarthritic articular cartilage [59, 6, 42], along with evidence from an animal model of osteoarthritis (OA) [45] and cartilage wounding experiments [99, 94], have led to the implication of aberrant apoptosis in the pathogenesis of OA.

Hypocellularity has been associated with both osteoarthritic tissue and normal carti-

lage tissue in joints affected with osteoarthritis (OA) [62]. This hypocellularity is believed to be both a risk factor and a contributor in the disease pathogenesis, and the finding of markedly increased levels of apoptotic chondrocytes in diseased tissue implicates apoptosis mediated cell-loss as a potential cause of OA hypocellularity. The method by which apoptosis may mediate or cause OA is not currently known, but mechanisms involving calcium precipitation by apoptotic bodies [43], matrix degradation by apoptotic bodies [42], and the inability of hypocellular tissue to maintain and repair itself [1] have been proposed.

Further evidence of a role for aberrant apoptosis in articular cartilage comes from correlations of tissue age and the numbers of apoptotic chondrocytes found in normal tissue of adult animals [1]. Since cartilage exhibits an age-related decrease of chondrocytes in both animal and human tissue [68], there is a strong expectation that this decrease in cellularity arises through apoptosis mediated cell loss. While a correlation between apoptotic chondrocytes and age in normal human cartilage has not been observed [42], this finding may be due to the particularly long life span of this particular species.

The cause of chondrocyte apoptosis is not currently known, but *in vitro* autoradiography studies with injuriously compressed cartilage have shown non-viable cell populations exhibiting condensed nuclei [81] reminiscent of apoptosis. This, coupled with the previous observations, has led to the hypothesis that injurious mechanical compression of articular cartilage may be a cause of chondrocytic apoptosis and in turn subsequent OA degeneration. This thesis will examine a model of injuriously compressed articular cartilage, and the apoptotic cellular response to loading, along with other related markers of tissue degeneration.

1.1 Articular Cartilage

Articular cartilage is a dense, highly hydrated, connective tissue that lines the articulating surfaces of synovial joints. In its mature form, the tissue is aneural, avascular, and alymphatic, with the tissue's native cells (chondrocytes) being fed entirely by diffusion [91] and convection from outside of the tissue. Articular cartilage acts as a flexible, shock-

absorbing, and wear-resistant surface [74] for the rigid underlying bone, and also provides for joint lubrication during motion [67].

1.1.1 Molecular Composition

The major constituent of articular cartilage tissue is water, consisting of 70-80% of the tissue by weight [39, 63]. The remaining components include collagen type II fibrils (50-65% or tissue dry weight), the cartilage specific proteoglycan "aggrecan" [63], and other molecular components (Fig: 1-1).

The collagen fibers form a network that provides the tissue with its tensile and sheer strength. This network is under constant internal tension, arising from the tissue's intrinsic tendency to swell due to the negatively charged aggrecan molecules. Any decrease in the tensile strength of the collagen network will manifest itself as an increase in tissue swelling [64], a hallmark of early-stage osteoarthritic cartilage.

The aggrecan molecules, on the other hand, are responsible for the compressive stiffness of the tissue [39]. This compressive stiffness arises from the glycosaminoglycan (GAG) side chains of the aggrecan molecules, which are highly anionic at physiological conditions. These fixed, negatively charged groups exert mutually repulsive forces against each other creating a swelling pressure that is counteracted by the collagen fiber network.

1.1.2 Cellular Structure

The remaining volume of the tissue (less than $\sim$10% [41, 90]) consists of a sparse population of articular cartilage chondrocytes that is embedded in and protected by the extracellular matrix (ECM) [79]. Due to the avascular nature of cartilage tissue, nutrients for the cells arise entirely from diffusion, and oxygen tension levels may be as low as 1% [12] (the normal atmosphere is 24%). Consequently, chondrocyte metabolism occurs primarily by glycolysis [91]. Convective fluid flow due to joint loading may also significantly affect the transport of larger protein and soluble factors [29].

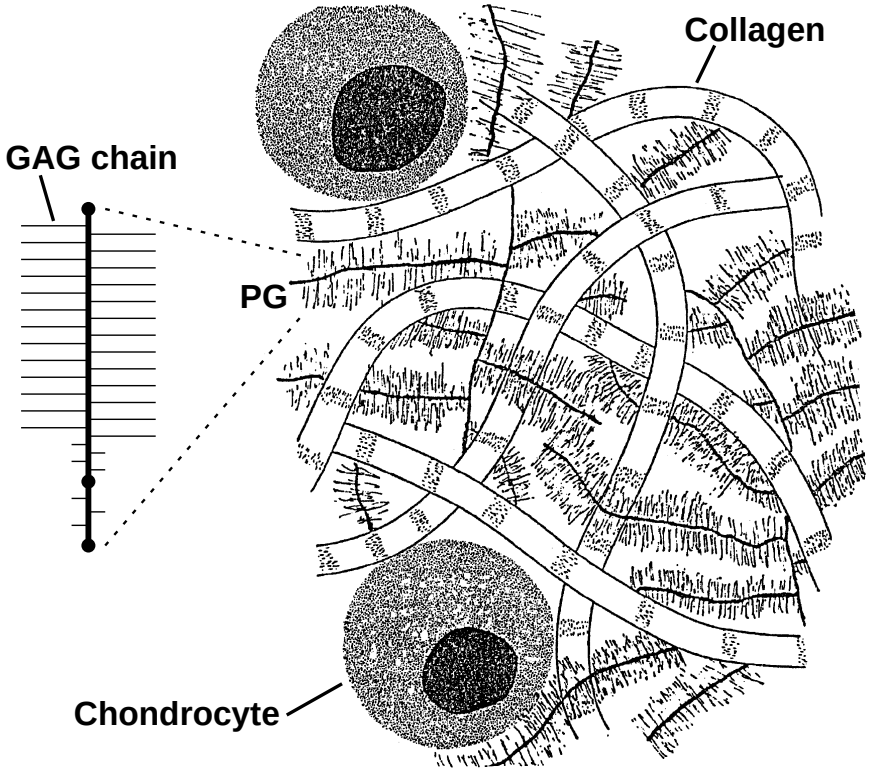

Figure 1-1: A drawing of the extracellular matrix of articular cartilage, showing the collagen network, the proteoglycan “aggrecan”, and the chondrocytes embedded in the ECM.

The chondrocytes maintain the ECM’s integrity by providing for the synthesis and secretion of the ECM’s constituent molecules, along with their degradation and turnover [46, 96]. Collagen and aggrecan macromolecules are synthesized inside the cell, but final assembly of these macromolecules into a functional matrix takes place in the extracellular space.

1.2 Osteoarthritis

Osteoarthritis (OA) is a common degenerative disease that primarily affects the load-bearing areas of articular cartilage containing joints. [13]. In OA, fibrillation of the cartilage occurs, which is then followed by erosion of the articular surface and mechanical softening of the cartilage. In severe cases, the underlying bone can be damaged. The main

consequences of OA are loss of free joint movement, lose of joint stability, and pain. In severe cases, the disease can be debilitating, requiring total joint replacement.

OA cases can be divided into two major groups, primary and secondary, based upon the origin of the disease [70]. Primary osteoarthritis develops in joints without any known cause, and affects predominantly the hands, the spine, and weight-bearing joints such as the hips and knees. Secondary osteoarthritis is classified under the basis that there is an identifiable cause for the condition, and may result from events that alter either metabolism or joint mechanics, such as infection, Wilson's disease, and simple trauma. Secondary OA is not as strongly correlated with particular joints as primary OA. In either case, once cartilage damage has begun the end results are frequently indistinguishable.

Lesions associated with OA are usually concentrated in the load-bearing areas of joints, and increased occurrences of OA are seen when unusual joint loading is present. These two observations suggest that mechanical factors play an important role in the progression of OA [49]. Additionally, apoptotic chondrocytes have been observed in human OA cartilage [59, 6, 42], leading to the speculation that apoptosis may also play a role in the development of OA.

Severe mechanical loading, such as what occurs in a fall from a height or a traffic accident (often called impact loading or injurious compression) can directly injure articular cartilage. Secondary OA is often reported some time after such an event. These observations have been confirmed by animal studies in which degenerative changes were seen in the cartilage of knee joints subjected to blunt trauma *in vivo* [21, 95].

Little, however, is currently known about the ability of articular cartilage to withstand and repair itself after impact loads, and a full understanding of the underlying factors involved are vital for the creation of treatment and prevention schemes. Therefore, the influences of mechanical loading on the ECM and chondrocyte viability are of significant interest.

1.3 Chondrocyte Response to Mechanical Loading

Maintenance of the ECM has been found to be influenced by mechanical loading of the tissue [40]. This finding has been reported in both *in vitro* [34, 78, 85] and *in vivo* [14, 56] studies.

In brief, static compression of cartilage, compressing cartilage tissue to a fixed thickness, has been found to cause a compression level dependent decrease in metabolic activity [78]. Dynamic compression, compressing cartilage tissue to a fixed thickness and then oscillating 1-10% around that point, has been found to up-regulate metabolic activity when the applied oscillations were comparable to physiological frequencies [85].

Injurious compression, on the other hand, involves compressing cartilage at rates and levels far in excess of what is typical in either static or dynamic compression experiments, and is meant to simulate an injury event rather than normal physiological levels of compression. These compression levels have been previously accomplished with the use of dropped weight systems [54, 55] and manually operated compression chambers [80], and have been shown to predispose the ECM to further cell-mediated degradation [80].

Autoradiography studies have shown that following an injurious compression, the chondrocytes can be grouped into two distinct populations [80]. The first group consists of cells that are larger than normal and have elevated rates of matrix turnover, which may indicate a repair response. The second group of cells do not mediate the normal turnover of matrix molecules and exhibit condensed nuclei and cytoplasm. It is currently believed that this latter group represents cells that have died through apoptosis.

1.4 Processes for Cell Death

There are two basic processes through which a cell can die. Apoptosis, which is often referred to as “programmed cell death”, and necrosis, which encompasses all other forms of non-programmed or “accidental cell death”.

1.4.1 Necrosis

When large scale cell death is encountered in a tissue, the cells are usually dying via a necrotic process. While it is often called "accidental cell death", this phrase only implies that the death was not part of the normal life cycle of the cell, as necrosis can be caused by both physiological and non-physiological processes.

The general pattern for necrotic cell death starts with the disruption of the cell membrane, either by a protein insertion into or actual physical disruption of the membrane. A large Ca^{++} influx follows, arising from the equalization of the physiologic Ca^{++} concentration gradient maintained across the cell membrane. The cell then proceeds to consume all of its energy supplies in a futile attempt to regain homeostasis. One key distinction between necrotic and apoptotic cell death is this complete consumption of energy. After running out of energy, the hypertonic cell expands, causing the cell membrane to tear open and the cell to lyse. Degradation of the cytoskeleton and organelles follows.

To be technically accurate, necrosis refers to the histologically identifiable swelling that occurs in dead cells, which usually occurs 12 to 24 hours after the cells have passed the point of no return [61], and is not intended to refer to a mode of cell death. Nevertheless, it has become common practice to refer to non-apoptotic forms of cell death (more properly termed oncosis [47]) as necrosis, and this convention will be followed in this text.

1.4.2 Apoptosis

Apoptosis, as opposed to necrosis, does not involve energy depletion, but rather involves the invocation of a biological pathway that leads to the ordered death and breakup of the cell, and the advantageous conservation of the energy and nutrients stored therein. Apoptosis is usually encountered as part of normal physiological homeostasis, being used within the body to regulate levels of mitosis, to provide for the efficient removal of tissue during embryogenesis and development (i.e. removal of finger webbing), and to remove cells that have been irreversibly damaged (i.e. sunburn). Only a small percentage of a cell population goes through apoptosis at the same time, with larger percentages usually being indicative

of the cell death arising via necrotic means [61]. Aberrant apoptosis is also thought to be the causative agent in some diseases, such as the neurodegeneration in Alzheimer's [18] and in neuronal cell death following spinal cord injury [22].

1.4.2.1 Causative Agents

Apoptosis starts with the cell receiving either an internal or external signal to begin the apoptotic process. Important internal signals that initiate apoptosis include the actions of cellular clocks, the detection of deoxyribonucleic acid (DNA) damage, and the infliction of irreparable internal damage. The term "programmed cell death" actually arose from observations of cells that were genetically predisposed to dying at fixed times during development [57]. The ability of a cell to respond to overwhelming DNA damage by inducing apoptosis, such as when a cell is exposed to ultra-violet light [53, 76], is an important evolutionary advantage as it reduces the risk of potentially carcinogenic DNA alterations in multi-cellular organisms. Finally, internal damage to mitochondria, the mitochondria being important elements of most if not all apoptosis biological pathways (see section: 1.4.2.3), has the potential to induce apoptotic cell death, allowing the mitochondria to serve as a form of cellular stress sensor.

External signals come from hormones and cytokines, along with viral, chemical, and physical agents. Most if not all mammalian cells are dependent on continual signaling by growth hormones for survival, and will automatically undergo apoptosis in the absence of these endogenous survival factors [52]. For instance, mesangial cells undergo apoptosis when IGF-1 and bFGF are removed from their environment [69]. Chondrocytes undergo apoptosis when cultured in low cell densities without supplemental growth factors and anti-oxidants [52], leading to the belief that intercellular signaling between chondrocytes is an important cue for continued survival of these cells. That cells will undergo apoptosis when they lose contact with their correct surroundings acts as an important cancer fighting mechanism in multicellular organisms.

Mammals have the ability to induce particular cells to undergo apoptosis via the use of apoptosis inducing cytokines, an ability that is important for the action of the mammalian

immune system [8], where killer T-cells need to selectively deactivate virally infected cells. These proteins are members of the tumour necrosis factor (TNF) receptor gene superfamily described further in section: 1.4.2.2. The most two well known and understood are tumor necrosis factor receptor 1 (TNFR1, also called p55 or CD120a) and CD95 (also known as Apo-1 or Fas). Activation of a TNF family receptor (such as CD95) by the appropriate TNF family ligand (such as CD95L) will induce the cell to undergo apoptosis. A subpopulation of cells in articular cartilage have been found to express CD95 and can be induced to undergo apoptosis via an antibody to the receptor [44].

Non-physiological external agents include aberrant disease processes and the action of drugs. The camptothecin topoisomerase I inhibitor family of drugs is used in chemotherapy as they induce apoptosis in dividing cells [77]. Camptothecin's inhibition of topoisomerase I prevents the enzyme from fulfilling its normal role of altering DNA topology, resulting in DNA damage during replication and apoptosis. Beta-amyloid peptides in Alzheimer's are neurotoxic and induce apoptotic cell death of the neurons in the brain [18].

Finally, mechanical injury of tissue has also been found to lead to the induction of apoptosis. Overstretching of muscle tissue has been shown to induce myocytic apoptosis [15]. The creation of lesions in chick hyaline cartilage has been shown to induce apoptosis in nearby cells [99]. The bovine articular cartilage injurious compression model developed in this thesis is also an example of mechanically induced apoptosis (see section: 3.1.1.1). The transduction mechanism that regulates mechanically induced apoptosis is currently unknown.

1.4.2.2 Signal Transduction

Following the initial signaling event, the cell may proceed through a number of different biochemical pathways. A schematic of some of the more important and common biological pathways and proteins involved in the process of apoptosis are shown in Figure: 1-2. The more important initiators of apoptosis are shown, including ligand binding to the CD95 and TNFR1 receptors, and direct action on the mitochondria.

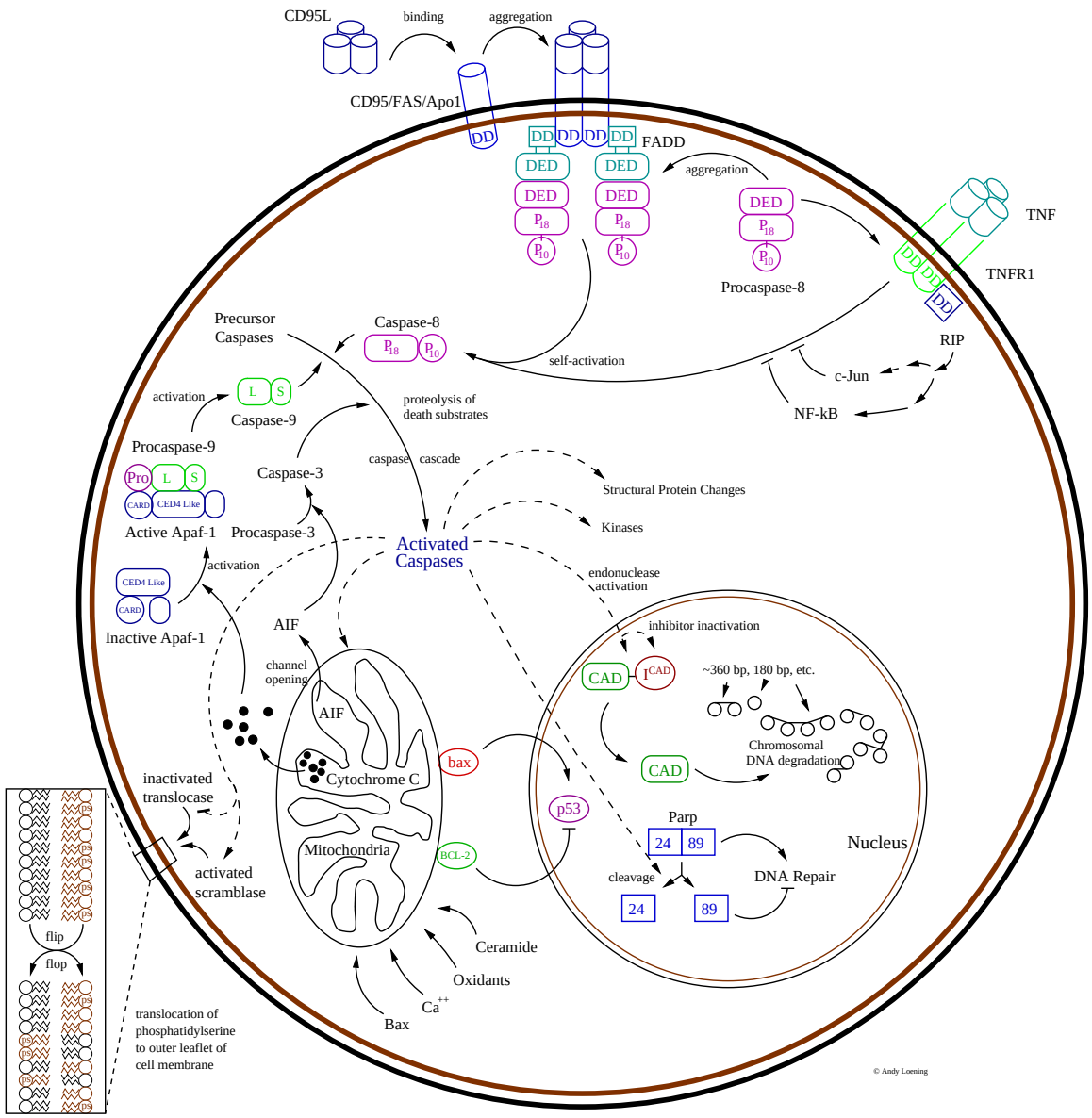

Figure 1-2: Flow diagram of biological pathways commonly associated with the induction and process of apoptosis.

The receptors responsible for mediating cytokine induced apoptosis belong to the TNF receptor gene superfamily and have similar, cysteine-rich extracellular domains [88]. Additionally, these receptors have a homologous intracellular sequence called the "death domain" (DD) [92]. Examples of death receptors are CD95, TNFR1, DR3 (also called Apo3 and Wsl1), DR4 or DR5, DcR2, and DcR1, with CD95 and TNFR1 being the best known examples.

1.4.2.2.1 CD95 The CD95 receptor is perhaps the best understood of the cytokine apoptosis signaling pathways. CD95 has three main roles under physiological conditions. It is used in the killing of activated T cells at the completion of an immune response, the killing of virus-infected and cancer cells by cytotoxic T cells and natural killer cells, and the killing of inflammatory cells at immune-privileged sites such as the eye [3].

Signaling with CD95 begins with binding of the ligand for CD95, CD95L, which is a homotrimeric molecule like all other ligands in the TNF family members. Since death domains (DD) tend to associate with one another, ligation of CD95L to 3 individual CD95's leads to the intracellular aggregation of the three DD's on the CD95 proteins [50]. The adapter protein FADD (for Fas-associated death domain, also called Mort1) binds to the aggregated death domains of CD95 with its own death domain [17].

The next step in the CD95 transduction pathway involves the clustering of procaspase-8 proteins (the zymogen form of caspase-8, which is also called FLICE or MACH), which are attracted by procaspase-8's "death effector domain"(DED) to an analogous domain on FADD [9, 72]. This aggregation of procaspase-8 creates a high local concentration of the zymogen, allowing the small proteolytic activity inherent in the protein to induce proteolytic activation through intermolecular self-cleavage [73]. The role of caspase-8 in the inducement of apoptosis is covered further in section: 1.4.2.4.

1.4.2.2.2 TNF TNF is the other well known apoptosis inducing cytokine pathway and is the namesake for the TNF gene super family. The ligand (called TNF or alternatively TNF-α) is produced mainly by activated macrophages and T cells in response to infection.

However, there is some evidence that the TNF ligand may play a role in inducing focal losses of cartilage in OA [101] due to enhanced expression of the TNF-α receptor p55 in OA chondrocytes [51].

While the receptor for TNF, TNFR1, is expressed in all cell types [93], ligation of TNF to TNFR1 rarely induces apoptosis unless protein synthesis is blocked. This is the opposite of CD95, which is not expressed in all cell types but generally induces apoptosis upon ligation of CD95L. The suppressive proteins involved in the TNF pathway are probably controlled through the NF-κB and JNK/AP-1 pathways [5].

When the TNF pathway does induce apoptosis, it proceeds via a mechanism analogous to that of CD95. The TNF ligand trimerizes TNFR1 [88], which leads to aggregation of FADD, clustering of procaspase-8, and finally self-activation. The role of caspase-8 in the inducement of apoptosis is covered further in section: 1.4.2.4.

1.4.2.2.3 Other Signaling Proteins There are other signaling proteins in the TNF gene super family that can induce apoptosis. Apo2 ligand (Apo2L, or TRAIL) is constitutively expressed in many tissues [104], binds to either DR4 or DR5 to induce apoptosis, and proceeds via a FADD independent pathway [107]. As DR4 and DR5 are expressed in many tissue types, there is most likely a mechanism that protects cells from induction of apoptosis in the Apo2L pathway.

The Apo3 signalling pathway has overlapping functions with TNF, but is found in a greater variety of tissues [65]. Apo3 ligand (Apo3L, or TWEAK) is constitutively expressed in many tissues [16], while its receptor, Apo3 (also DR3, WSL-1, TRAMP and LARD), is expressed mainly in the spleen, thymus, and peripheral blood.

1.4.2.3 Mitochondrial Roles

The mitochondria play both central roles in most of the apoptosis pathways and have the ability to induce apoptosis on their own, in effect serving as both stress sensors and executioners. This role makes sense from an evolutionary standpoint, as a cell without mito-

chondria, and therefore without a key anti-cancer weapon, is a cell that cannot metabolize efficiently and is not a cancer threat to begin with [35].

The mitochondrial role in apoptosis depends on the release of the electron-transport chain molecule cytochrome c (cyto c) and/or the protein apoptosis-inducing factor (AIF) from within the mitochondria. This release can be caused by a variety of factors including caspase activity, oxidants, the protein Bax, and direct mitochondria membrane damage [35].

Following release, the cytostolic cyto c conjugates with Apaf-1, and the complex then conjugates with procaspase-9 [60], causing self-activation of procaspase-9 into caspase-9 in a manner analogous to the self-activation of caspase-8 in the CD95 pathway. The activated caspase-9 then cleaves procaspase-3 into its activated form, caspase-3. The continued role of activated caspase-3 in apoptosis is covered further in section: 1.4.2.4. The release of cyto c is inhibited by Bcl-2 [58]. Some pro-apoptotic proteins, notably Bax, can induce mitochondrial damage, cyto c release and resultant cell death even when caspases are inactivated [106]. This demonstrates that release of cyto c from the mitochondria commits the cell to death, whether it be by a fast apoptotic death via Apaf-1 and resultant caspase activation, or a slow, necrotic death due to the collapse of the electron transport chain and energy starvation.

The release of AIF, which is currently thought to be a caspase, by the mitochondria causes the activation of caspase-3 from procaspase-3. Following activation, caspase-3 continues on as described in section: 1.4.2.4.

1.4.2.4 Caspases

All of the biological pathways through which apoptosis is induced eventually proceed via the caspase proteins (*C*ysteinyl-*asp*artic acid prote*ases*, also called interleukin converting enzymes, or ICE's), which appear to be the point of no return in the process [4]. The caspases are a highly conserved set of proteins specific to the apoptosis process and are constitutively expressed in most if not all mammalian cells [102], even "life-time cells"

such as neurons.

Caspases share similarities in amino acid sequence, structure, and most importantly, substrate specificity [75]. Caspases are among the most specific of proteases, having an absolute requirement for cleavage after aspartic acid and recognition of an at least four amino acid sequences NH_2-terminal to the cleavage site. This specificity is consistent with observations that apoptosis does not lead to indiscriminate protein digestion.

Caspases are created as pro-enzymes, or zymogens, with extremely low levels of activity and consisting of three domains, the pro-domain, the large-domain, and the small-domain. The low catalytic activity allows large quantities of the caspase precursors to be built up and stored within the cell. Since proteolysis is an irreversible process, activation of caspases by cleavage allows the cell's commitment to apoptosis to be an irreversible process.

Activation of a caspase requires cleavage between the prodomain and the other two domains at a site whose sequence is specifically recognized by the catalytic site of caspases. A structural change can then occur whereby the small and large domains form a heterodimer. Two separate heterodimers then associate to form a tetramer, with two independent catalytic sites.

There are two basic processes by which the zymogen pro-caspases can be cleaved into their active forms. The simplest is proteolysis of the pro-caspase by a previously activated caspase. Since all activated caspases can cleave and activate all pro-caspases, a "caspase cascade" can occur whereby a small, threshold level apoptotic signal can be amplified and lead to the activation of all caspases and resultant apoptosis.

The second method of activation is by induced proximity and appears to be the common method for the initial transduction of the apoptosis signal to the caspases. In induced proximity, pro-caspases are aggregated, and due to the high local concentration the inherent low protease activity of the pro-caspase zymogens is sufficient to drive intermolecular proteolytic activation. This activation method was first observed for caspase-8 in the CD95 pathway [73] and is thought to be the method whereby cyto c bound Apaf-1 is able

to activate caspase-9 [89].

Only a few of the roles that the different caspases play in effecting cell death are known. Known roles include endonuclease activation, destruction of the nuclear lamina, cleavage of proteins important in cytoskeleton regulation, and shutdown of DNA repair, mRNA splicing, and DNA replication.

Endonuclease activation is partially accomplished by cleavage of the caspase-activated deoxyribonuclease (CAD) inhibitor (I^{CAD}, or DFF45) by caspase-3 from the CAD-I^{CAD} complex [86]. This leaves the endonuclease CAD free to act upon the chromosomal DNA and helps lead to the internucleosomal cleavage discussed further in section:1.4.2.6.2. Caspase activation also leads to the destruction of the nuclear lamina [82], the rigid structure composed of intermediate filaments underlying the nuclear membrane, causing the condensation of the chromatin. Furthermore, caspase cleavage of several proteins important in the regulation of the cytoskeleton leads to the reorganization of cell structures. Proteins effected include gelsolin, focal adhesion kinase (FAK), and cleavage induced activation of p21-activated kinase 2 (PAK2) [84].

1.4.2.5 Other Apoptosis Associated Proteins

There are many other proteins involved in the process of apoptosis. Some of the more important ones not covered so far are Bcl-2, Bax, p53, and Parp.

Bcl-2 is the prototype for a large family of proteins that can either prevent or promote apoptosis. Bcl-2 is an important anti-apoptotic protein that is localized near the mitochondria membrane. How it performs its anti-apoptotic role is unclear, but Bcl-2 is thought to prevent the release of AIF and cytochrome C from the mitochondria. In chondrocytes, Bcl-2 has been implicated in regulating the apoptotic response of chondrocytes subjected to serum-withdrawal or retinoic acid treatment [26]. Additionally, increased expression of Bcl-2 has been reported in chondrocytes near defects in OA tissue [23].

Bax is a pro-apoptotic member of the Bcl-2 family that induces apoptosis by acting on the mitochondrial membrane. Levels of Bax were unchanged in response to serum-

withdrawal or retinoic acid treatment of chondrocytes [26]. P53 blocks the process of DNA repair, playing a critical role in the induction of apoptosis due to chromosomal damage. Finally, Parp, normally responsible for DNA repair, is cleaved into an inactive form by the caspases.

1.4.2.6 Cellular Effects

1.4.2.6.1 Phosphatidylserine Translocation One of the earliest detectable changes in apoptotic cells is the translocation of phosphatidylserine (PS) to the outer leaflet of the cell membrane [98]. Under normal physiological conditions, the enzyme aminophospholipid translocase maintains the asymmetrical distribution of PS toward the inner leaflet of the plasma membrane. Shortly after the inducement of apoptosis, translocase is inactivated and the distribution of PS between the outer and inner leaflet becomes symmetric by nonspecific flip-flop of phospholipids between the leaflets [11] and/or the activity of a hypothesized enzyme "scramblase" [97] (depicted in Figure: 1-2). The exposure of PS serves as a marker for phagocytosis allowing a non-inflammatory response by macrophages [24].

Since this translocation occurs in apoptosis without the accompanied disruption of the plasma membrane found in necrosis, it can be used as a method for the distinguishment of necrotic, apoptotic, and viable cells. Annexin V staining makes use of FITC labelled Annexin V, a Ca^{++} dependent phospholipid-binding protein that binds to PS, to detect the presence of PS on the outer leaflet [109].

1.4.2.6.2 Chromosomal DNA Cleavage Another detectable change that is commonly used for assaying apoptosis is internucleosomal cleavage of the chromosomal DNA by endonucleases. Although the mechanism of this cleavage is not completely understood, caspase activated endonucleases such as CAD certainly play a role in the process along with Ca^{++} and Mg^{++} dependent nucleases such as DNAse I.

The actual degradation of the chromosomal DNA begins with it breaking up into large, $\sim$300 kbp fragments, which are then further degraded into $\sim$50 kbp fragments. Both the $\sim$300 kbp and $\sim$50 kbp fragments can be detected with the use of pulsed field gel elec-

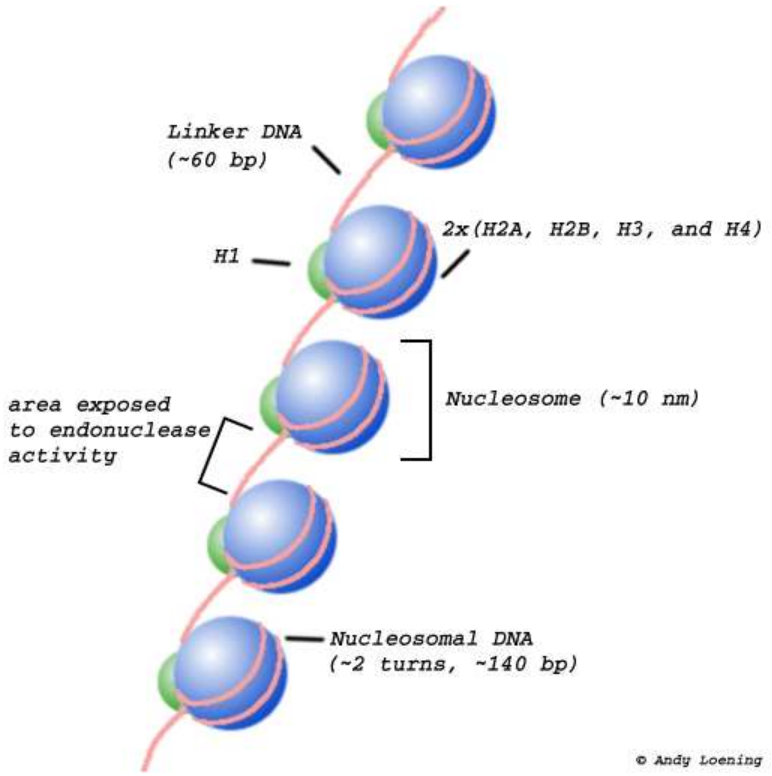

Figure 1-3: A diagram of the Nucleosomes showing typical DNA lengths.

trophoresis [100]. The chromosomal DNA in most cells is then further cut into < 40 kbp fragments by random endonuclease activity, from which small oligonucleosome fragments with lengths that are multiples of $\sim$185 bp are released. It is these oligonucleosomes that allow for the classic dna laddering shown on agarose gels [32].

That the oligonucleosomes come in lengths that are multiples of $\sim$185 bp arise from the physical structure of chromosomal DNA. When DNA is not being transcribed or replicated, it is wrapped in structures called nucleosomes, which are composed of $\sim$140 bp of DNA wrapped around 8 histone proteins (two each of H2A, H2B, H3, and H4) with a H1 histone protein locking the DNA into the assembly (Fig: 1-3). Since the DNA is not released from the nucleosomes during apoptosis, cleavage must occur in the linker DNA region between the nucleosomes [105], which leaves fragments that are multiples of $\sim$185 bp (Fig: 1-4).

The chromosomal DNA cleavage leaves many cut edges of DNA, which lend themselves to apoptosis identification by the nick-end labeling methods. Both TUNEL (terminal

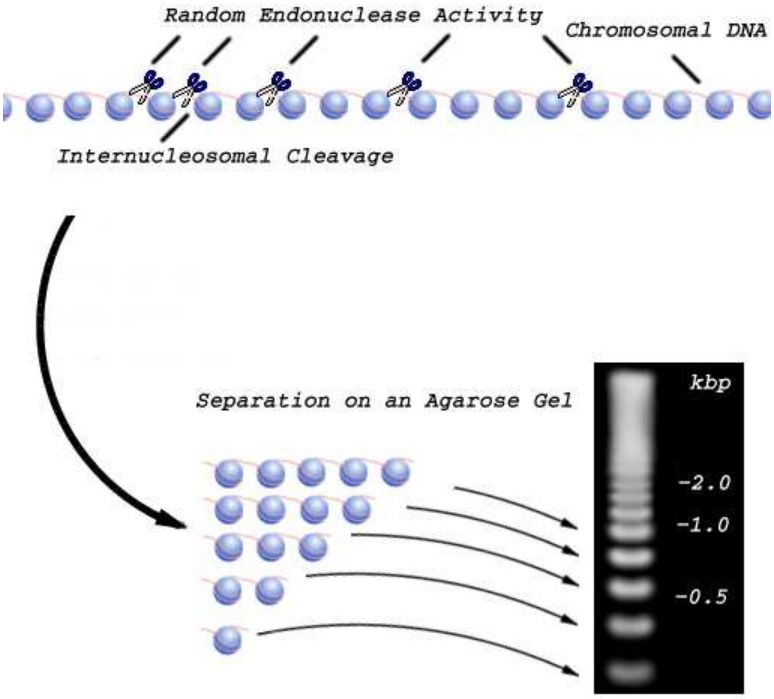

Figure 1-4: A diagram of the endonuclease activity that leads to the characteristic laddering pattern of apoptotic DNA on an agarose gel.

deoxynucleotidy transferase mediated UTP nick end labeling) [30] and ISEL (*in situ* end labeling) [103] work by incorporating artificial nucleotides into the DNA where it is cut, allowing identification of apoptosis even when only large ($\sim$300 kbp) fragments are available. The only difference between the two methods is the enzyme used for the artificial nucleotide incorporation. ISEL uses DNA Polymerase I (or the Klenow fragment of DNA Polymerase I), which can label 3' recessed ends of the cut DNA. TUNEL uses of terminal deoxynucleotidy transferase (TDT, or terminal transferase), which can label 3' recessed, 5' recessed, and blunt ends of the cut DNA. This ambivalence to the shape of the cut ends makes TUNEL more sensitive [71] and the more commonly used of the two assays.

The artificial nucleotides used in the nick-end labeling methods tend to either be fluorescein or digoxigenin conjugated. In the case of digoxignenin, an anti-digoxigenin antibody that is either conjugated to fluorescein or peroxidase is then used. In any case, since viable cells do not have large numbers of DNA ends, they will show very little signal. Necrotic cells generally do have large numbers of DNA ends due to degraded chromosomal DNA, but since the nuclear membrane is ruptured, the DNA will diffuse and a concentrated signal will not be displayed. Only in the case of apoptotic cells will a concentrated and strong signal be seen.

1.4.2.6.3 Apoptotic Body Formation Following the fragmentation of the cell's DNA, the cell begins to convolute and form buds. These buds eventually separate and the cell disintegrates. These separated buds are called apoptotic bodies and are generally phagocytosed by neighboring cells and macrophages [47]. In cartilage, no phagocytic cells exist and the apoptotic bodies are likely to remain in the cartilage extracellular matrix. Most proteins, nucleotides, and other important molecules are recovered by these phagocytosing cells. While the cell membrane and other membranes are not compromised during these processes, the cell membrane does lose most of its function and its permeability is altered.

1.5 Thesis Objectives

In an effort to better understand the conditions under which apoptosis occurs in articular cartilage and the role apoptosis may play in both normal cartilage function and osteoarthritic degeneration, this thesis focuses on an *in vitro* model system for apoptosis induced by injurious mechanical compression in articular cartilage. The creation and understanding of a well-defined and repeatable model for the generation of apoptosis in articular cartilage is a necessary prerequisite for quantitative studies. Cartilage specimens are subjected to graded levels of mechanical compression, and the TUNEL method is used to assess the extent of chondrocyte apoptosis. These results are compared to additional metrics of tissue injury including cell viability and biochemical changes. Threshold levels of mechanical stress, strain, and strain rate that result in biochemical and apoptotic changes are identified and compared.

Chapter 2

Materials and Methods

2.1 Materials

Dulbecco's phosphate buffered saline (PBS), gentamicin, non-essential amino acid solution, HEPES, and Dulbecco's modified Eagle's medium (DMEM) were purchased from Gibco, Grand Island, NY. L-proline, shark chondroitin sulfate, ascorbic acid, sulfanilamide, napthylethylenediamine dihydrochloride, ethidium bromide, and sodium nitrite were purchased from Sigma, St. Louis, MO. Ethanol was from Pharmco, Brookfiled, CT. Dimethylmethylene blue and fluorescein diacetate were from Polysciences, Warrington, PA. Dimethyl sulfoxide (DMSO) was from from Mallinckrodt, Paris, KY. IL-1β was provided by MERCK Research Laboratories. TNF-α was obtained from R & D systems, Minneapolis, MN. Z-VAD-fmk and SB-279885 was provided courtesy of Dr. Michael Lark and associates at SmithKline Beecham, King of Prussia, PA.

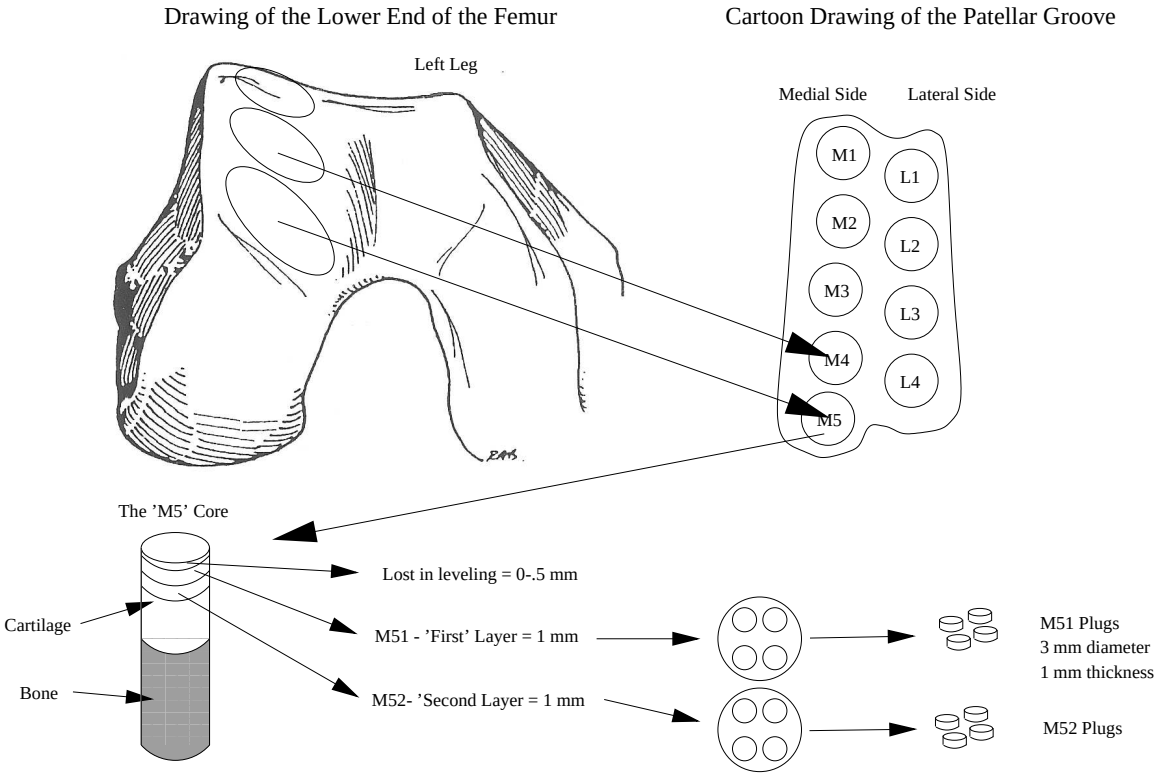

Figure 2-1: The general procedure used for the explanting of cartilage disks is shown. Full-thickness cores are cored out of the femoropatellar groove. Two 1 mm thick slices are then taken, and four 3 mm diameter by 1 mm thick cartilage disks are obtained from each slice.

2.2 Methods

2.2.1 Tissue Protocols

2.2.1.1 Tissue Harvesting

Articular cartilage tissue was harvested from the femoropatellar groove as previously described [85]. Briefly, 1 mm thick by 3 mm diameter cartilage disks ($\sim$8 mg wet weight at time of explant) were explanted from the femoropatellar grooves of 1-2 week old calves using a 3/8 inch coring bit mounted on a drill press, a sledge microtome (Model 860, American Optical, Buffalo, NY) and a 3 mm dermal punch (Miltex Instruments, Lake Success, NY) (Fig: 2-1). The joint surface and explanted tissue was kept moist at all times by immersing in or irrigating with a phosphate-buffer saline (PBS) solution containing 50 μg/ml gentamicin.

2.2.1.2 Feeding

During the course of an experiment, the cartilage tissue disks were maintained in low-glucose, 10% serum-supplemented DMEM with 10 mM HEPES buffer, 110 mg/ml sodium pyruvate, 0.1 mM non-essential amino acids, 0.4 mM proline, 0.1 mM ascorbate acid (20 μg/ml) and gentamicin (50 μg/ml, reduced to 25 μg/ml after the first day). During experiments involving cytokines, high-glucose serum-free DMEM was used to avoid any ambiguities arising from growth factors and other proteins inherent in the serum. In experiments involving apoptosis inhibitors, a 10 mM stock solution was made by dissolving the inhibitors in appropriate volumes of 100% DMSO. The stock solutions were then used in preparation of the medium, and an equal volume of 100% DMSO was added to the control medium.

2.2.2 Injurious Compression Protocols

Injurious Compression

Following 1-2 days in culture, between 3 and 10 disks of tissue to be loaded were placed inside of a 12 well polysulfone compression chamber (Fig: A-1) with 0.5 ml media per well. Inside the compression chamber, the disks were sandwiched between two impermeable platens, allowing uniaxial, radially unconfined compression to be applied by loading of the top of the compression chamber. The compression chamber was then placed inside a custom built incubator housed compression apparatus [28] (incustat, appendix: A) for the application of the injurious compression protocol (calibration procedure is described in section A.5). The number of disks in the chamber was picked so that the peak load attained during the compressive phase of loading would not exceed the incustat server motor's limit of around 45 kg.

The disks in the chamber were then subjected to an injurious compression protocol (Fig: 2-2). The protocol consisted of:

1. A quick compression to 50-70% of cut thickness (30%-50% strain) at a strain rate of

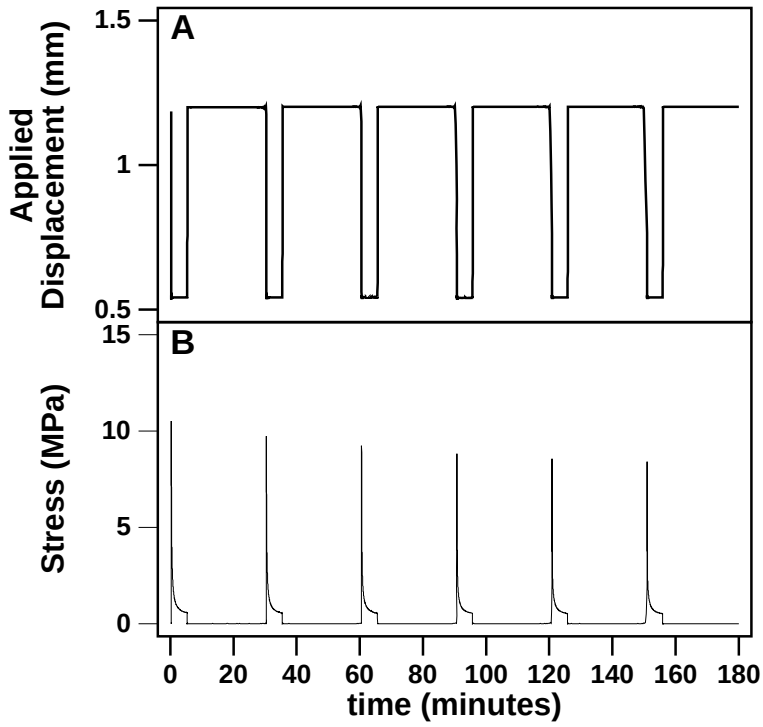

Figure 2-2: Output from a typical injurious compression protocol is shown. Peak stress generated was $\sim$ 10 MPa for this example. Displacement corresponds to the expected thickness of the cartilage disk.

100% of the disks thickness per second (1000 μm/s)

2. Maintaining this strain level for 5 minutes

3. Releasing the compression for 25 minutes

4. And repeating this on/off compression cycle for a total of 6 times

Load measurements were recorded during all experiments, and the peak stresses produced during the compression (between 4 and 25 MPa depending on the chosen strain level) were used for comparisons between different experiments. (Compressive strains were not used to compare these experiments due to problems with machine compliance and displacement calibration, as discussed in section: A.5.

Anatomically matched free-swelling disks served as controls and were maintained in an unloaded compression chamber alongside the loaded chamber during the course of

the experiment. Media and handling conditions were identical to that of the compressed disks.

Following the compression, the disks were maintained in media for zero to six days, depending on the experiment. Conditioned media samples were stored at -20° C for later analysis (described in section: 2.2.3).

2.2.3 Biochemical Assays

2.2.3.1 Wet Weight Measurements

Wet weights of cultured tissue were taken by patting each disk dry with sterile gauze, placing it inside of a pre-weighed sterile vial, and differentially weighing the disk (AE 163 Balance, Mettler Instrument Corp, Hightstown, NJ).

2.2.3.2 Sulfated GAG Assay

Conditioned media was assayed for sulfated glycosaminoglycan (sGAG) released into the media using the dimethylmethylene blue (DMMB) dye method [25] with chondroitin sulfate from shark cartilage used as the standard. Briefly, 20 μl media was mixed with 200 μl DMMB dye, 20 μl of 70% ethanol was added to remove bubbles, and the absorbance at 520 nm was measured using a microplate reader (Vmax microplate reader, Molecular Devices, Menlo Park, CA)

2.2.3.3 NO Assay

Nitric oxide levels in the conditioned media were assessed by placing media samples through the Griess reaction [36, 37, 38] and measuring the absorbance at 560 nm, with the use of sodium nitrite for standards. Briefly, media was spun at 16,000 g for 1 minute to remove any debris. 100 μl of the media supernatant were then mixed with 50 μl 1% sulfanilamide in 5% H_3PO_4 and 50 μl 0.1% naphthylethylenediamine dihydrochloride, with 20μl of 70% ethanol added to remove bubbles, incubated at room temperature for

20 minutes, and measured for optical absorbance at 560 nm in a microplate reader (Vmax microplate reader, Molecular Devices, Menlo Park, CA).

2.2.3.4 Apoptosis Assays

Levels of apoptosis were measured in cartilage tissue through a collaborative effort with Smith-Kline Beecham (SKB). Injurious compressed disks were flash frozen by direct immersion in liquid N_2, stored at $-80\ ^{\circ}C$ prior to shipment, and shipped on dry ice to SKB for further processing.

At SKB, each disk was serially cryostat sectioned into semi-thin (8 μm) sections ($\sim$125 sections/disk) and immobilized on glass slides. The sections were then air-dried, fixed, and stained for the presence of apoptotic nuclei following the manufacturer's protocol (ApopTag peroxidase *in situ* apoptosis detection kit, Oncor, Gaithersburg, MD). The peroxidase enzyme label used yielded an insoluble brown stain in positive nuclei. All $\sim$125 sections/disk were scored blind for the presence of apoptotic nuclei. Sections with positive staining nuclei at their periphery were considered negative (score of -1, 0, or 1), as these apoptotic cells were artifacts of the cutting process [99]. Sections considered positive had apoptotic nuclei away from their edges and were scored according to whether there were small (score of 2) or large numbers (score of 3) of positive nuclei. The final number reported for each disk was the percentage of positive sections (score 2 or 3) to the total number of sections from the disk. In another series of experiments, the percentage of apoptotic cells was also assessed. This was done by counting and averaging positive and negative staining cells in the central region on 3-5 separate sections (300-500 cells total) of a given disk.

2.2.3.5 Red/Green Fluorescence Cell Viability Assay

Viability in cartilage tissue disks was assessed with the vital dyes ethidium bromide (EtBr) and fluorescein diacetate (FDA) [2, 87]. Each disk to be assayed was sliced completely into $\sim$200 μm sections with a scalpel blade and then immersed into an 18 μM EtBr (25 μg/ml),

250 μM FDA (10 μg/ml) in PBS solution. (For an explanation of the theory behind the assay, please see section: B.1) The tissue sections were immediately examined under fluorescence microscopy (Nikon Diaphot, Japan) using a 450-490 nm excitation filter, a 510 nm dichroic mirror, and a 520 nm barrier filter (B-2A filter set). Viability was then determined for a random location near the center of 3-4 sections, and these viability numbers were averaged together to form a viability score for the entire disk.

2.3 Statistics

Control and experimental groups were compared using Student's paired t test when appropriate and Student's t test assuming equal variances otherwise, with significance at the level $p < 0.05$.

Chapter 3

Results of Injurious Compression on Articular Cartilage

3.1 Effects on Cellular Viability

3.1.1 Apoptotic Response

3.1.1.1 Induction of Apoptosis

Injurious mechanical loading of bovine articular cartilage disks resulted in an increase in the number of cells staining positive for apoptosis via the TUNEL method that was dose-dependent on the applied peak stress (Figs: 3-1 & 3-2). This increase was significant at 10 and 20 MPa, with the number of cells staining positive for apoptosis nearly 50% for the 20 MPa condition. Loading with even a relatively mild injurious compression protocol ($\sim$4.5 MPa) resulted in a significant increase in the number of sections judged positive for apoptosis (score of 2 or 3) for loaded cartilage tissue versus free swelling controls (Fig: 3-3).

In both the loaded disks and the unloaded control disks, numerous cells at the cut-edge stained positively for apoptosis, as has been reported previously for the cutting of articular cartilage [99]. In contrast, there was a significant increase in apoptotic nuclei in

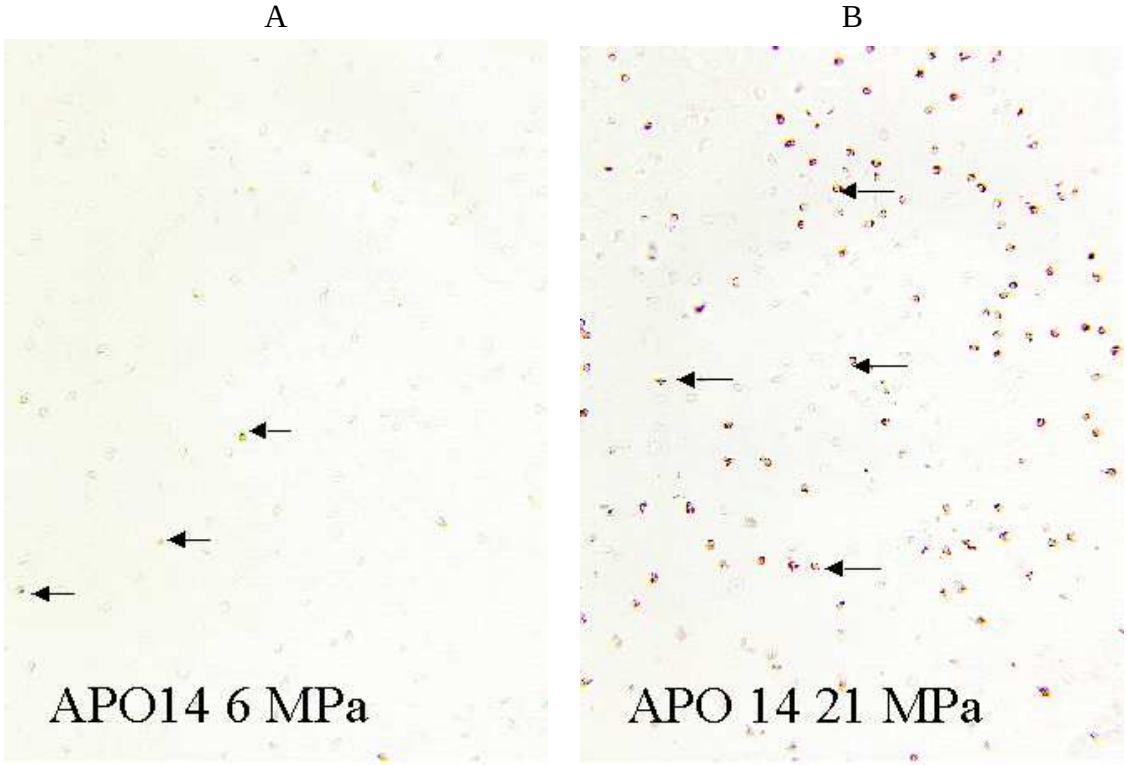

Figure 3-1:
Examples of cartilage tissue stained with TUNEL. A) Tissue loaded with a peak stress of ~6 MPa showing scattered positive TUNEL staining. B) Tissue loaded with a peak stress of ~21 MPa showing a large number of positive staining cells.

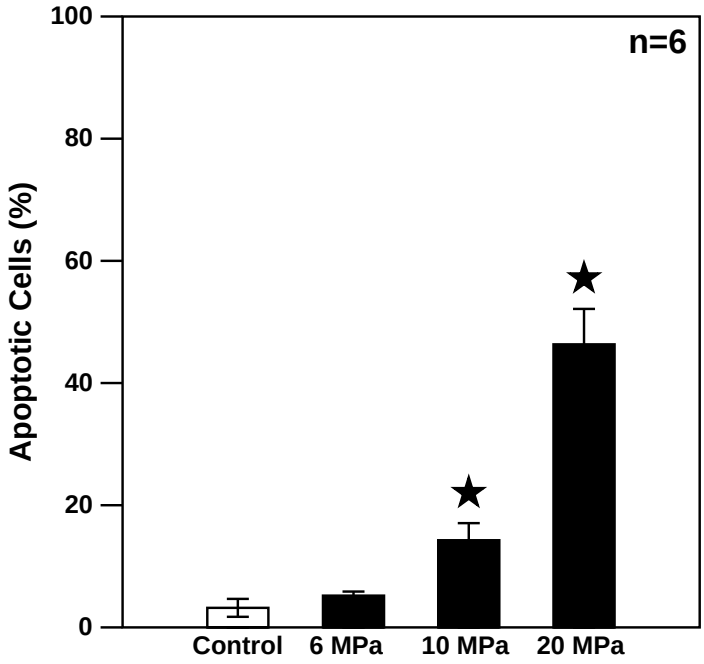

Figure 3-2: Apoptosis was induced in cartilage tissue by application of different levels of injurious compression. Cartilage explant disks were subjected to peak compressive stress of 0 (control), 6, 10, and 20 MPa, subsequently incubated for 4 days, and then analyzed for apoptotic nuclei with the TUNEL assay. Data are mean$\pm$SEM; $\star$ indicates $p < 0.05$ by paired t test.

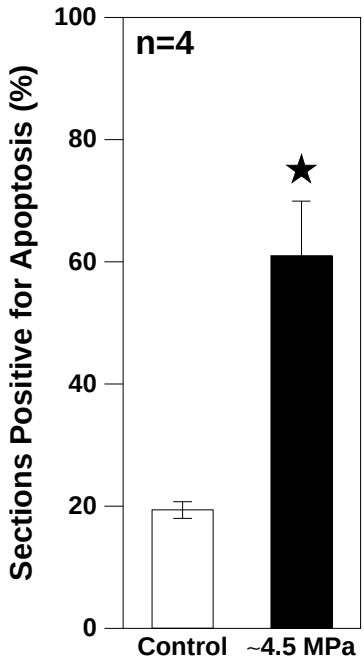

Figure 3-3: Apoptosis was induced in tissue with a relatively mild injury ($\sim$4.5 MPa) protocol. Results are shown as the precentage of sections considered positive for apoptosis (score of 2 or higher). Data are mean$\pm$SEM; $\star$ indicates $p < 0.05$ by paired t-test.

the central region of the loaded cartilage disks (e.g., Fig: 3-3).

Although the TUNEL staining portion of a time course study had not yet been completed at the time of this writing, experiments in other labs have shown that apoptotic chondrocytes in articular cartilage remain stainable via TUNEL for apoptosis for at least 20 days in explant culture [94]. An experimental wounding model in embryonic chick hyaline cartilage has also shown that an apoptotic response can be detected after only 10-20 minutes post-wounding and that the apoptotic effect of the wounding reached a maximum at two days post-injury [99].

3.1.1.2 Effects of Apoptosis Inhibitors

Preliminary data from the TUNEL staining of cartilage tissue that had been given a $\sim$20 MPa peak stress injury and had been maintained in media containing the general caspase inhibitor Z-VAD-fmk (Z-Val-Ala-Asp Fluoromethyl Ketone) before, during, and for the four days after injury before being frozen is shown in Figure: 3-4. The SmithKline

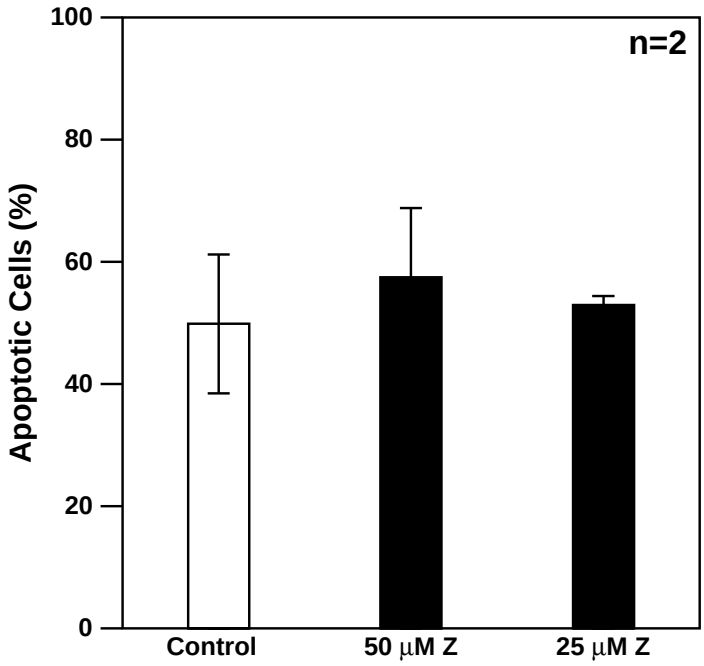

Figure 3-4: Tissue was given a ∼20 MPa peak stress injury, incubated for four days with or without the use of inhibitors, and then stained for apoptotic cells using the TUNEL assay. 50 μM Z indicates 50 μM Z-VAD-fmk, 25 μM Z indicates 25 μM Z-VAD-fmk.

Beecham inhibitor SB-279885 at a concentration of 25 μM had also been used, but data from that condition had not yet been generated at the time of this writing. There were no apparent differences between the different conditions, but a conclusive answer cannot be given due to the small sample size (n=2).

3.1.1.3 Effects of Apoptosis Inducing Cytokines

The effects of cytokines that are known to induce apoptosis in certain cell types were examined in order to verify the accuracy of the apoptosis assay. The two cytokines used were TNF-α and IL-1β. TNF-α at 100 μmol/ml produced an apoptotic signal, as expected, that was slightly higher than that seen in injuriously compressed samples (Table: 3.1). No apoptosis was seen with 100 μmole/ml of IL-1β, which is consistent with previously published reports that examined the effects of IL-1β on chondrocytes [7]. Only a single section was looked at from each disk in this study, so the results were non-quantitative and should be regarded with caution.

Group	Result of TUNEL
Control (no cytokine)	Some Postive Staining
IL-1β (100 ng/ml)	No Staining
TNF-α (100 ng/ml)	Some Positive Staining
IL-1β (100 ng/ml) + TNF-α (100 ng/ml)	No Staining

Table 3.1: Effects of Apoptosis Inducing Cytokines

3.1.2 General Viability Changes

3.1.2.1 Results of Cell Viability Assay

Injurious mechanical compression of cartilage disks resulted in marked decreases in cell viability in the centers of the disks, as measured by the vital dyes ethidium bromide and fluorescein diacetate 6 days post-compression (Figs: 3-5 & 3-6). This decrease in cell viability was strongly dependent on the peak stresses generated, with significant changes between loaded and control disks beginning around 10 MPa peak compression stress and a $\sim$25% reduction in viability being seen around 20 MPa. For all loaded disks, the viability was best in the center, were the viability measurements were taken, and worsened traveling toward the sides of the disk. Control and loaded disks always displayed 2-6 cell layers of dead cells along all of the edges that were artifacts of the cutting process. Fracturing of the cartilage tissue was not seen until the disks were compressed above a peak stress of $\sim$15 MPa and was usually associated with extremely low (5-10%) viability.

A time course study done with an 18-20 MPa peak stress injurious compression applied to the disks showed that the change in vital dye staining was apparent even directly after the completion (3 hrs after initiation) of the injurious compression protocol and remained constant at $\sim$30% for the following two days (Fig: 3-7).

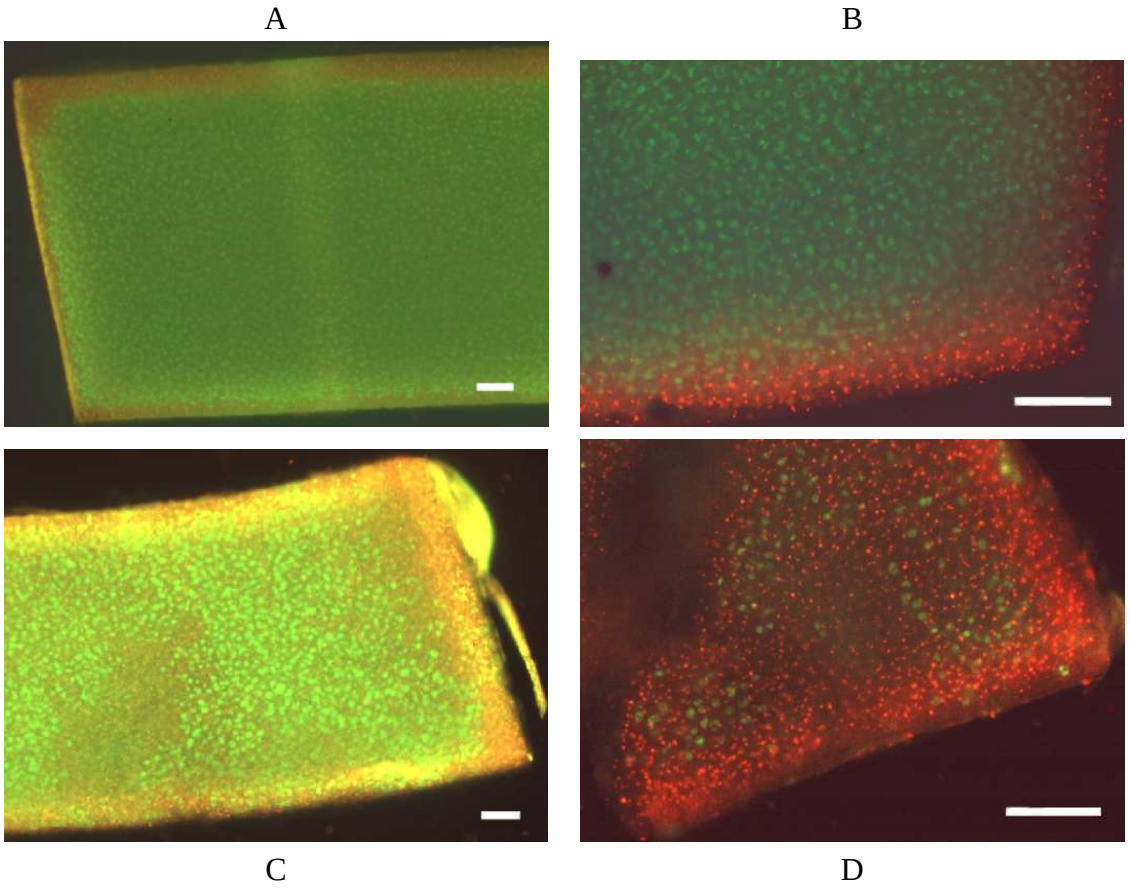

Figure 3-5: Examples of cartilage tissue sections stained with ethidium bromide and fluorescein diacetate. A) Section of an unloaded control disk showing cutting artifacts along the edges. B) Higher magnification of an unloaded control disk, again showing the cutting artifacts. C) Section of a loaded explant disk subjected to 17 MPa peak stress exhibiting $\sim$50% viability and cutting artifacts along the edges. D) Higher magnification of a different loaded explant disk compressed with $\sim$17 MPa peak stress. The tissue exhibits deep fissures and extremely low viability. Bar indicates 100 μm.

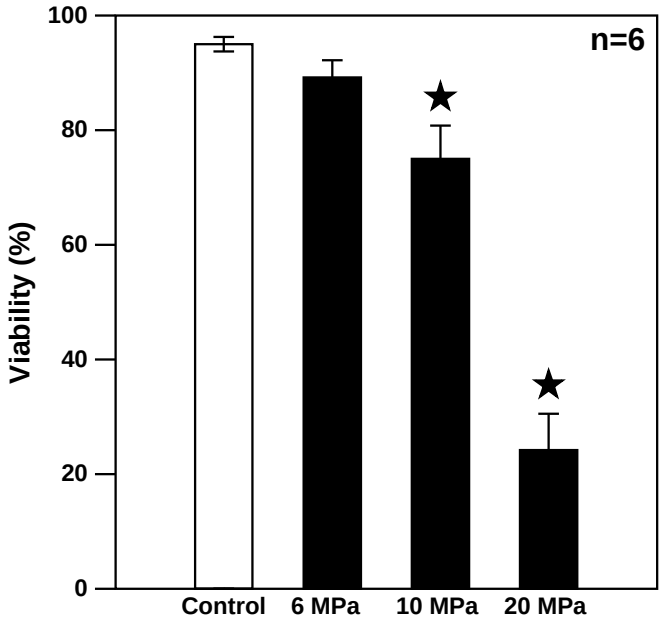

Figure 3-6: Changes in cell viability were measured using the red/green assay 6 days after injurious compression to peak streses of 0 (control), 6, 10, and 20 MPa. Data are mean$\pm$SEM; $\star$ indicates $p < 0.05$ by paired t-test.

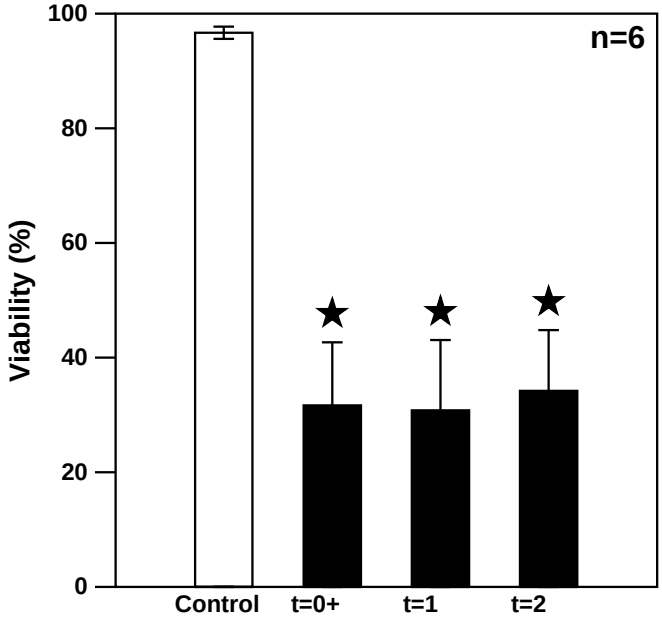

Figure 3-7: Changes in cell viability were measured using the red/green assay 0,1, and 2 days after a relatively high loading condition to a peak stress of 18-21 MPa. Data are mean$\pm$SEM; $\star$ indicates $p < 0.05$ paired t-test.

3.2 Effects on Tissue Properties

3.2.1 Biochemical Changes

3.2.1.1 Wet Weight

Tissue wet weights were measured daily for 6 days following injury at several different injurious compression levels (Fig: 3-8) and showed a clear dose-dependent response. At the lower compression levels (7 and 8.5 MPa peak stress) no significant changes were seen in the wet weights of loaded tissue compared to that of free swelling controls. At 12 MPa, the loaded tissue showed a significant increase in wet weight compared to control, and by 13 MPa this difference between control and loaded wet weights was even more apparent. The 17 MPa condition clearly showed the effect of the collagen network damage and rapid swelling and was the only condition in which the loading was severe enough to produce a significant increase in tissue swelling even directly after the injurious compression. An analysis of the rate of tissue swelling (Fig: 3-9) showed that any increase in wet weight over that of controls occured within one day of compression.

3.2.1.2 Sulfated GAG Loss

The cumulative sGAG release from injured disks paralleled changes in the tissue wet weights (Fig: 3-10), also showing a clear dose response. At the lower injury levels (7-8.5 MPa), significant differences in sGAG release were not generally seen. At the 8.5 MPa condition, the cumulative sGAG release was higher directly after compression, but fell back to normal levels immediately afterwards. Around 12 MPa, a small yet significant change from control values was apparent. By 13 MPa, a strong and significant difference in sGAG loss arose, with the cumulative loss nearly 75% greater than that of the free-swelling controls for the 13 and 17 MPa loading conditions by day 6. A look at the sGAG release rates (Fig: 3-11) shows that the rates were sharply increased during the compression and remained significantly elevated for 2-5 days before returning back to control values.

In a separate series of experiments, the cumulated sGAG released by day four was

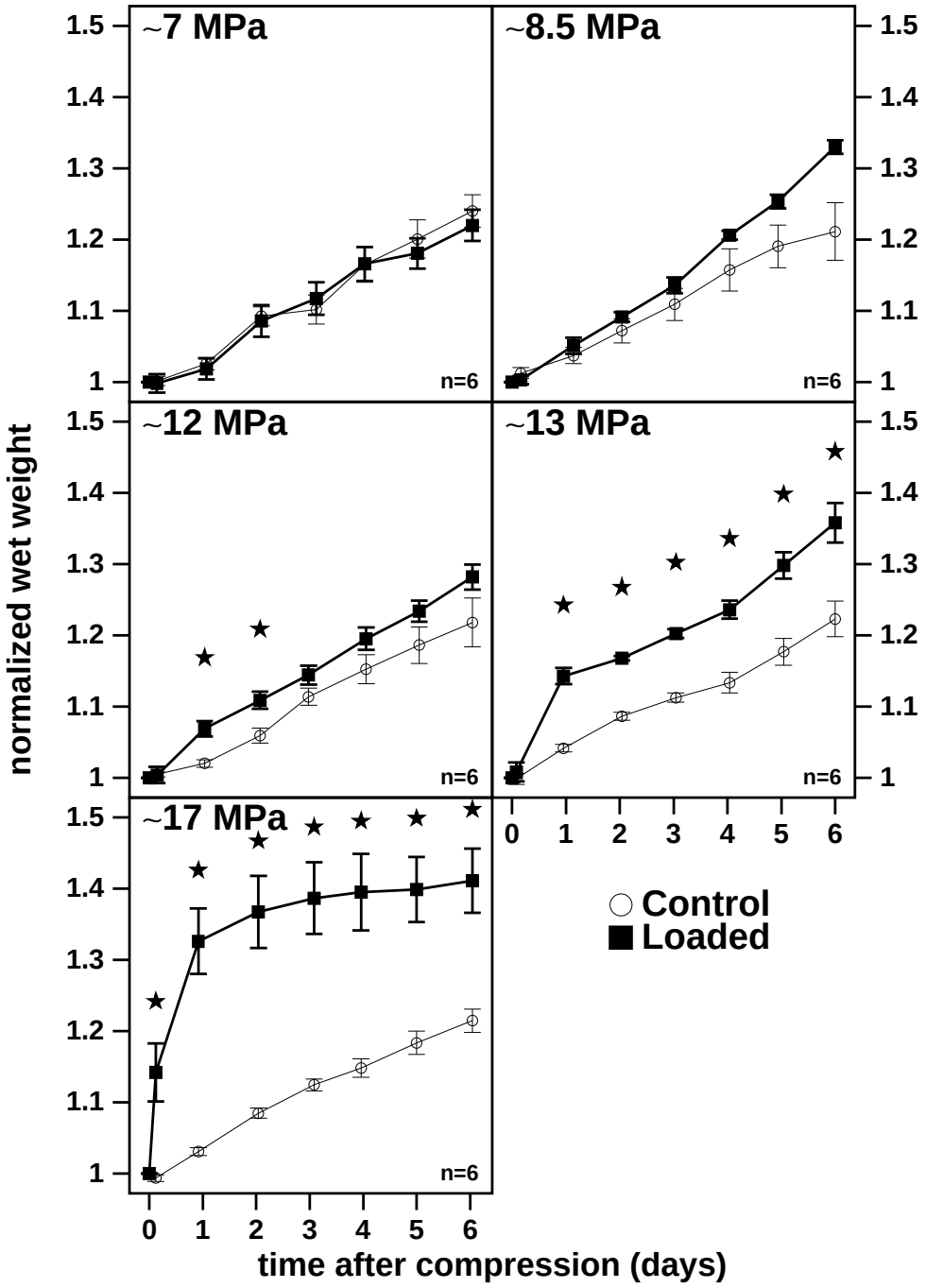

Figure 3-8: The wet weights of injured cartilage disks are shown along with their matched controls for different peak stress loading conditions. Tissue wet weights were recorded immediately before and immediately after compression to 7, 8.5, 12, 13, and 17 MPa peak stress and every day afterwards for 6 days Data are normalized to the measured wet weight before compression;mean$\pm$SEM, n=6; $\star$ indicates $p < 0.05$ by paired t test.

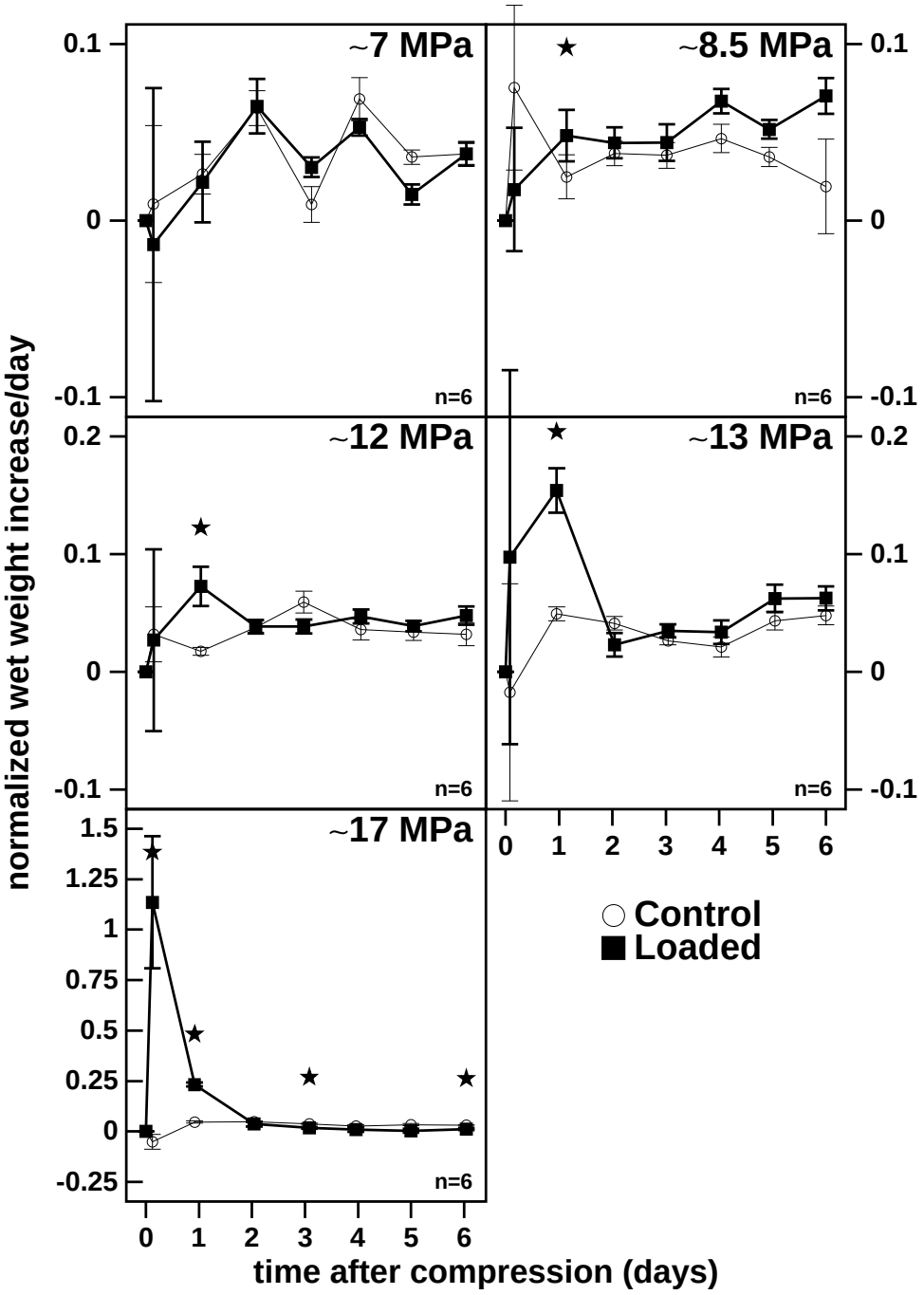

Figure 3-9: The rate of increase in wet weight of injured cartilage disks, shown along with their matched controls for different peak stress loading conditions. The weights are normalized to the weight of the tissue immediately prior to compression. Data are mean$\pm$SEM; $\star$ indicates $p < 0.05$ paired t-test.

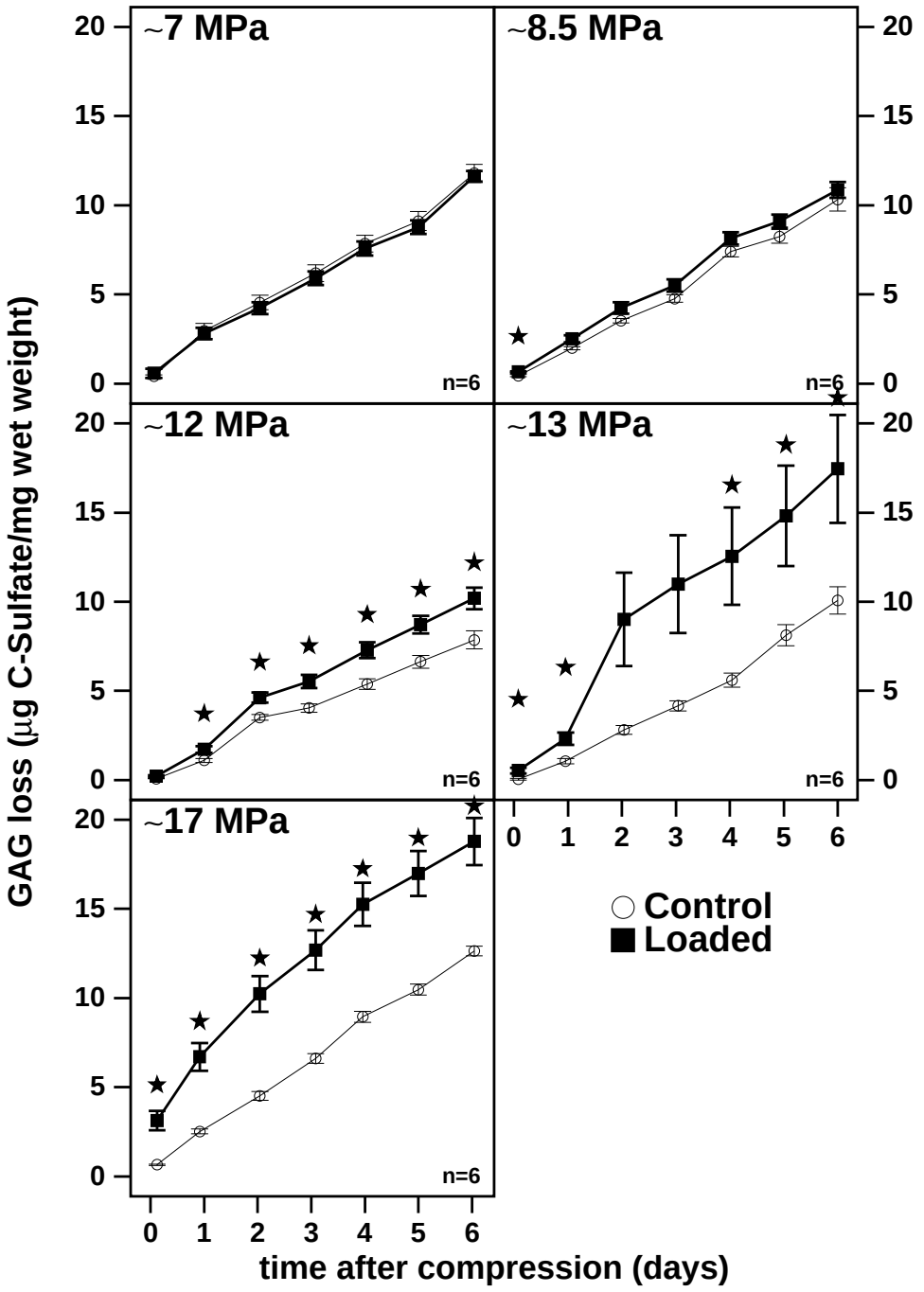

Figure 3-10: The cumulative release of sulfated-GAG's to the media are shown for injured cartilage disks along with their matched controls for different peak stress loading conditions. Cartilage explants were subjected to peak stresses of 7, 8.5, 12, 13, and 17 MPa, with free-swelling anatomically matched tissue serving as control. Conditioned media was stored directly after compression and every day thereafter, and analyzed for sGAG. Each data point represents the total GAG lost to the medium by that day. The results are normalized to the tissue's wet weight at time 0. Data are mean$\pm$SEM, n=6; $\star$ indicates $p < 0.05$ by paired t test.

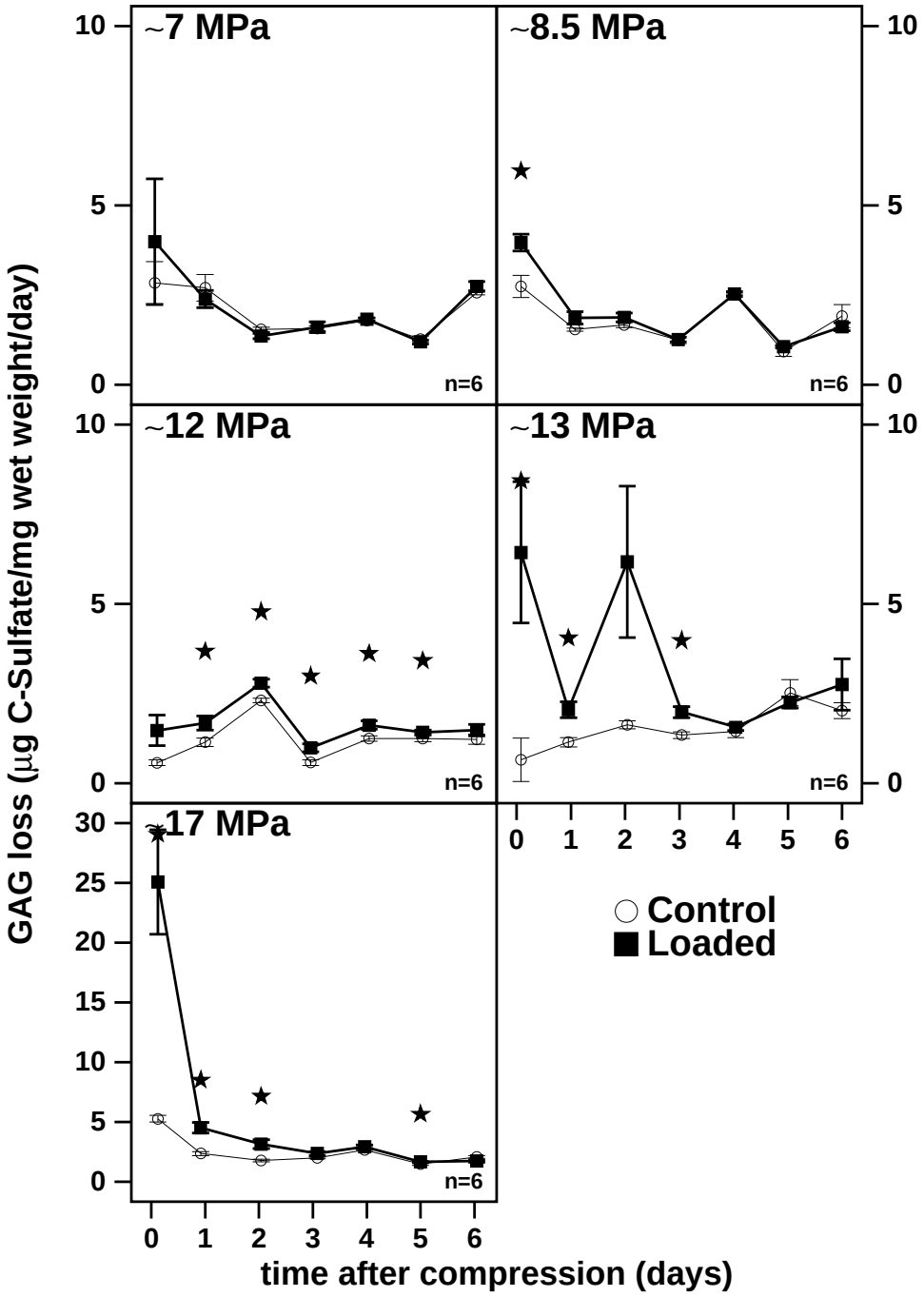

Figure 3-11: The release rate of sulfated-GAG's to the media are shown for injured cartilage disks along with their matched controls for different peak stress loading conditions. Each data point represents the GAG lost to the medium at that time point divided by the amount of time the tissue was in that particular medium. The values are normalized to the tissue's wet weight at time 0. Data are mean$\pm$SEM; $\star$ indicates $p < 0.05$ by paired t-test.

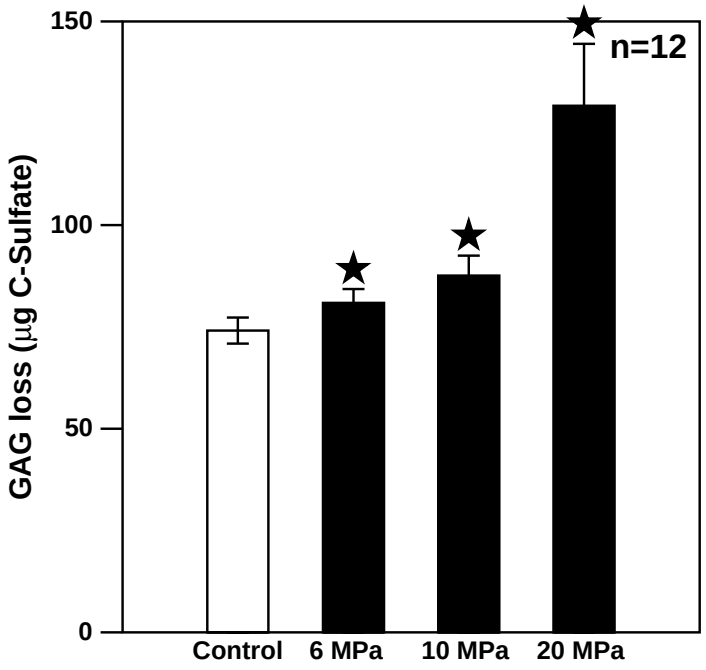

Figure 3-12: The total sGAG lost to the media by day 4 following injurious compression on day 0 is shown for different levels of injurious compression. Data are mean±SEM; $\star$ indicates $p < 0.05$ by paired t-test.

measured using disks subjected to 0, 6, 10, and 20 MPa peak stress (Fig: 3-12). A small but significant increase in cumulative sGAG loss at four days was observed in both the 6 MPa and 10 MPa peak stress loading conditions. Not only did all three stress values show significantly increased sGAG loss compared to free-swelling controls, but all three groups were significantly different from each other, again showing a clear dose-dependency.

In a parallel experiment, the use of the general caspase inhibitor Z-VAD-fmk and the SmithKline Beecham manufactured inhibitor SB-279885 failed to significantly reduce the amount of sGAG lost to the media for an injurious compression of 20 MPa peak applied stress (Fig: 3-13).

3.2.1.3 Nitric Oxide Release

Since nitric oxide (NO) has previously been shown to induce apoptosis in chondrocytes [7], levels of nitric oxide production were measured to assess whether NO was a component of the transduction pathway associated with injurious compression. Looking at the cumulative

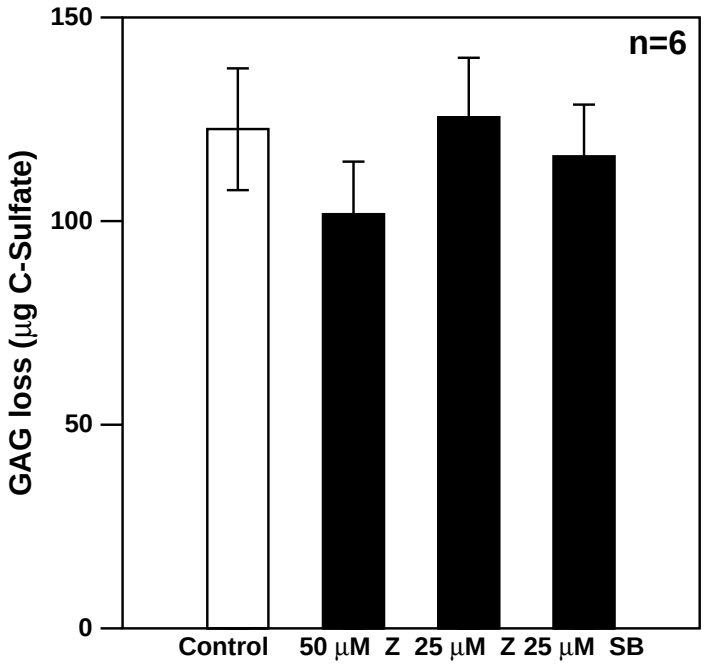

Figure 3-13: The total sGAG lost to the media by day 4 following a 20 MPa peak stress injurious compression on day 0 is shown for different apoptotic inhibitors. *Z* stands for Z-VAD-fmk, *SB* stands for SB-279885. Data are mean±SEM; No changes were significant.

nitric oxide released to the media by day four of the dose response experiment of Fig: 3-12, only the most severely loaded condition presented a significant increase in nitric oxide production versus free-swelling controls (Fig: 3-14). It should be noted that the detection limit of the Griess reaction is $\sim$1 μM nitrite [66] in biological fluid, and that many of the samples were close or even below this level. Therefore, the possibility of finite NO production at the 6 and 10 MPa levels, but below the detection limit of the assay, remains.

The accumulated NO levels were also measured in the conditioned media for an experiment involving the use of the general caspase inhibitor Z-VAD-fmk and the SmithKline Beecham inhibitor SB-279885 (Fig: 3-15). The groups in this experiment were cultured in different inhibitors and all exposed to a 20 MPa peak stress injury. The cumulative NO release as of day 4 shows a non-significant (p=0.13) trend toward decrease for the 25 μM SB-279885 condition, but all other differences were not significant.

The NO levels from spent media taken from the cytokine experiment (see section: 3.1.1.3) were also assessed for nitrite content and showed levels of NO that were

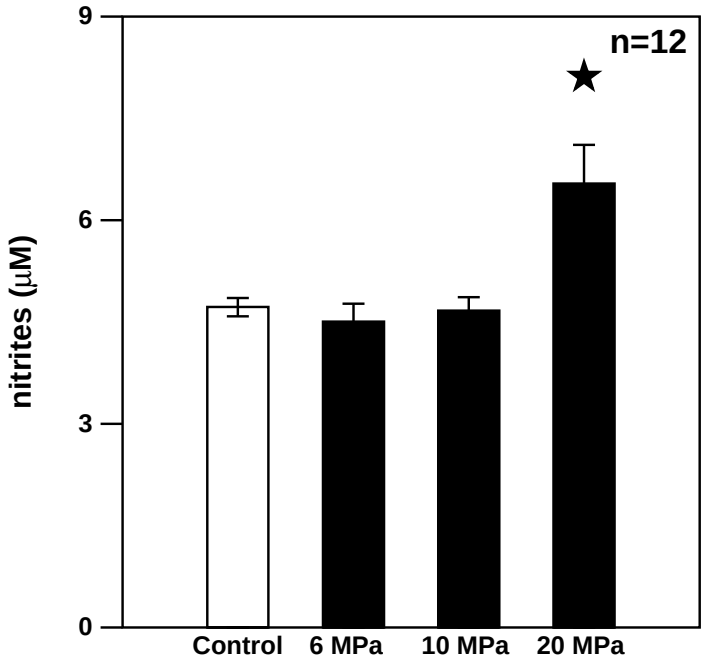

Figure 3-14: The total nitrite found in the media by day 4 following injurious compression on day 0 is shown for different levels of injurious compression. Data are mean±SEM, $\star$ indicates $p < 0.05$ by paired t-test.

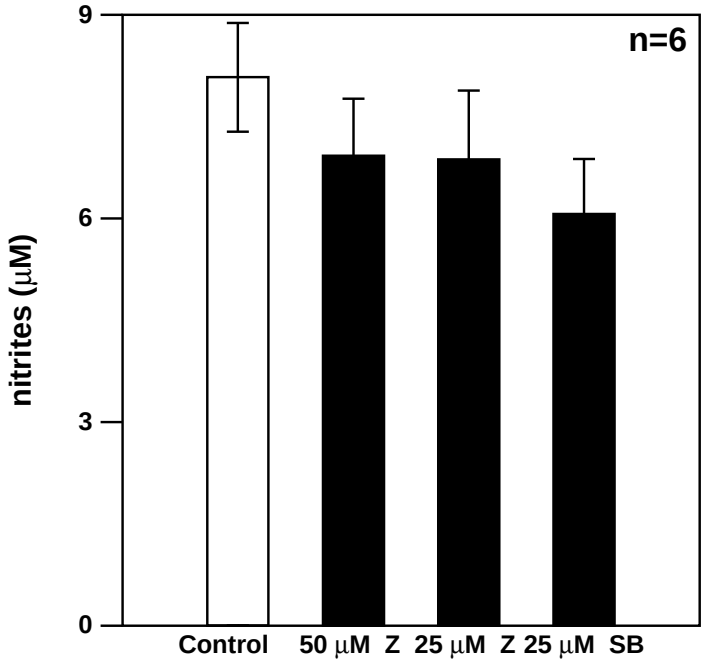

Figure 3-15: The total nitrite found in the media by day 4 following a 20 MPa peak stress injurious compression on day 0 is shown for different apoptotic inhibitors. *Z* stands for Z-VAD-fmk, *SB* stands for SB-279885. Data are mean±SEM; 25 μM SB showed a non-significant (p=0.13) trend toward decrease.

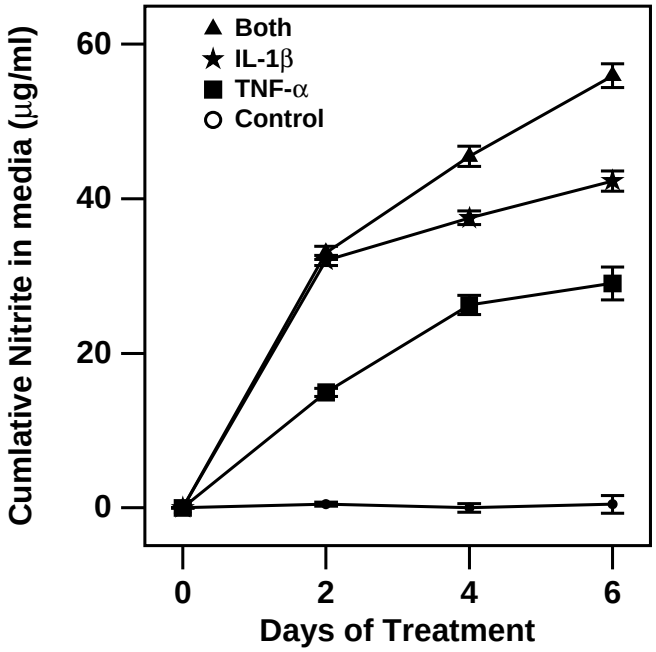

Figure 3-16: The cumulative release of nitric oxide into the media is shown for disks treated with 100 ng/ml TNF-α, 100 ng/ml IL-1β, both, and anatomically matched controls. Data are mean$\pm$SEM, n=12,12,8,4.

40-70 times that of control disks for both TNF-α and/or IL-1β (Fig: 3-16).

Chapter 4

Discussion and Conclusion

4.1 Apoptosis Findings

The presence of nuclei staining positive for apoptosis via TUNEL demonstrates that injurious mechanical compression can induce chondrocytes to undergo apoptosis in articular cartilage. This effect was observed to be dose-dependent, with detectable increases beginning at 4.5 MPa and close to 50% of chondrocytes staining positive at 20 MPa. Previous studies of cartilage explants wounded by cutting [94, 99] have shown that cartilage tissue assayed via TUNEL for apoptotic chondrocytes began to display positive staining of cells as soon as 10 minutes following injury, showed a maximum staining at 2 days post-injury, and retained positive staining cells for at least 20 days. These findings should also be representative of *in vivo* studies, as articular cartilage does not possess phagocytic cells. In light of this evidence, a detection window for apoptotic chondrocytes does not appear to exist, and the analysis of injuriously compressed tissue at 4 days post-injury would not be expected to be confounded by artifactual loss of apoptotic cells.

Preliminary results indicate that mechanically induced chondrocytic apoptosis is not inhibited using the non-specific caspase inhibitor Z-VAD-fmk. This suggests that chondrocytic apoptosis following injurious compression may proceed via a non-caspase dependent mechanism, such as a mitochondria related pathway. Experiments involving

chondrocytes isolated from growth plate tissue have demonstrated that the expression of the mitochondria associated anti-apoptotic protein Bcl-2 is reduced in cells subjected to serum withdrawal and retinoic acid [26]. A similar response may be occuring in injuriously compressed cartilage.

Currently, all assessment of apoptosis in this thesis has been done using the TUNEL assay. While the TUNEL assay is generally considered to be a reasonable measure of apoptosis, it does have the possibility of staining necrotic DNA [33]. It can be imagined that DNA from necrotic cells, while not condensed and no longer bound inside of a nuclear membrane, may be insufficiently degraded to diffuse out of the lacuna into the ECM and give rise to false positive signals. Additionally, the failure of caspase inhibitors to prevent apoptosis could just as easily be explained by necrotic cell death as a mitochondrial pathway. Without electron-microscopy (EM) studies to look at the cell morphology (the definitive test of apoptosis) and DNA laddering via agarose gel electrophoresis, the most convincing supporting evidence of chondrocytic apoptotic cell death is other studies showing apoptotic chondrocytes in similar conditions [94, 99, 20] that have used EM, TUNEL, and Annexin V staining.

4.2 Viability Findings

Vital dye staining of injuriously compressed cartilage tissue yielded results that closely followed those of the apoptosis studies. In most cases the viable and non-viable cells were interspersed among each other in a fashion similar to that found in previous studies [81]. Viability results were consistent with a previous study on calf cartilage tissue [81] but were reduced at peak stresses lower than what was needed to reduce viability in young (16-20 month) bovine tissue (0.2 J, drop tower injury) [54] and adult human tissue (20 MPa, strain of 25%, strain rate of 500/s) [83]. A time course study looking at vital dye staining of 20 MPa injuriously compressed tissue as a function of time following compression showed no significant changes between directly after, one day, two days and six days after compression. This result again validates the stability of non-vital cells inside of the ECM, and

it also points out that much shorter post-incubation times than the current four days could likely be used. The correspondence between the vital dye staining and the TUNEL labelling results indicate that the apoptotic cells are most likely staining as red by the time of analysis. Whether apoptotic chondrocytes will stain green, green and red, or red with ethidium bromide(red)/fluorescein diacetate(green) is currently unknown, but it will depend on how long it has been since the apoptotic event has occurred. From these results, it would appear that apoptotic chondrocytes begin to stain exclusively red before the end of the compression, and vital dye staining has the potential of serving as an effective primary assay for analyzing new conditions within this injury model.

4.3 Changes in Biochemical Properties

Wet weight increases and sGAG loss both increased in a dose-dependent manner. The sudden increases in tissue wet weights that were observed following injurious compression (within 1 day) indicate collagen network damage from the physical trauma [81] rather than cell-mediated proteolysis. The increased sGAG release rates, observed for two to three days following the more severe compressions, are also consistent with collagen network damage. The increase in sGAG release can be at least partially attributed to increased proteoglycan diffusivity due to the greater effective pore size of the damaged collagen network [55].

Previous researchers have found evidence for a nitric oxide (NO) related pathway in chondrocytic apoptosis [7, 45]. NO release from injuriously compressed tissue was elevated from control at the 20 MPa peak stress compression level but was very close to the detection limit of the assay and still far below the NO levels induced using either TNF-α or IL-1β. While these results did not rule out an NO mediated pathway at this time, they do not lend much weight to this hypothesis.

4.4 Conclusions

In an effort to understand the conditions under which apoptosis occurs in articular cartilage, an *in vitro* model system was developed to study chondrocyte apoptosis induced by injurious compression of articular cartilage. The apoptotic response corresponded well with other markers of tissue damage, including tissue swelling, sGAG loss, and vital dye staining. Interestingly, this apoptotic response was detectable under loading conditions (4.5 MPa peak applied stress) below what was need to produce detectable changes in viability (10 MPa), sGAG loss (6 MPa) and wet weight (13 MPa). Therefore, the threshold mechanical loading responsible for induction of chondrocyte apoptosis may not necessarily be the same as for damage of the ECM.

The finding of increased numbers of apoptotic cells in OA tissue [59, 6, 42] indicates a possible role for aberrant apoptosis in the pathogenesis of OA. At what point this role would come into play is currently unknown. The present results indicate that mechanical compression alone is sufficient to induce chondrocyte apoptosis in articular cartilage, and this leads to the interesting hypothesis that injurious joint loading could cause chondrocyte death even in the absence of other observable changes to the tissue. This apoptosis mediated cell loss could then lead to the remaining chondrocytes being too few in number to counter the normal catabolic metabolism of the ECM, resulting in subsequent degradation of the tissue into OA [1]. Conversely, fibrillation of the cartilage tissue exposes the chondrocytes to non-physiological levels of mechanical stress and would also lead to apoptosis. In both cases, the induction of apoptosis could be ascribed to mechanical compression, but in the second case apoptotic chondrocytes come about as a secondary result of OA and are not the primary cause.

The stresses that were applied to the articular cartilage tissue disks in this thesis matched the range of physiological stresses felt by articular cartilage *in vivo* (0-20 MPa) [48]. However, other studies have noticed that removal of cartilage from bone has an amplifying effect on tissue damage [54], and the removal of the superficial layer will also expose the tissue to greater damage. Since the stress levels in this injury model do

not map directly to physiologic stress levels, it is difficult to distinguish between the two hypotheses presented for the *in vivo* findings of apoptotic chondrocytes in OA tissue from the *in vitro* data presented in this thesis. One advantage of the injury model developed in this thesis is that it is a pure cartilage system, and the effects of non-chondrocytic cells do not need to be accounted for.

The biological pathway through which articular chondrocytes are induced to undergo apoptosis is currently unknown, but several hypotheses have appeared in the literature including binding of CD95 [44], elevated levels of NO [6, 7], and loss of extracellular matrix survival signals [42, 45]. This last hypothesis is the most consistent with a mechanical origin of the initial apoptosis inducement signal, as a mechanical insult could cause the chondrocytes to be detached from these survival-promoting ECM signals. An alternative hypothesis that is also consistent with a mechanical origin and the lack of caspase inhibitor effects is mechanically induced mitochondria damage. In many ways, mitochondria act as stress sensors for cells, and mechanical damage to the mitochondria could cause release of cytochrome c into the cytosol and/or interfere with the normal anti-apoptotic ability of Bcl-2.

4.5 Future Experiments

The full potential of the *in vitro* cartilage injury model developed in this thesis is not close to having been reached. Many open ends remain, and every answer asks many more questions.

- A confirmatory experiment needs to be done to verify the results of the TUNEL assay for this cartilage explant system. Agarose gel electrophoresis to look for DNA laddering (preliminary results discussed in section: D.3) or electron microscopy to look for characteristic changes in morphology would serve as conclusive checks of the validity of the TUNEL assay.

- The biological pathway along which the apoptotic process propagates in injuriously compressed articular cartilage has not been identified. Although caspase activity is

generally studied in cell culture systems, quantification of caspase activity in this tissue culture system, if technically possible, would provide valuable insights into the mechanism and propagation of the apoptotic response. Caspase inhibition studies in this thesis have shown no effect, but other researchers have found that caspase inhibitors, specifically Z-VAD-fmk [20], prevented apoptosis in injuriously compressed cartilage. Further experiments with higher concentrations of Z-VAD-fmk and other inhibitors should be attempted. Finally, looking for cytochrome c and/or Bcl-2 might provide information on whether this apoptotic response is proceeding via a mitochondria regulated pathway.

- The current method for detection of apoptotic nuclei is time intensive and does not readily provide a quantitative number. Other methods for apoptotic analysis, such as TUNEL analysis via flow cytometry D.1, would be useful and should be developed.

- The current injury model, while useful, is not directly physiologically relevant. Cartilage deformation upon loading of intact joints is not directly comparable to either unconfined or confined compression but is somewhere inbetween. Applying confined or unconfined compression to full thickness cartilage-bone cores would be more physiologically relevant due to the intact superficial layer and support provided by the underlying bone. Additionally, the peak stresses generated in such an experiment would correspond more closely to the stresses generated in the physiological condition and in osteochondral autograft surgeries.

- Finally, the injury model has not yet been used in any real capacity to examine the effects of tissue injury on possible degeneration of cartilage tissue into OA. Many experiments using this injurious compression model can be envisioned, including examining the role of matrix metalloproteinase (MMP) activity using techniques such as immunocytochemistry or Western blotting and looking for gene (up and down) regulation using techniques such as differential mRNA displays and Atlas blotting.

Appendix A

The Incustat and its Controller

A.1 Introduction

Previous compression studies in this lab have made use of dynamic mechanical spectrometers (dynastats) or static compression chambers (Fig: A-1) for the mechanical loading of cartilage tissue. While the dynastats provide extremely accurate and precise dynamic movement, their large size makes them impractical to maintain inside of a sterile environment and therefore limits dynamic loading experiments to short time spans. The static chambers, on the other hand, can be autoclaved and used inside of sterile incubators, but they are not as accurate and cannot provide true dynamic loading.

The solution has been to construct a miniature dynastat that can fit inside an incubator (hence, incustat, also called the CA2000) (Fig: A-2). This apparatus was originally conceived so as to allow for dynamic compression experiments longer than one day (experiments in which the use of dynastats would have created a serious risk of infection). The machine has also proven extremely useful for the application of the injurious compression protocols used in this thesis, as it has the ability to apply a controlled and monitored mechanical load to cartilage tissue within a sterile environment, thereby allowing for post-compression culturing.

The incustat (Fig: A-3) was constructed by Dr. Eliot Frank and consists of a high-

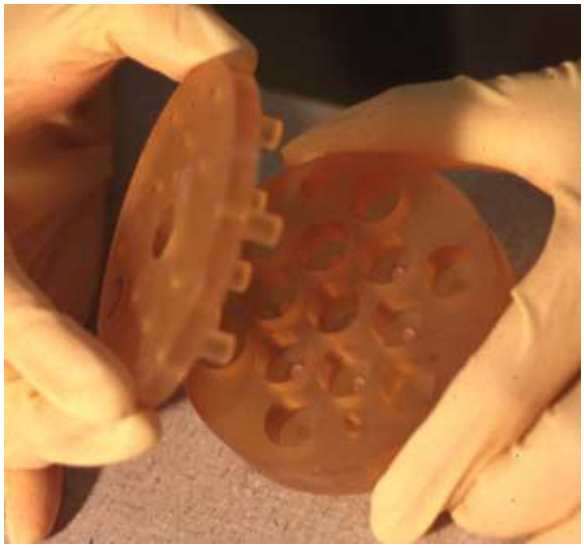

Figure A-1: A typical static compression chamber. These chambers have been used in both static loading experiments and previous injurious compression experiments. Note the hole in the center of the chamber through which the LVDT passes.

precision stepper motor connected through a worm gear to a loading frame, allowing the loading frame to move up and down so as to apply load to a polysulfone chamber containing the cartilage disks. The chamber used is identical to the ones used for static loading experiments (Fig: A-1). A load cell is connected between the chamber top and the loading frame, and measures the applied load. A linear velocity displacement transformer (LVDT) is connected between the loading platform and the load cell, going directly through the center hole of the compression chamber (see Fig: A-1). This arrangement allows direct measurement of the thickness of the chamber and side-steps some of the problems encountered with machine compliance.

A.2 Non-linearities

As built, the machine suffered severe performance problems arising from backlash in the motor train. This nonlinearity was unaccounted for in the original feed-forward control design and was only partially compensated for by the later addition of springs. Besides not fully correcting the problem, the springs limited the range of the device and more importantly for injurious compression experiments, reduced the maximal load that could

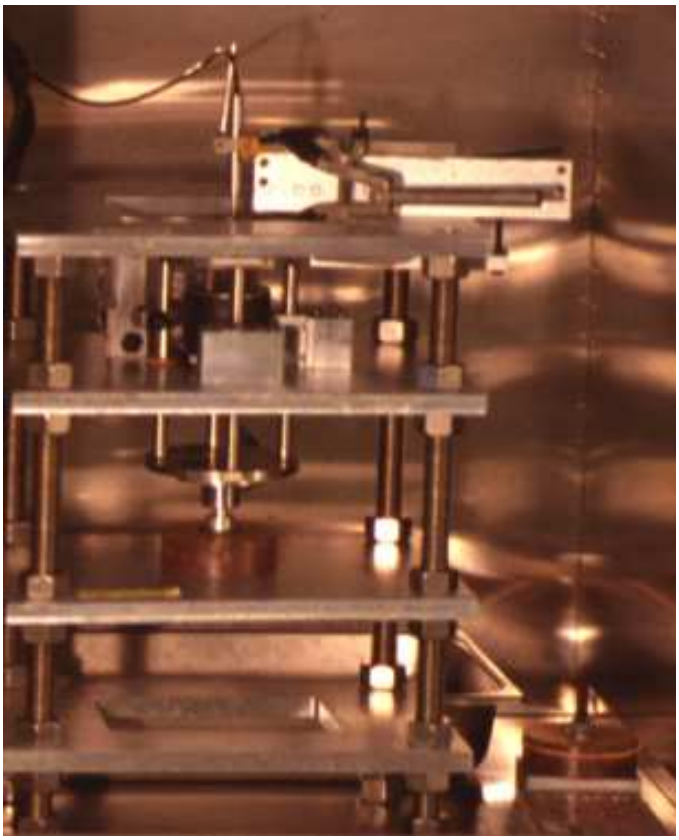

Figure A-2: The incustat machine inside a standard cell culture incubator. The chamber in the machine is being compressed. The chamber to the right of the incustat is being used as a static control.

be applied to tissue samples.

A.3 Feedback Compensation

A better solution than the use of springs in the gear train is feedback compensation to eliminate the system's nonlinearities (Fig: A-4). This feedback was originally accomplished through software control, and a further improved hardware implementation of the feedback loop has been built and incorporated into the current design (CA2000, Fig: A-6) and the second generation (CA2001) incustat machines. A schematic of the feedback loop is shown in Figure: A-5.

The feedback allows the full loading capabilities of the machine to be used in in-

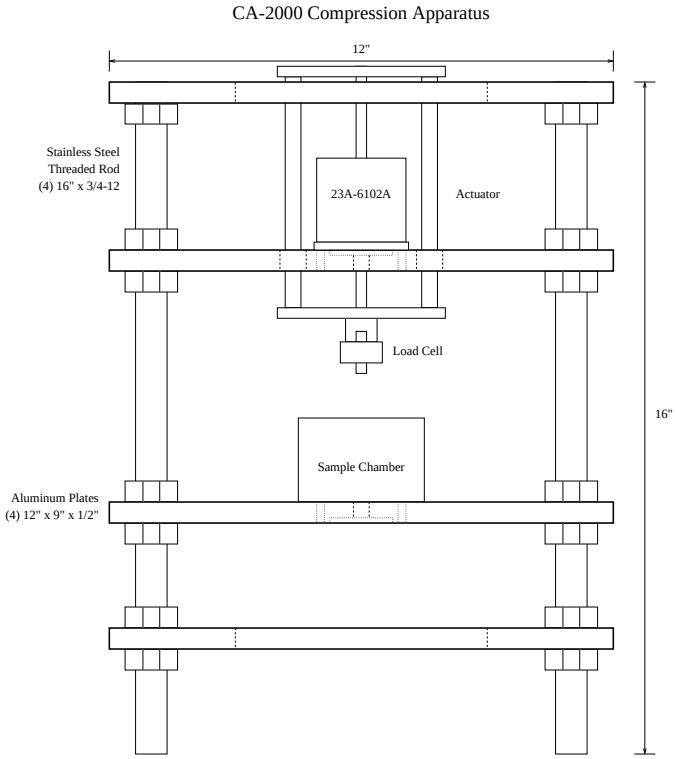

Figure A-3: Schematic drawing of the incustat showing stepper motor, loading frame, load cell, and the compression chamber. The displacement transducer (not shown) is positioned between the load cell and the plate the sample chamber rests on, passing through the center of the compression chamber.

jurious compression experiments by eliminating the need for springs in the design. The maximum load of the machine has been further increased by the removal of a 35 kg hardware cut-out, allowing the machine to induce loads up to the stepper motor stalling level of $\sim$45 kg. Additionally, the feedback improves performance sufficiently that the rate of compression can be precisely controlled and sinusoids at any frequency can be imposed for the purposes of dynamic compression experiments.

The feedback control scheme in both the hardware and software version is a simple proportional compensator. Solving for the transfer function of the feedback system in Figure: A-4 yields:

$$\frac{Y(s)}{X(s)} = H(s) = \frac{K_1 K_2 H_1(s)}{1 + K_1 K_2 H_1 H_2(s)} \tag{A.1}$$

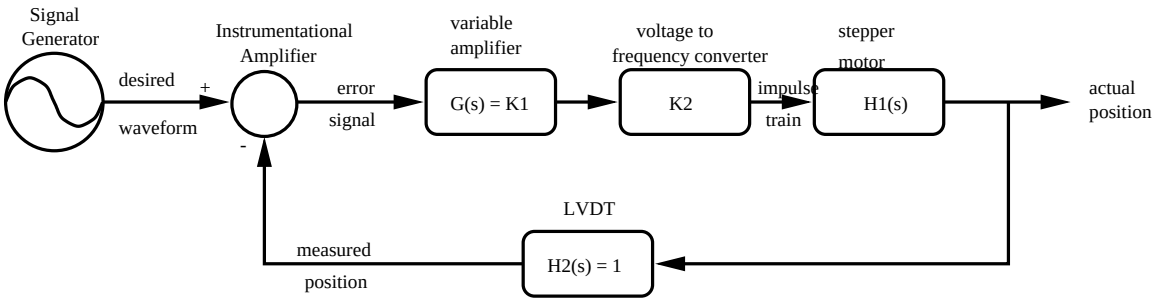

Figure A-4: Diagram showing the basic components of the hardware feedback scheme. H_2 is assumed to be linear, and a proportional gain is used for the amplifier G.

where $H_1(s)$, representing the transfer function of the stepper motor, is not known, but can be expected to be nonlinear, $H_2(s)$, representing the LVDT, is approximately unity, and K_1 and K_2, the 2 points of feedback adjustment, are assumed to be proportional and can be combined as one gain, K.

To linearize the system as a whole, K is increased, which allows the system transfer function H(s) to go to 1. Empirically, it has been found that to maintain stability in the software case, the gain K must be set to less than unity. This limit on stability arises from the non-linear delays involved in data acquisition, software computation, and data output. In the hardware feedback case, the delay in the system is essentially non-existent and an upper limit on stability for K has not been reached.

A.4 Software Issues

The hardware feedback implementation for controlling the incustat has demonstrated very satisfactory results. However, there are currently several issues with the available software for controlling the incustat machine that makes full use of the machine's capabilities slightly more complicated.

Briefly, the "Incustat Controller" program is currently at version 1.5 and does an adequate job of running scripts and saving and displaying data. The program does not make use of the hardware feedback electronics and uses only software feedback to control the machine, making it unsuitable for higher frequency sinusoidals ($>$0.1 Hz). Additionally,

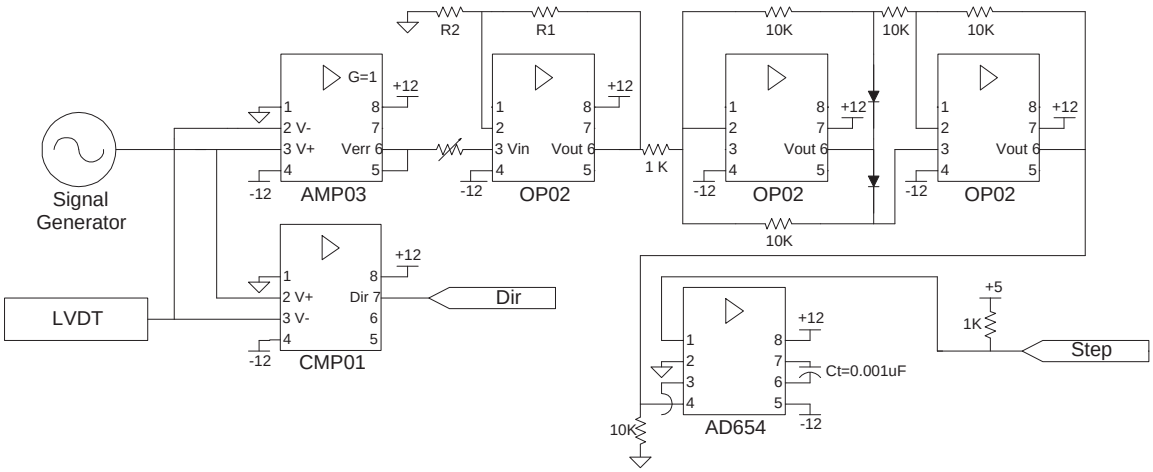

Figure A-5: A Schematic of the hardware feedback circuit. The *AMP03* is the instrumentational amplifier used for generating the error signal. The *CMP01* is a simple comparator and provides the directional bit for the stepper motor. The error signal is amplified with the first *OP2* and then rectified with the next two *OP2's*. Finally, the rectified amplified error signal is converted to a pulse sequence with the voltage controlled oscillator chip *AD654*.

the program, while simple, has some usability issues, such as sinusoids needing to be done at a DC level of 0 for optimal resolution, which requires manual zeroing of the LVDT to the desired DC level.

There is an alpha level version 2.0 "Incustat Controller" that is approximately 80% complete that was to incorporate both open and closed loop control, with both hardware and software feedback, but development of this software was dropped leaving the program in an unusable state when "Cassp" version 8.8 incorporated hardware feedback control.

"Cassp", while the most full-featured of the three programs and the only one not to be written in Labview (a good thing), has several problems that still need to be addressed. The DC level of sinusoids have a habit of drifting with time under "Cassp", which has led to quite a few ruined experiments. Additionally, due to a design "feature" of the voltage-controlled oscillator chip in the hardware feedback loop, the hardware feedback loop stalls if the error signal goes over 1.5 V, a common occurrence in injurious compression experiments. "Cassp" has no mechanism for recovering from such an occurrence, which limits the program's usefulness for injurious compression protocols. Finally, "Cassp" provides

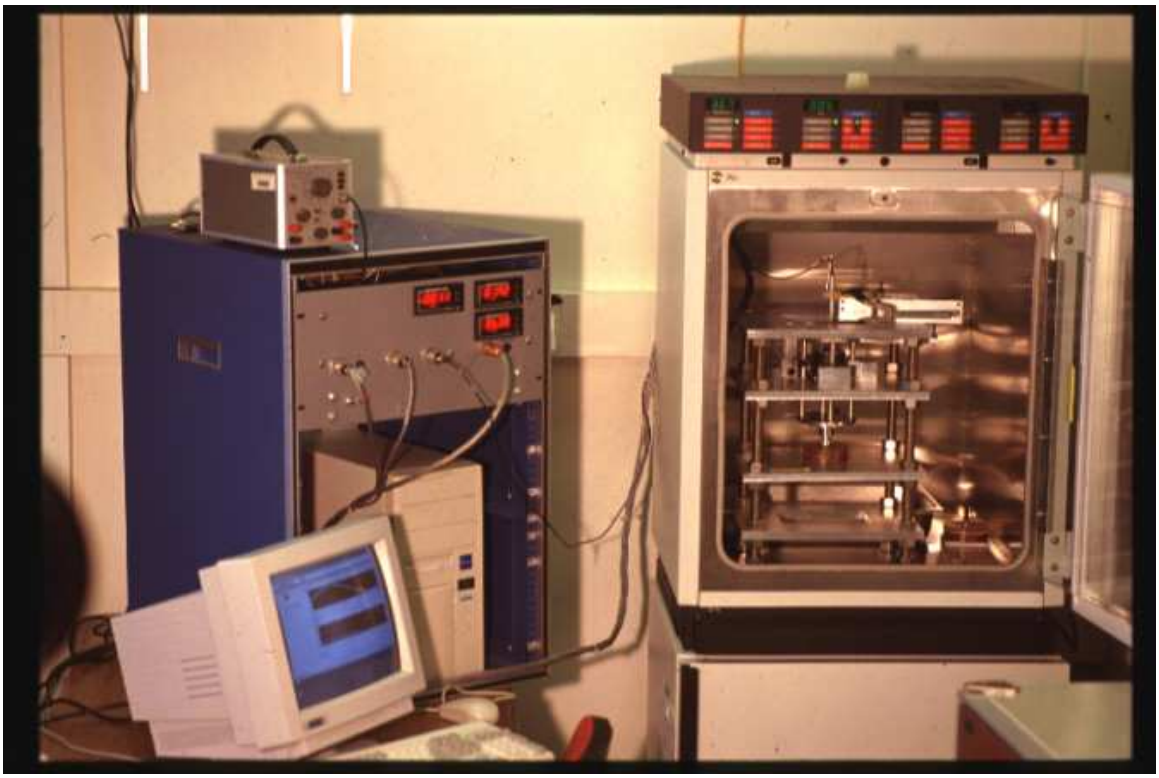

Figure A-6: The incustat within its incubator along with the controlling computer and electronic hardware. This is an old picture taken when an actual signal generator was used to drive the hardware feedback circuitry in dynamic compression experiments.

few mechanisms for viewing what is being done to the tissue in real-time.

Since the problems in "Cassp" are real show-stoppers, and the problems with version 1.5 of the "Incustat Controller" are only usability and performance annoyances, the "Incustat Controller" program has been used for all injurious compression protocols in recent history. The problems in "Cassp" should, however, be fixed shortly and it is anticipated that "Cassp" will be the only controlling software package maintained and used sometime in the near future.

A.5 Calibration Procedures

Calibrating the incustat is more of an art of approximation then engineering. Several of the factors that make precise calibration difficult include: (1) the compressibility of the polysulfone chambers, (2) the aluminum plates on which the chamber sits and the aluminum plate the stepper motor is bolted to are not parallel, (3) machine compliance, due to the "threaded rods and bolts" construction and choice of materials, and (4) tissue swelling. While these factors make knowing exactly what you are doing to the tissue difficult, consistent loading of explant tissue between different experiments and therefore consistent results can be obtained by strict adherence to the following guidelines.

1. Use tissue that is between 1 and 2 days old. Cartilage tissue swells over time during explant culture, so using the tissue soon after performing the explant minimizes variability due to swelling. It also allows the use of a measured thickness at the time of cutting to be used to offset the variability in thickness arising from the explant sectioning process.

2. Calibrate the incustat so that 1 kg of load on the polysulfone chamber after stress-relaxation corresponds to a displacement of 0 μm. Since the wells of the compression chambers are 500 μm deep, in a perfect world 0 μm displacement on the machine would correspond to 50% compression of a 1 mm thick cartilage disk (not the case, see below).

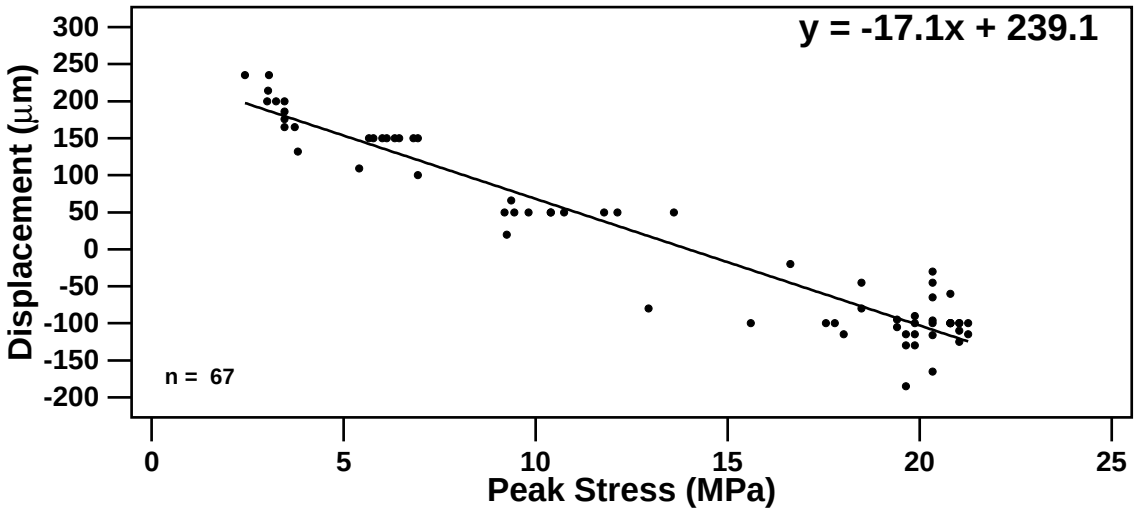

Figure A-7: Displacement is shown as a function of peak stress. All data comes from 1-2 day old tissue compressed in the incustat using the described calibration procedure. In the fitted equation, x represents the desired peak stress and y the appropriate displacement.

One may note, as an example of the combined effects of the chamber compressibility and machine compliance, that the difference between 1 kg of load on the empty polysulfone chamber and 10 kg of load is around 100 μm. Therefore, for repeatability, it is very important that zero should always correspond to the somewhat arbitrary 1 kg of load on the chamber.

3. Examine Figure: A-7 to calculate the strain needed for the desired peak stress.

From examining Figure: A-7, one can see that compressing below the zero point is necessary for higher level loading. While at first non-intuitive, one must keep in mind that the offset load of 1 kg during calibration is fairly arbitrary, and zero does not correspond to compressing the disk to 500 μm because of the previously mentioned problems with the incustat and the chambers. In fact, when compressed to -100 μm using this calibration scheme, the load is only around 10 kg due to compressibility and compliance.

Another important thing to realize is that in all experiments to date, any effects of the chamber on the load reading have been ignored for the calculation of peak stress. The main reasons are that the polysulfone chambers have their own stress-relaxation times, and at the higher loads, the peak stress is often achieved before arriving at the final strain level,

both of which make calculating the effects of the chamber on the peak stress difficult.

Other things to worry about include using the “Greg Allen” chambers (500 μm deep well divets) and avoiding the “Tom Quinn” chambers (100μm deep well divets). In the future, the “Tom Quinn” chambers might be preferable, due to their ability to compress a 1 mm thick cartilage disk to more than 50%, but at the present, “Greg Allen” chambers have been used and should continue to be used for consistency.

While there are problems with the current calibration procedure, adherence to the current protocol will allow for repeatable results. In the future, several changes should be made to enhance the repeatability of experiments. Use of the new incustats (i.e. version 2001) should avoid some of the mechanical compliance problems due to their more rugged construction. Further, use of stainless steel chambers would reduce the compressibility problems of the current chambers. Finally, updates to “Cassp” should allow for hardware feedback to be used in injurious compression experiments and further remove problems with non-linearities.

Appendix B

Quantitative Analysis of Ethidium Bromide and Fluorescein Diacetate Stained Cartilage Tissue Sections

B.1 Introduction

When running experiments using tissue or cell culture systems, the viability of the cells is a parameter of great interest. In most cases, such as checking that cells are alive before beginning an 8 week metabolic experiment, a qualitative assessment of the viability is more than sufficient. In certain experiments, however, a quantitative analysis of the cell viability is desirable. An example of this would be animal models and tissue systems used for studying osteoarthritis, such as in this thesis, where the effect of mechanical insult on the viability of the chondrocytes needs to be assessed and correlated to the level of damage.

There are many ways to measure cell viability. As the relative advantages and disadvantages of all these different methods are outside the scope of this thesis, the interested reader is referred to the Molecular Probes web page for further information. Image enhancement will be applied using the Ethidium Bromide (EtBr) and Fluorescein Diacetate (FDA) method, better known as the red/green assay [2, 87].

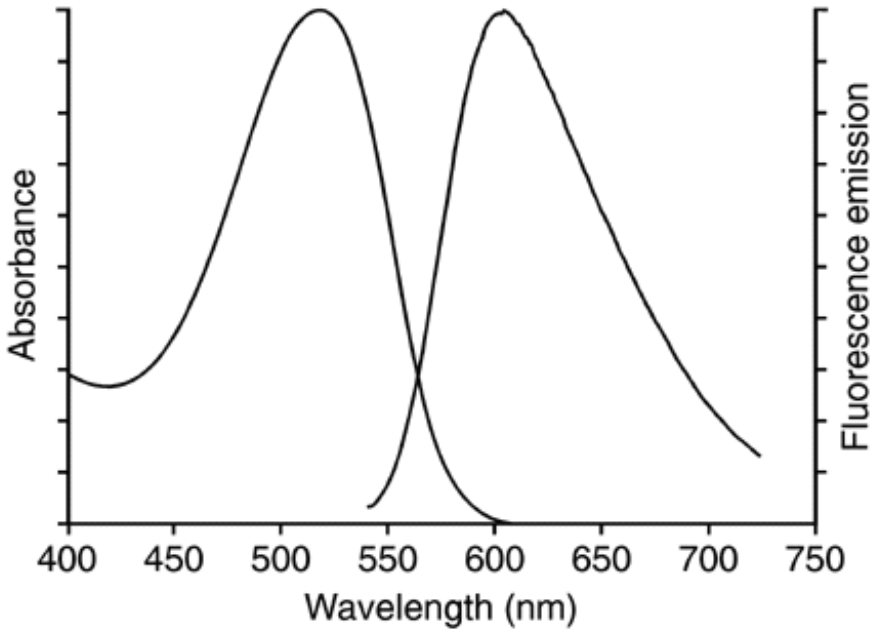

Figure B-1: Excitation and Emission Spectra of intercalated Ethidium Bromide. The excitation peak is $\sim$510 nm, the emission peak is $\sim$ 610 nm.

In this method, either cells or thin sections of tissue are immersed in a solution containing EtBr and FDA. EtBr cannot diffuse through the cell membrane of viable cells and only diffuses through the cell and nuclear membranes of non-viable cells. Once in the nucleus, EtBr intercalates with the chromosomal DNA, enhancing fluorescence 30-40 fold and shifting the excitation maxima $\sim$3040 nm to the red and the emission spectra $\sim$15 nm to the blue. At an excitation of 490 nm, bound EtBr has an emission maxima at $\sim$610 nm (Fig: B-1). FDA, in contrast, diffuses into all cells. However, only viable cells contain active lipases, which break FDA down into fluorescein. Fluorescein has an excitation/emission maxima of $\sim$494/520 nm (Fig: B-2).

In short, under a fluorescent microscope using the appropriate filters, the nuclei of dead cells will fluoresce reddish-orange, while live cells will fluoresce green.

There are several major problems with this method. First, fluorescein leaks out of cells, creating a background green fluorescence that rises rapidly with time. This is especially apparent with tissue sections, where the slide may be intelligible for less then 2 minutes. Second, fluorescein exhibits photo-bleaching, which takes place on a time scale

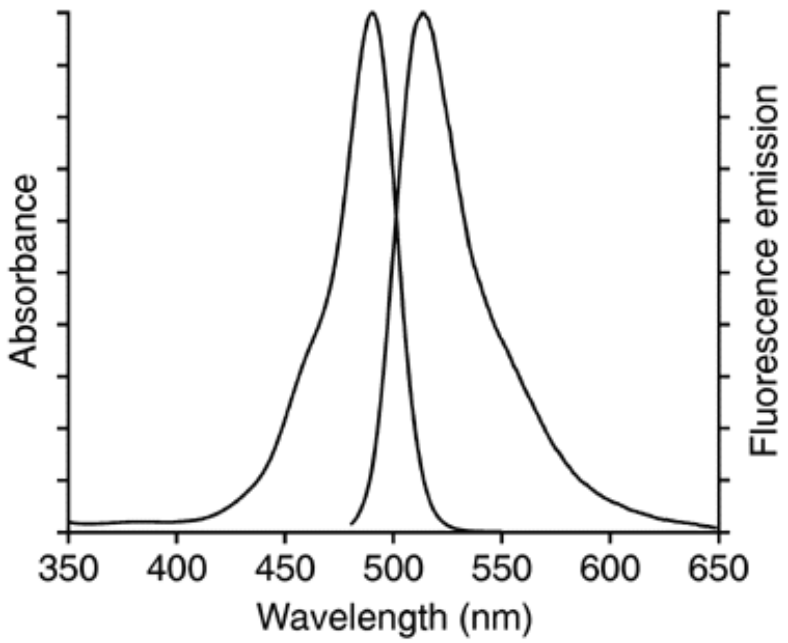

Figure B-2: Excitation and Emission Spectra of Fluorescein. The excitation peak is ∼490 nm, the emission peak is ∼ 520 nm.

of tens of seconds at higher magnifications. Third, the EtBr staining is concentration dependent, and at high concentrations EtBr will also diffuse into viable cells. Nevertheless, this method is still quite popular for two main reasons. First, the results are vivid and easy to quickly interpret. Second, and far more importantly, EtBr and FDA are astoundingly cheap (The total cost of the EtBr and FDA used in an average experiment is on the order of 40 μ\$).

There are two products put out by Molecular Probes that may be of interest for those looking to measure viability. The first, calcien AM, behaves quite similarly to FDA, with the added advantage that it has a relatively high cellular retention, reducing background fluorescence greatly. Ethidium homodimer is similar to EtBr but binds to DNA about 1000 times stronger than EtBr. Currently, both products are expensive enough to prohibit them from casual lab use. Additionally, work by Greg Allen has demonstrated that calcien AM has an extremely slow diffusion time compared to FDA.

The goal of this project will be to process images taken of EtBr/FDA stained tissue sections to improve the intelligibility of the images and to facilitate quantification of cell

viability. To achieve this, several issues need to be addressed:

1. The images contain high levels of background staining from unbound EtBr and fluorescein that has diffused out of cells.

2. The tissue sections are extremely thick (100-200 μm), so only a fraction of the cells will be in focus, the rest adding background noise.

3. The variability in image intensity varies greatly from slide to slide. This variability arises mainly from differences in the thickness of sections and in the amount of time between immersion in the EtBr/FDA solution and viewing the slide.

B.2 Methods

All cartilage tissue was explanted from the femoropatellar groove of freshly slaughtered calves, processed into groups of 3 mm diameter $\times$ 1 mm thick disks, and maintained in low-glucose, 10% serum-supplemented DMEM with ascorbate (20 μg/ml=.1 mM) and gentamicin antibiotic (50 μg/ml). Following an equilibration time (1-5 days), disks were subjected to an injurious compression protocol. This consisted of compressing a disk to 50-70% of cut-thickness under displacement control, holding at the compressed level for 5', releasing for 25', and repeating for a total of 6$\times$. Free-swelling disks acted as controls.

After a variable amount of time post-compression (0-6 days), small vertical sections (100-200 μm) were taken from the disks with a razor blade. The section was immersed on a slide in PBS w/ 18 μM EtBr and 150 μM FDA for $\sim$30 seconds before viewing on a fluorescent microscope. A 450-490 nm excitation filter was used with a 520 nm barrier filter on the emission. Photographs were taken immediately on ISO 100 slide film. Processed slides were scanned with a Nikon CoolScan slide scanner and saved as JPEG's. All subsequent image processing was done on SGI Indy computers using Matlab version 5.1. The images were trimmed when necessary to remove edge effects of the filtering operations.

B.3 Image Processing & Results

The basic process outlined so far is: Stain tissue with fluorescent compounds ▷ Photograph ▷ Scan the slide film ▷ Save the image ▷ Load into Matlab. This series of actions creates a system with an unknown amount of noise and distortion. The goal was to enhance the image so as to minimize the effects of this noise and distortion and facilitate quantification of the cell viability.

When scanned into the computer, the image was stored as an RGB color-indexed image. Each channel in the RGB image represented a sampled color of a different wavelength. The red, green, and blue channels represented samples at wavelengths of λ = 700 nm, 546.1 nm and 435.8 nm, respectively (Fig: B-3). However, the colors of interest from the fluorescence of DNA bound EtBr and fluorescein had peak wavelengths of 610nm and 520nm and wide spectrums that overlapped, as shown in Figures: B-1 and B-2. This meant that each of the RGB samples at λ=700 nm, 546.1 nm and 435.8 nm represented a combination of the EtBr and fluorescein spectrums. In order to process the EtBr and fluorescein components separately, the color portions of the RGB image corresponding to each chemical needed to be determined.

For any given pixel, the intensities of the red, green, and blue components depended on the relationship between the emission spectrums of EtBr and fluorescein and the absorption spectrums of the photographic film and scanning equipment. Rather than characterizing each of these spectrums, it was assumed that the intensity of the RGB components was directly proportional to the value of the emission spectra at the RGB peak wavelengths, and these values were simply read off of the graphs in Figures: B-1 and B-2.

Examining the emission spectra, it was apparent the EtBr spectrum completely dominated the red component of the scanned image, as the fluorescein had virtually no fluorescence at λ=700 nm. As a result, the red component of the image was taken to be a scaled representative of the EtBr distribution in the tissue section:

$$Red = x * EtBr \tag{B.1}$$

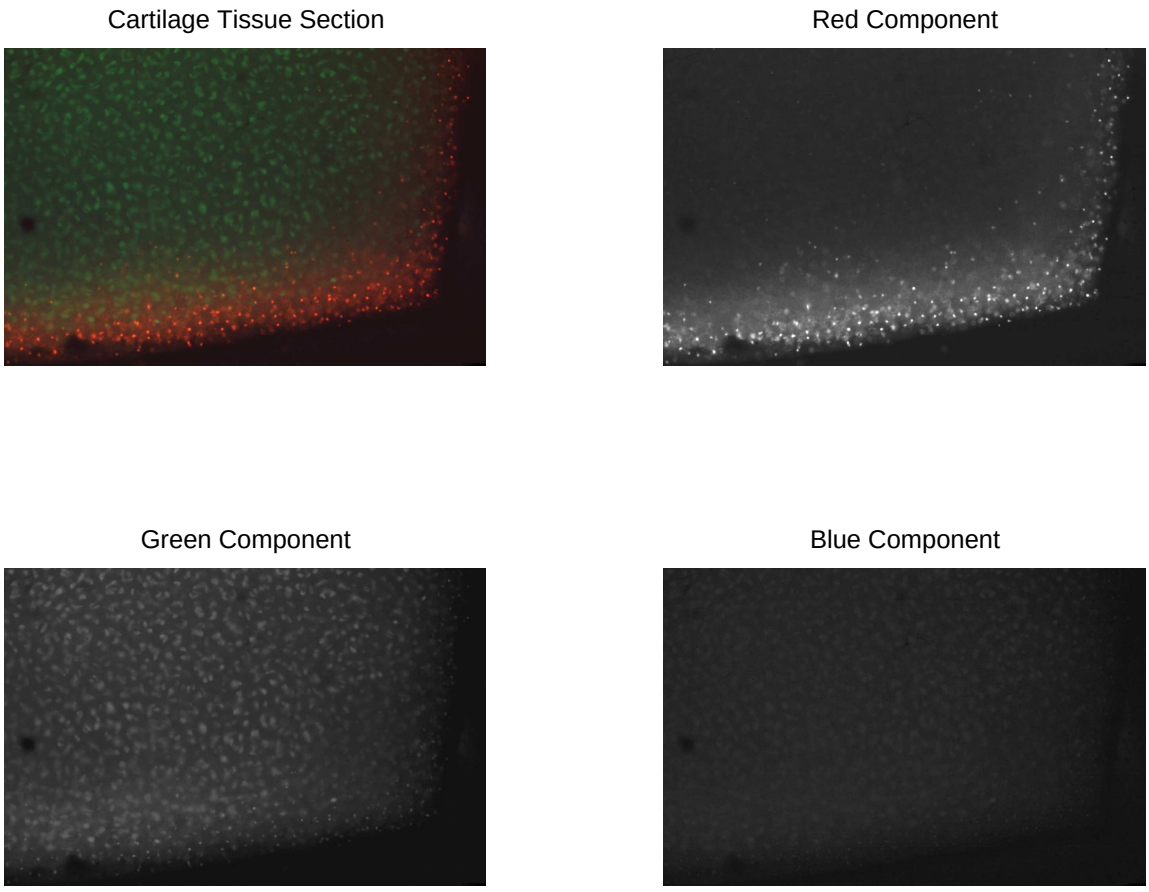

Figure B-3: The original image to be used as an example along with its red, green, and blue components.

$$0 < x < 1$$

The green component of the image, however, was at λ=546.1 nm, a wavelength at which both fluorescein and EtBr fluoresce. This meant that the green color component represented a linear combination of the light fluoresced by EtBr and the light fluoresced by fluorescein. The intensity of the green samples was modeled using the following equation:

$$Green = y * EtBr + z * fluorescein \tag{B.2}$$

$$0 < y < 1, 0 < z < 1$$

Equations: B.1 and B.2 form a linear system that can be solved to extract an image that more closely corresponds to the fluorescein component of the tissue section. For simplicity, x was chosen to be 1, as the actual magnitude of the image was not of real importance. Similarly, z was chosen as 1. The remaining constant, y, was found by examining the emission spectrum of EtBr. Continuing the approximation that the RGB components were directly related to the value of the emission spectra at the RGB peak wavelengths, the ratio of EtBr at λ=546.1 nm to EtBr at λ=700 nm was measured to be $\sim$ 0.25. Since x was chosen to be 1, this ratio was the value of y, or the relative proportion of the green image component that came from EtBr. Putting this into matrix form yields:

$$\begin{bmatrix} Red \\ Green \end{bmatrix} = \begin{bmatrix} 1 & 0 \\ .25 & 1 \end{bmatrix} \begin{bmatrix} EtBr \\ fluorescein \end{bmatrix} \tag{B.3}$$

The inverse of this equation is:

$$\begin{bmatrix} EtBr \\ fluorescein \end{bmatrix} = \begin{bmatrix} 1 & 0 \\ -0.25 & 1 \end{bmatrix} \begin{bmatrix} Red \\ Green \end{bmatrix} \tag{B.4}$$

Separating the EtBr and fluorescein components of the image was now a simple mathematical transform (Fig: B-4). Notice that the blue component was ignored when performing this transform, since its information was redundant in the model.

The process of picking distinct cells in the image could now begin. In counting cells, only the cells in a single focal plane of the cartilage section, which appear in sharp contrast in the image, were of interest. Cells from higher and lower layers that appear as low-contrast blurs in the image were ignored.

To remove the background noise that results from these blurred cells and background fluorescence, unsharp filtering was be used. Unsharp masking is akin to high-pass filtering and helped to remove background coloration while maintaining the high frequency components of the image (these should have been the in-focus cells).

The cutoff frequency of the low-pass filter was chosen so as to smooth out all in-focus cells while still passing the background coloration for a specific region. By analyzing images, it was determined that at the given level of magnification the nuclei of most non-viable cells were approximately 6 pixels in diameter. Similarly, the size of in-focus viable cells was approximately 16 pixels in diameter. Accordingly, a Gaussian low-pass filter with standard deviation $(6/2) = 3$ was chosen to smooth out the in-focus nuclei in the EtBr component, and a Gaussian low-pass filter with standard deviation $(16/2) = 8$ was chosen to smooth out the in-focus viable-cells in the fluorescein component (Fig: B-5). Both filters were chosen to be of size 21x21 as a compromise between distortion, speed, and the area of the image lost due to edge effects. The resultant smoothed EtBr and fluorescein components were then subtracted from their respective image components.

Next, the cells and nuclei from the filtered images were picked out. This entailed choosing which magnitudes of the unsharp filtered image corresponded to cells or nuclei and which are merely noise or blurred objects. Since most of the blurring had already been filtered out by the unsharp filter, simple thresholding was used to convert the 8 bit image

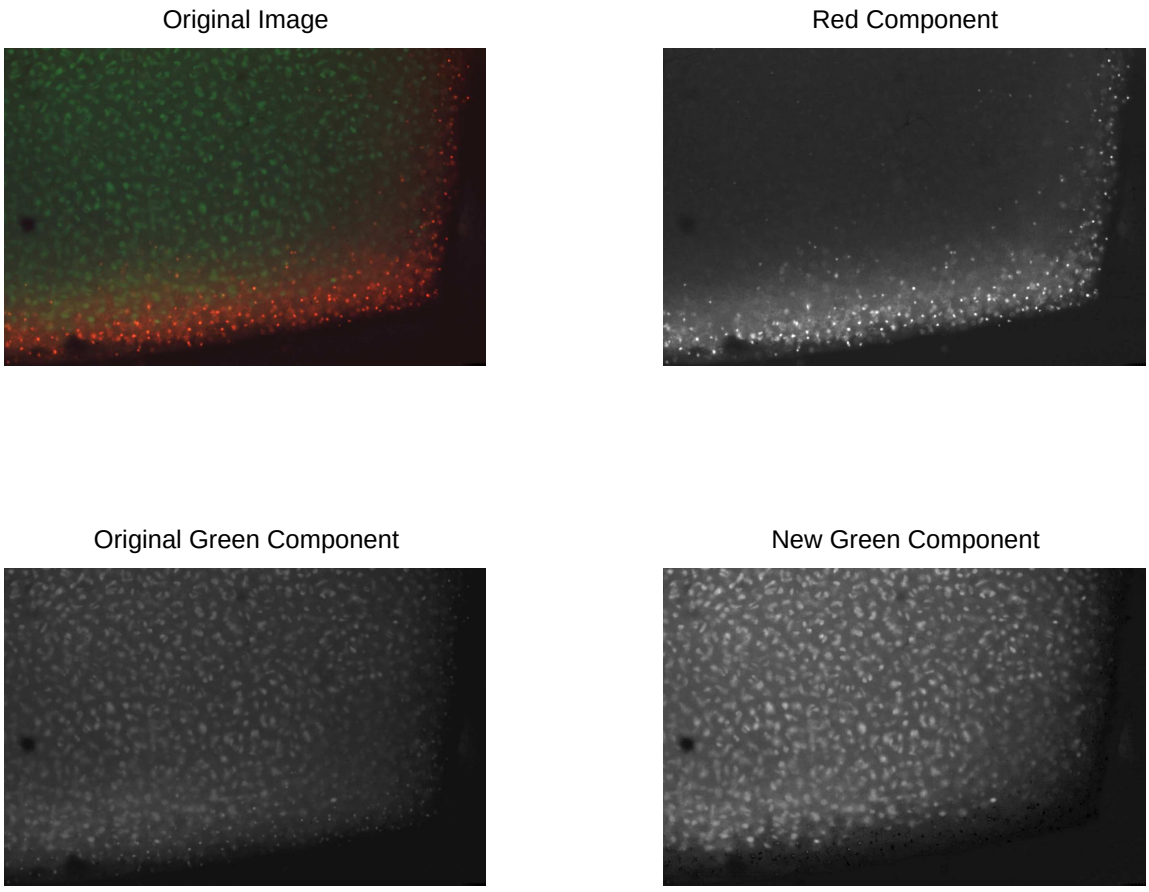

Figure B-4: The original image along with its green component, the EtBr component, and the fluorescein component.

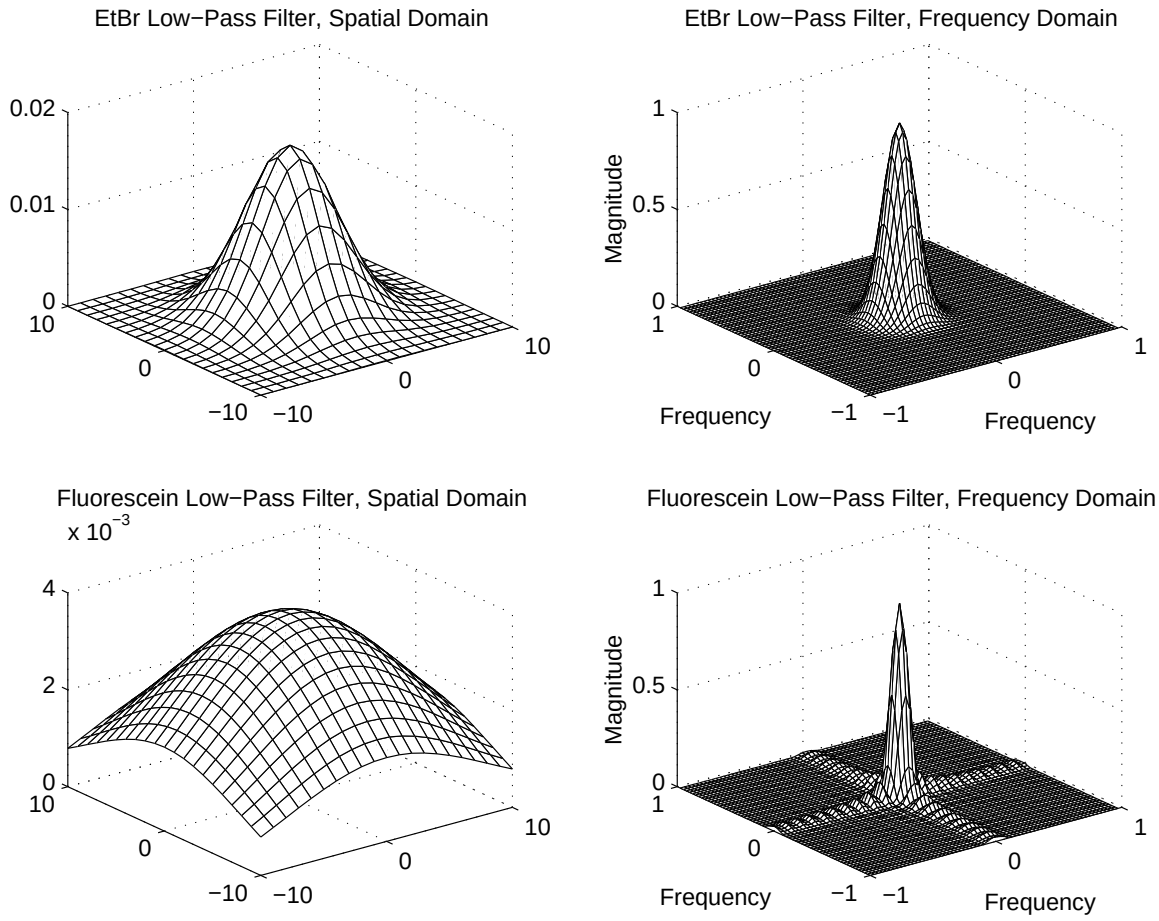

Figure B-5: Spatial and frequency perspectives of the Gaussian low-pass filters used for the unsharp filtering. The EtBr filter has a σ=3 and is 21x21. The fluorescein filter has a σ=8 and is 21x21.

components to binary components. Experimentally, it was determined that in general the best threshold values were 1/12 of maximum intensity in the filtered image component. This method was used for both the EtBr and fluorescein components. The result of the filtering and thresholding steps are shown for both the EtBr and fluorescein components in Figures: B-6 and B-7.

This thresholding process worked reasonably well, but often allowed random bright pixels to pass, or created holes in otherwise well-defined cells and nuclei. To remove these imperfections, a smoothing operation consisting of an erosion to remove unwanted bits followed by a dilation to restore the image was performed on both components (Fig: B-8). For the EtBr component, the erosion and the dilation were done with a 3 pixel diameter circle. For the fluorescein component, the erosion was done with a 5 pixel diameter circle and the dilation was done with a 4 pixel diameter circle (Fig: B-9).

Once the erosion and dilation were completed, it was a simple task (MATLAB even has a command for it) to count the number of cells in both of the processed image components. These numbers can then be recorded to show the number of live and dead cells in a particular slide and the ratio of cells that are alive (i.e. the viability).

Taking this one step further, the EtBr and fluorescein binary components were re-combined into an enhanced image of the original slide (Fig: B-10). This image clearly shows the distribution of live and dead cells in the tissue section without background and blurred object noise. Notice the occasional dead cell in the core of the tissue section that is visible but hard to discern in the original image, but clearly evident in the enhanced image.

B.4 Conclusion

The described method worked well on a variety of sample images with different levels of viability and blurring. Two other examples (Fig: B-11) are shown. The first of these examples highlights this technique's ability to pick up on EtBr stained cells that are usually lost to the human observer among the strong green fluorescein background fluorescence. The first example also displays an artifact of the slide scanner, appearing as a band of

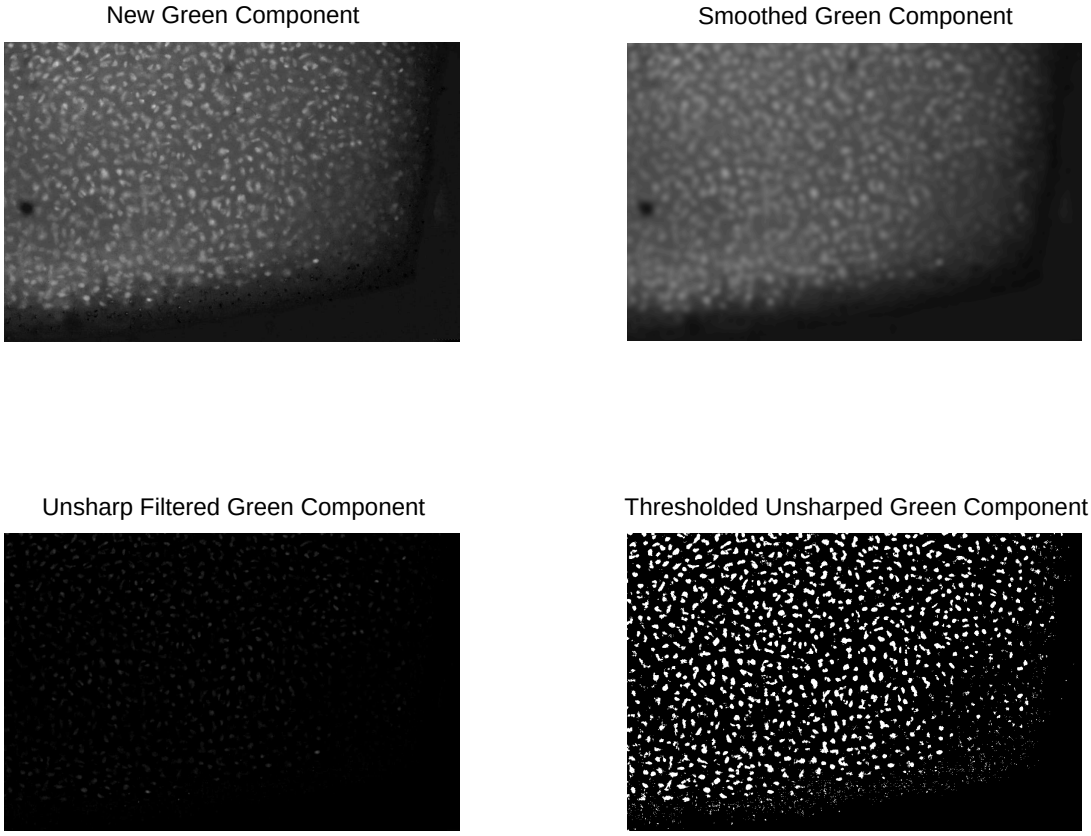

Figure B-6: The fluorescein component is shown, along with the results of the low-pass filter, the unsharp mask, and then the thresholding.

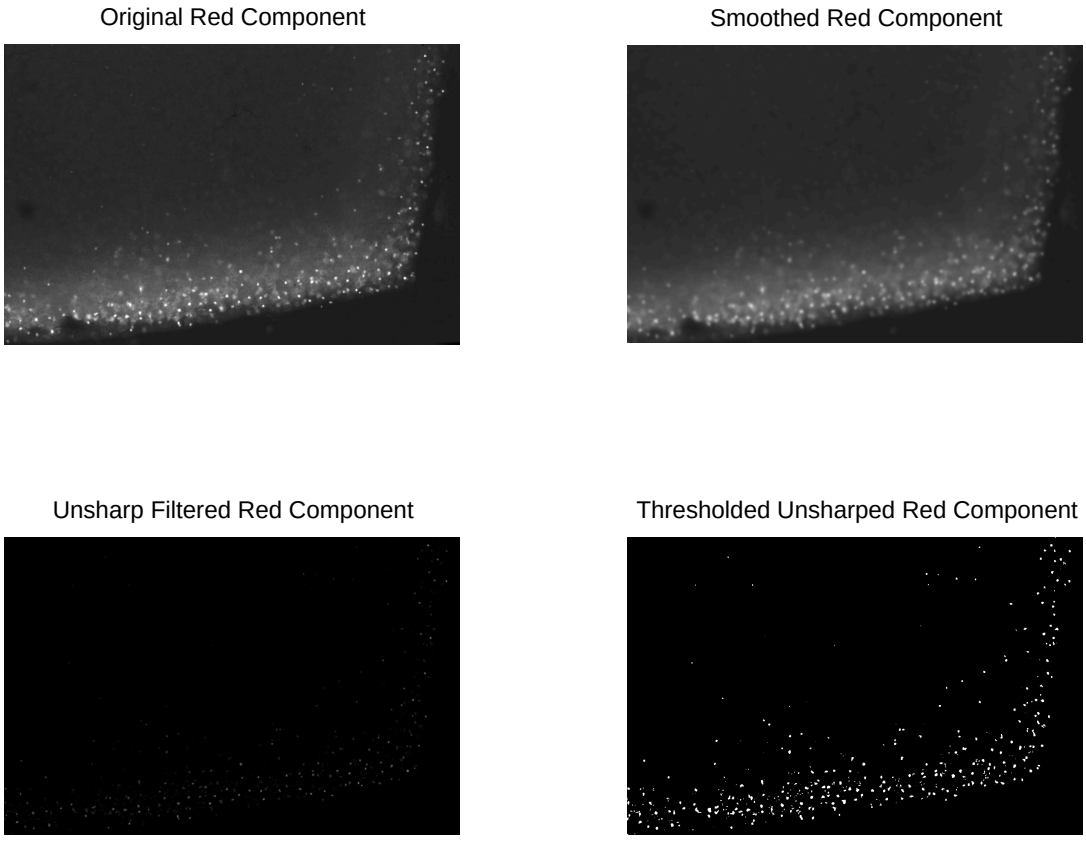

Figure B-7: The fluorescein component is shown, along with the results of the low-pass filter, the unsharp mask, and then the thresholding.

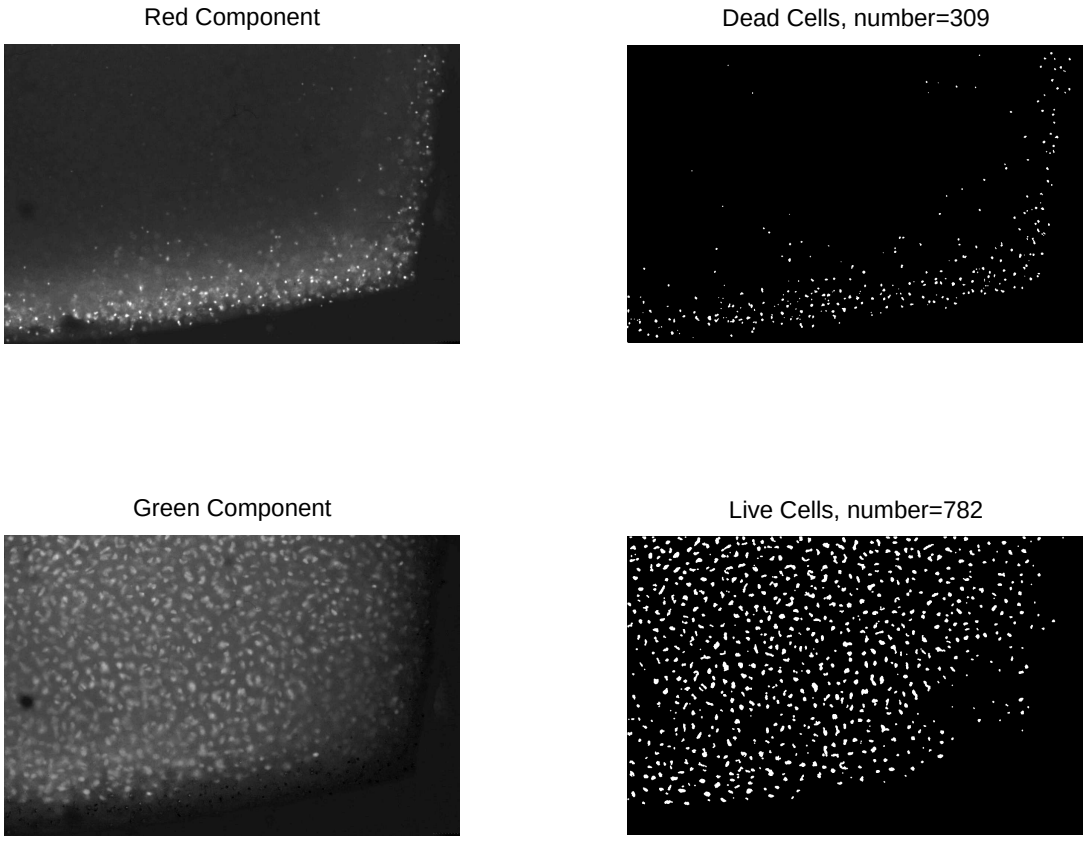

Figure B-8: The EtBr and fluorescein Components, along with the binary EtBr and fluorescein components computed from an erosion and dilation of the thresholded, unsharp-filtered components.

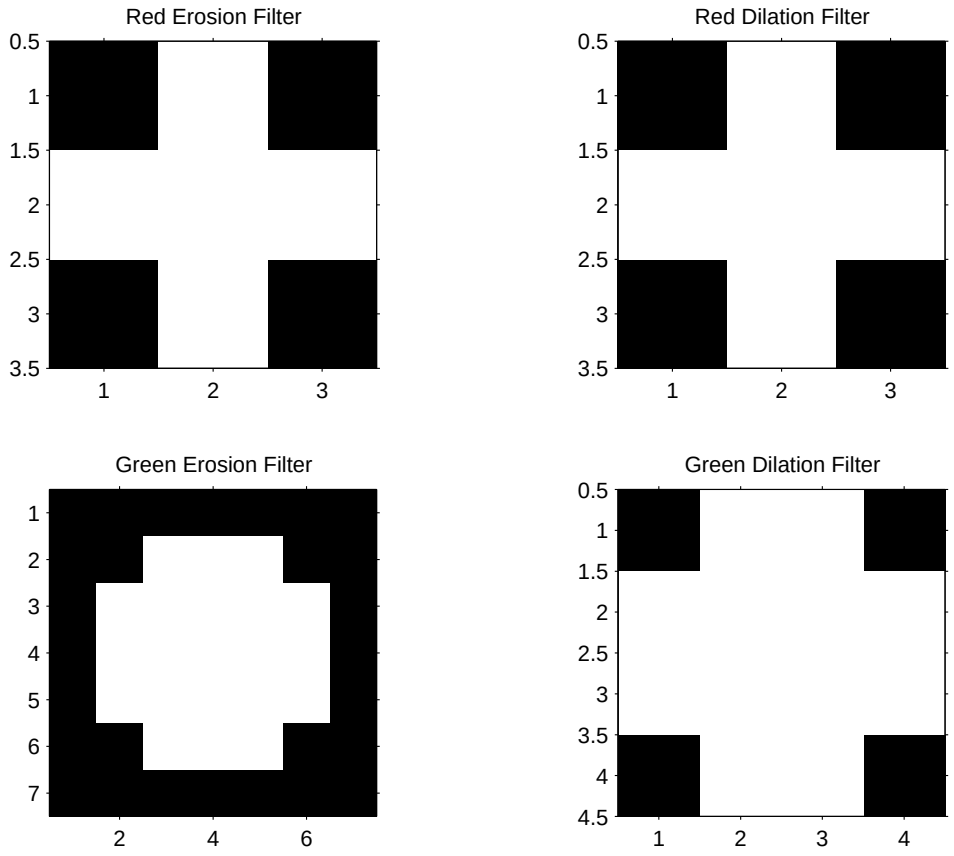

Figure B-9: The erosion and dilation filters used to process the fluorescein and EtBr components.

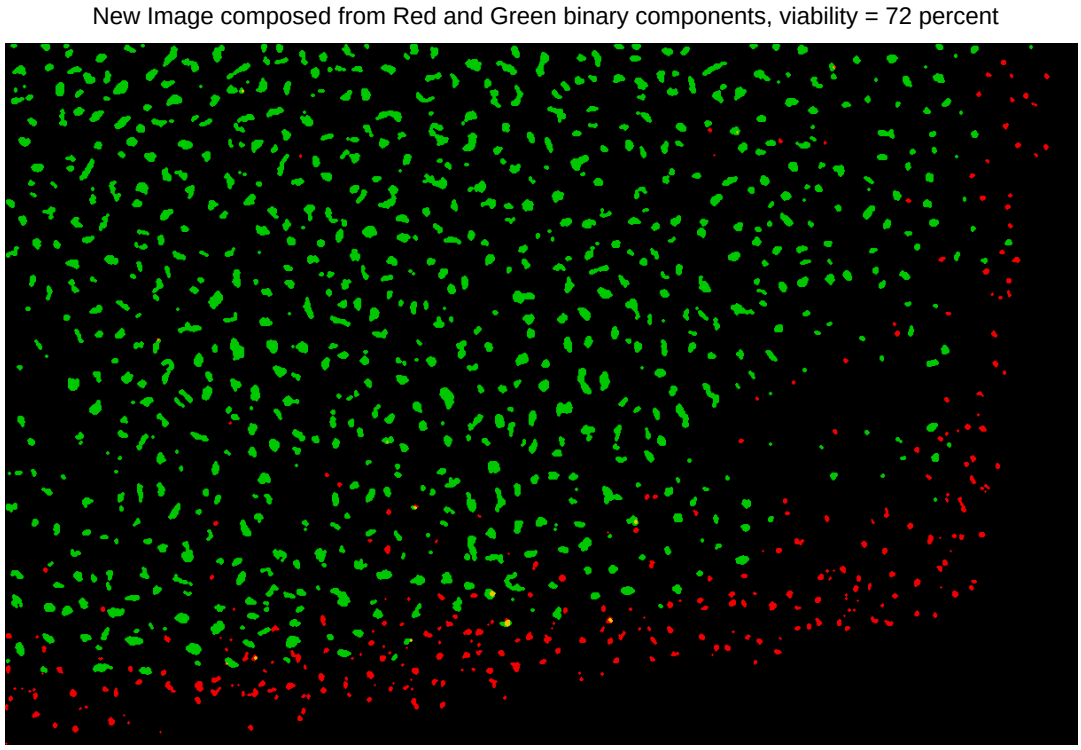

Figure B-10: An enhanced image created by combining the binary EtBr and fluorescein components into a full-color image.

extremely low intensity along the top. It was assumed that the photography, slide scanning, and image storing did not add any noise or distortion to the image, but the slide scanner often added very visible artifacts to the scanned images that were not present on the slides. This method does not try to address this problem, as it was felt this would be more easily fixed by an investment in new equipment.

While filtering the images on computer takes longer than the visual qualitative assessment that is usually used, this method represents a means of obtaining quantitative viability measurement from EtBr/FDA staining. It should also be noted that this is only one method of performing such a quantification. The color transformation, unsharp filtering and smoothing were all well-suited to this sort of problem, but it is certainly possible that other methods may work as well or better. In accordance with its goals, this project has demonstrated successfully one method of enhancing and automatically quantitating the results of an EtBr/FDA viability assay.

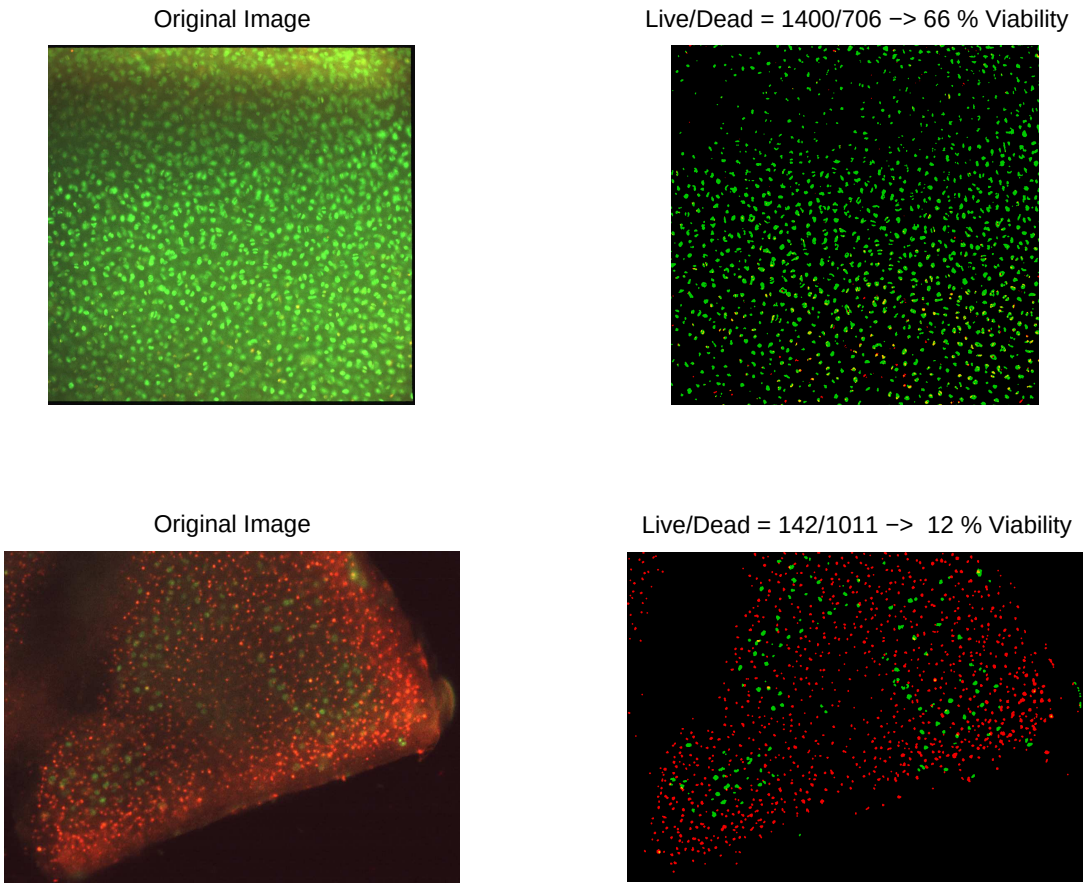

Figure B-11: Two further examples of the image processing, showing the scanned slide image, the newly generated image, and the calculated viability.

Appendix C

Biomechanical Characterization of Loaded Disks

C.1 Introduction

Biomechanical measurements of cartilage tissue provide an accurate and sensitive measure of the tissue's physical composition and status. Initial changes in the biomechanical properties were measured for the injurious compression model. These biomechanical measurements sought to examine the levels of peak applied stress at which tissue damage begins, and to elucidate whether the damage was associated with the collagen network and/or proteoglycan loss.

C.2 Methods

Cartilage disks were harvested and fed as described in sections 2.2.1.1 & 2.2.1.2. The disks were then subjected to graded levels of injurious compression as described in section 2.2.2, with anatomically matched disks serving as controls. Immediately after compression, the loaded and control disks were placed into a protease inhibitor PBS solution containing PMSF, leupeptin, and pepstatin with occasional use of E64 and/or Pefablock.

The disks were allowed to equilibrate in the inhibitor solution for at least 30 minutes before mechanical testing, and testing was generally completed within 8 hours of the completion of the loading protocol. Mechanical testing of the cartilage disks was done first in uniaxially confined compression and then in uniaxially unconfined compression using a Dynastat mechanical spectrometer (IMASS, Hingham, MA), as previously described [27]. For both testing modes the mechanical testing protocol was identical and consisted of a series of ramp-and-hold compression steps, allowing stress relaxation after each compression. At 0.92 mm compressed thickness, a series of 5 μm amplitude sinusoids at 0.01, 0.03, 0.1, 0.3, and 1 Hz was applied [10]. Total testing time for each disk was 2 hours. For both compression modes, a quadratic was fitted to the equilibrium stress versus equilibrium strain data. The equilibrium modulus at a given strain level was then obtained from the slope of the curve at that strain (strains corresponding to compressed thicknesses of 1 mm and 0.92 mm were examined here). The dynamic stiffness was calculated from the dynamic load amplitude, normalized to dynamic strain amplitude and disk area.

C.3 Results

C.3.1 Equilibrium Moduli

The equilibrium modulus was calculated at 1 and 0.92 mm for both confined and unconfined compression modes (Fig: C-1). Since the measured moduli exhibited specimen to specimen variation between different experiments, it was useful to normalize the values for injured disks to those of matched controls (Fig: C-2).

For confined compression testing of the injured tissue, no significant changes were seen for any loading condition between loaded and control tissue, although a non-significant trend toward decreased stiffness was observed.

In contrast, unconfined compression testing showed significant reductions in the equilibrium moduli of the injured tissue. For the equilibrium moduli calculated at 0.92 mm, these changes were significant at peak applied stresses of 12 and 24 MPa, with $\sim$30% and

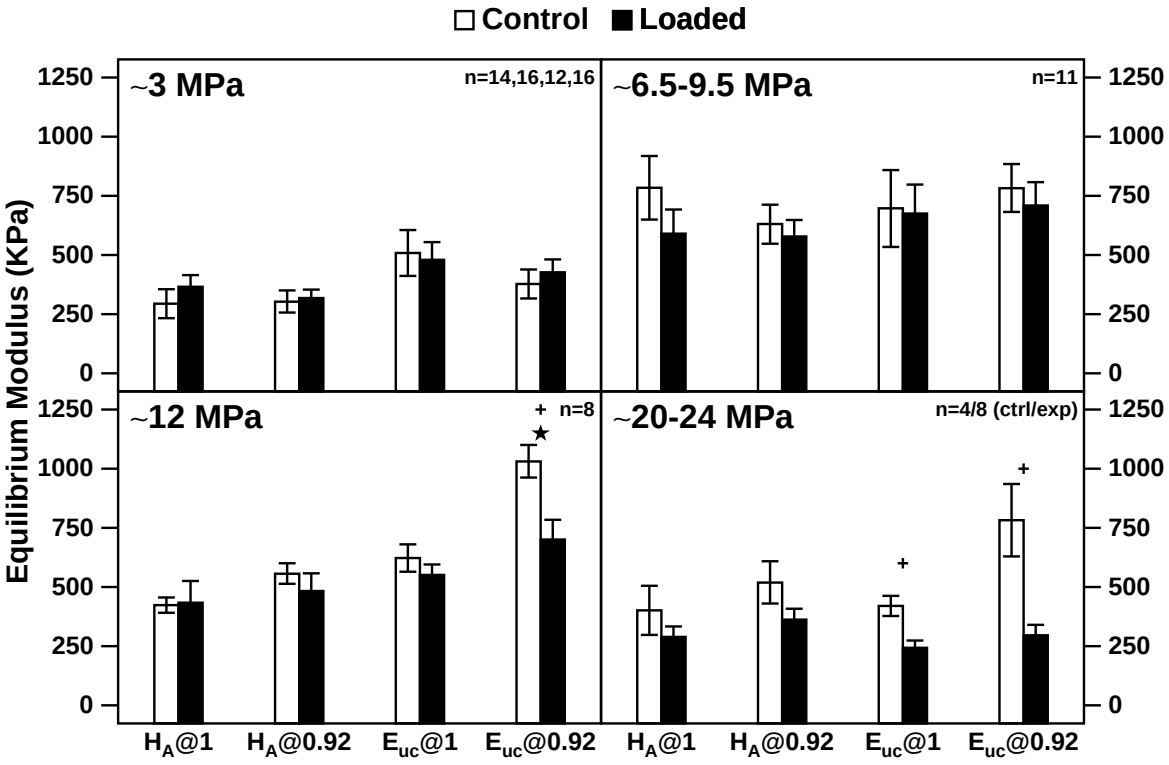

Figure C-1: The equilibrium moduli are shown for loaded disks at four different peak stresses versus uninjured controls, computed from confined and unconfined compression tests at 1 mm and 0.92 mm. H_A designates confined compression mode equilibrium modulus. E_{uc} designates unconfined compression mode equilibrium modulus. Data are mean$\pm$SEM; $\star$ indicates $p < 0.05$ by paired t-test, $+$ indicates $p < 0.05$ by t-test assuming equal variances.

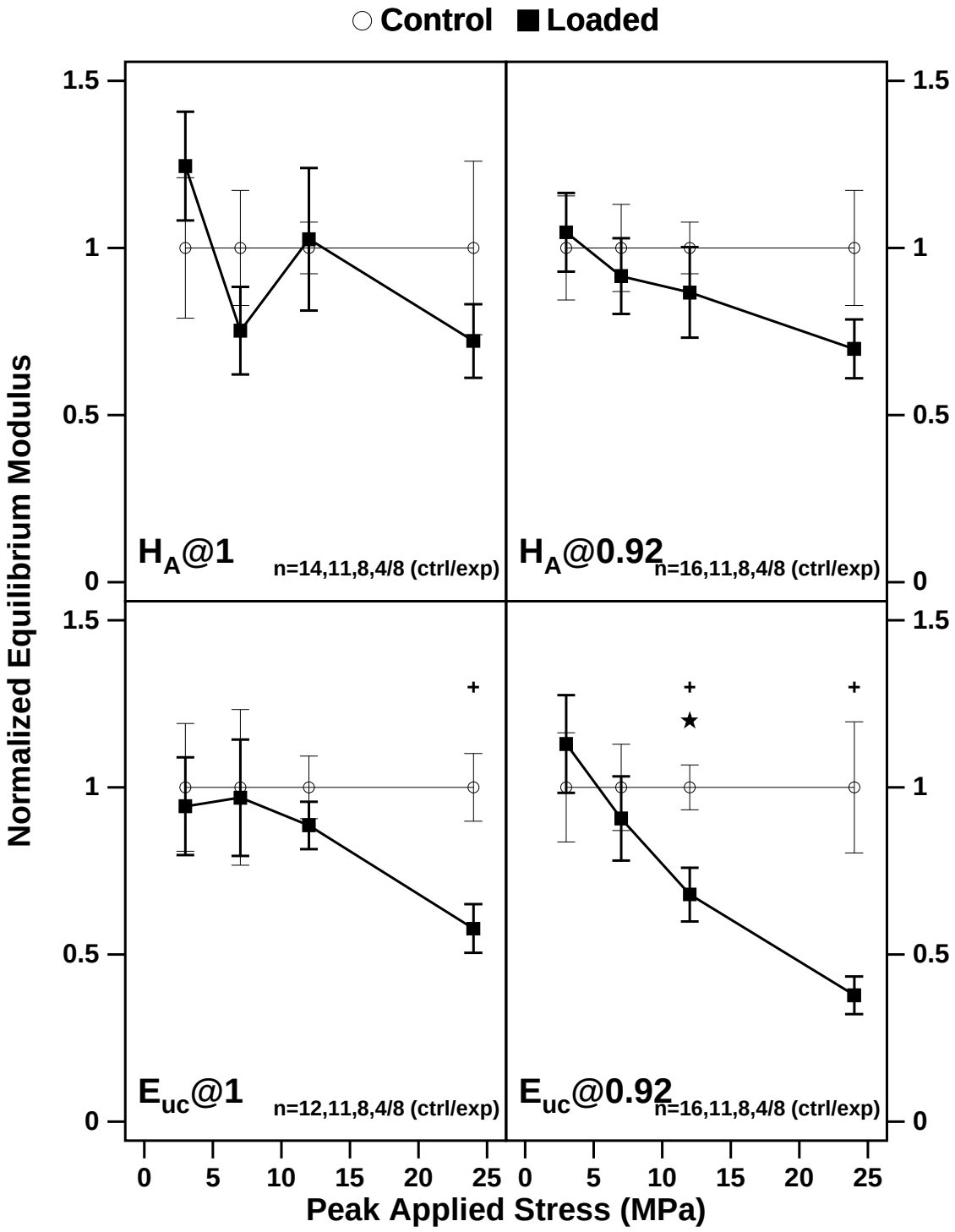

Figure C-2: The equilibrium moduli normalized to the average of the control values are shown versus peak injury stress, computed from confined and unconfined compression tests at 1 mm and 0.92 mm compressed thicknesses. Data are mean$\pm$SEM; $\star$ indicates $p < 0.05$ by paired t-test, $+$ indicates $p < 0.05$ by t-test assuming equal variances.

$\sim$60% reductions respectively. No significant differences were seen for the 3 and 7 MPa conditions.

C.3.2 Dynamic Stiffness

The dynamic stiffness was calculated for the frequencies used in the mechanical testing protocol (0.01, 0.03, 0.1, 0.3, and 1 Hz, Fig: C-3). Since the measured stiffness showed specimen to specimen variation between different experiments, it was again useful to normalize the values for injured disks to those of matched controls (Figs: C-4 & C-5).

For confined compression, the dynamic stiffness was significantly lower ($\sim$50%) only for the most severe case (24 MPa), and then only at 1, 0.3, and 0.1 Hz. A non-significant trend toward degraded stiffness could be observed.

In contrast, unconfined compression tests showed large and significant reductions in the dynamic stiffnesses of the injured tissue. At 0.01, 0.03, and 0.1 Hz, the injured tissue exhibited a significantly reduced (15-20%) stiffness at just 7 MPa. At higher peak applied stresses, all differences were significant, with the 12 and 24 MPa loading conditions showing a 50-60% and 90% reduction respectively at all frequencies. No significant differences were seen for the 3 MPa condition.

C.3.3 Other Measurements

Streaming potential measurements were taken during the confined compression tests. However, due to poorly conditioned electrodes and inter-experimental variation, these numbers had large associated errors and showed no significant differences.

C.4 Conclusion

The measured moduli and stiffness values showed large amounts of inter-experimental variation arising from joint to joint and specimen to specimen variation, combined with

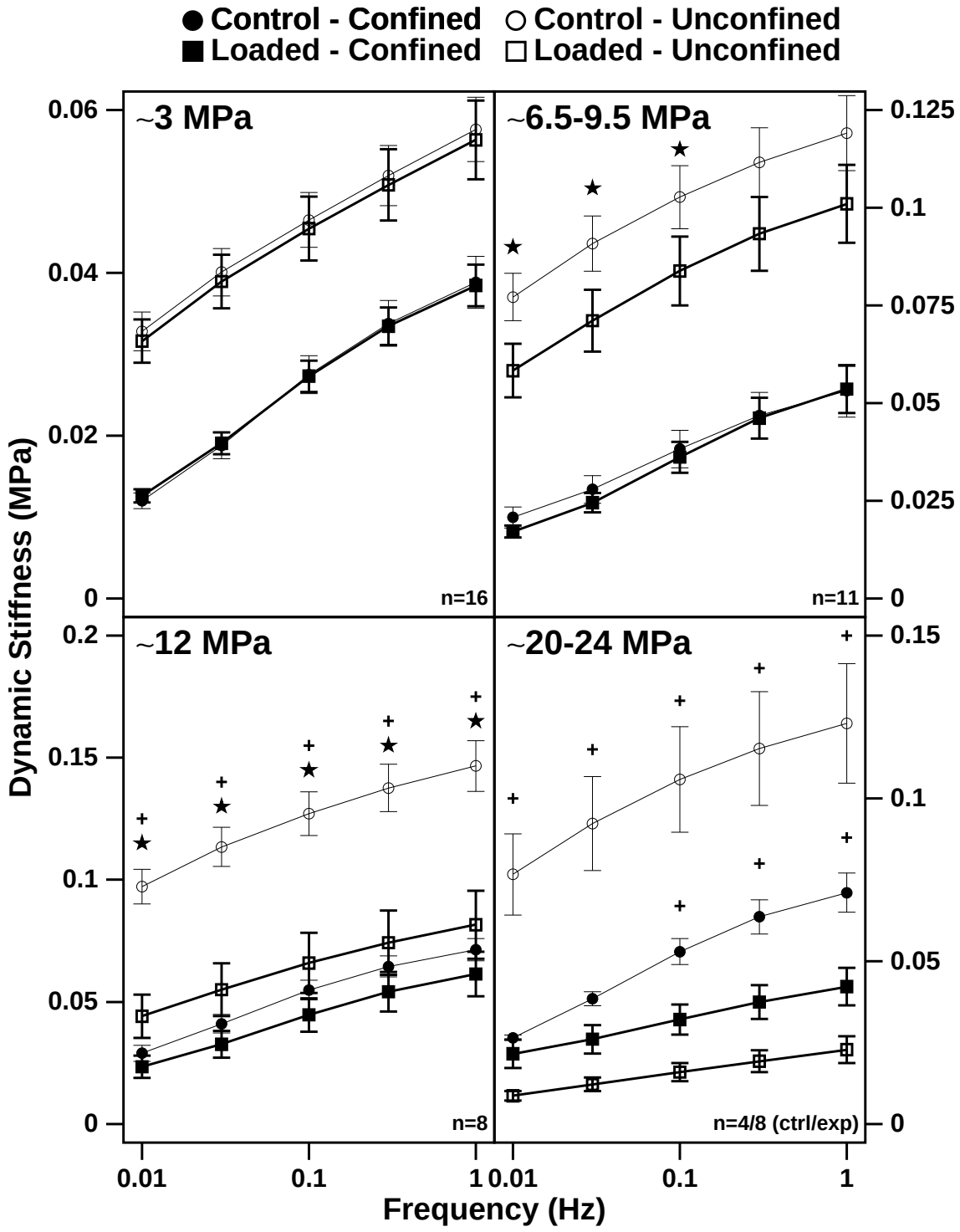

Figure C-3: Confined and unconfined compression dynamic stiffness measurements are shown versus frequency for disks loaded at different peak injury stresses. Data are mean$\pm$SEM; $\star$ indicates $p < 0.05$ by paired t-test, $+$ indicates $p < 0.05$ by t-test assuming equal variances.

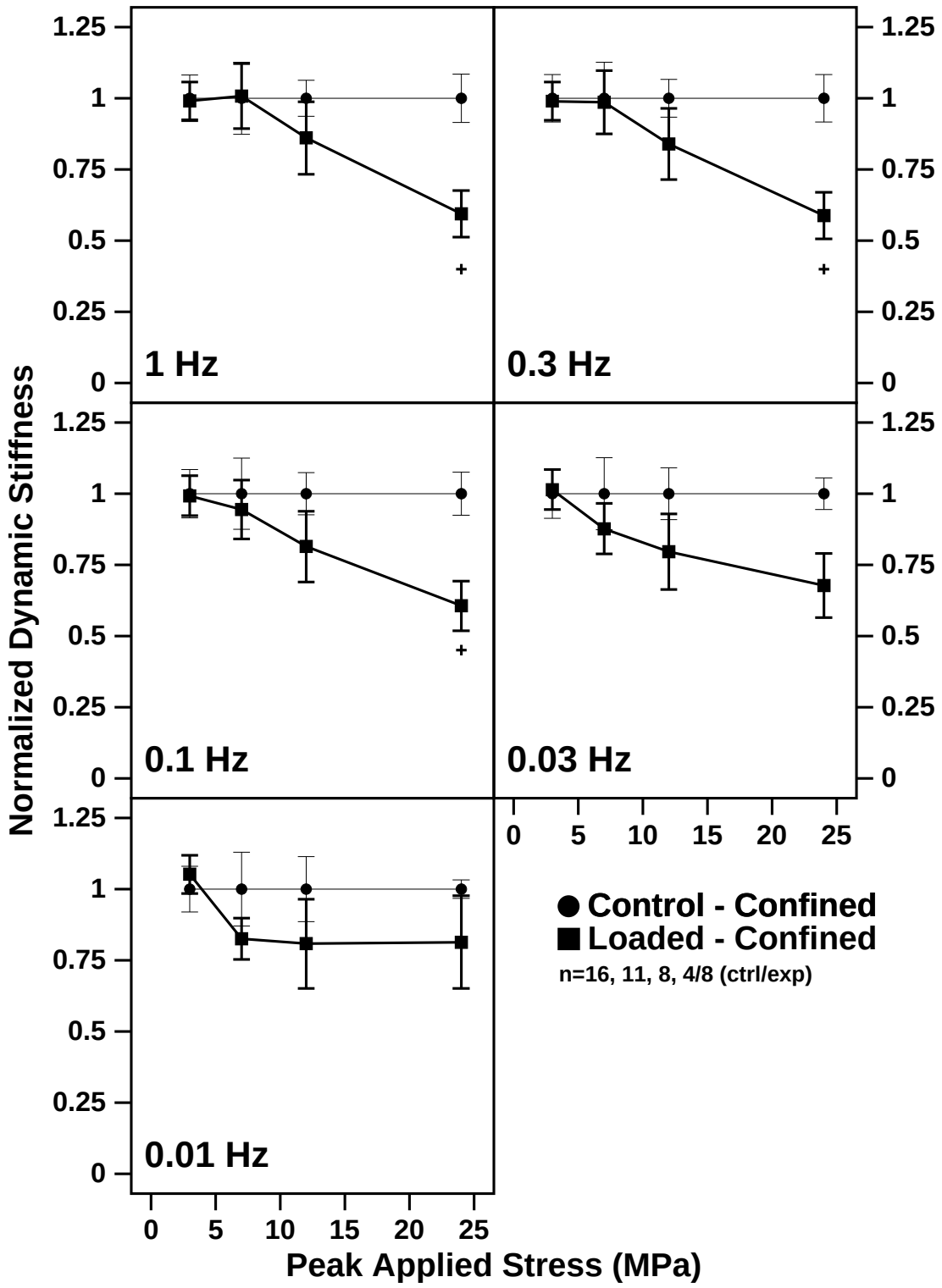

Figure C-4: Normalized confined compression mode dynamic stiffness measurements are shown versus peak injury stress at different frequencies. Data are mean$\pm$SEM, $\star$ indicates $p < 0.05$ by paired t-test, $+$ indicates $p < 0.05$ by t-test assuming equal variances.

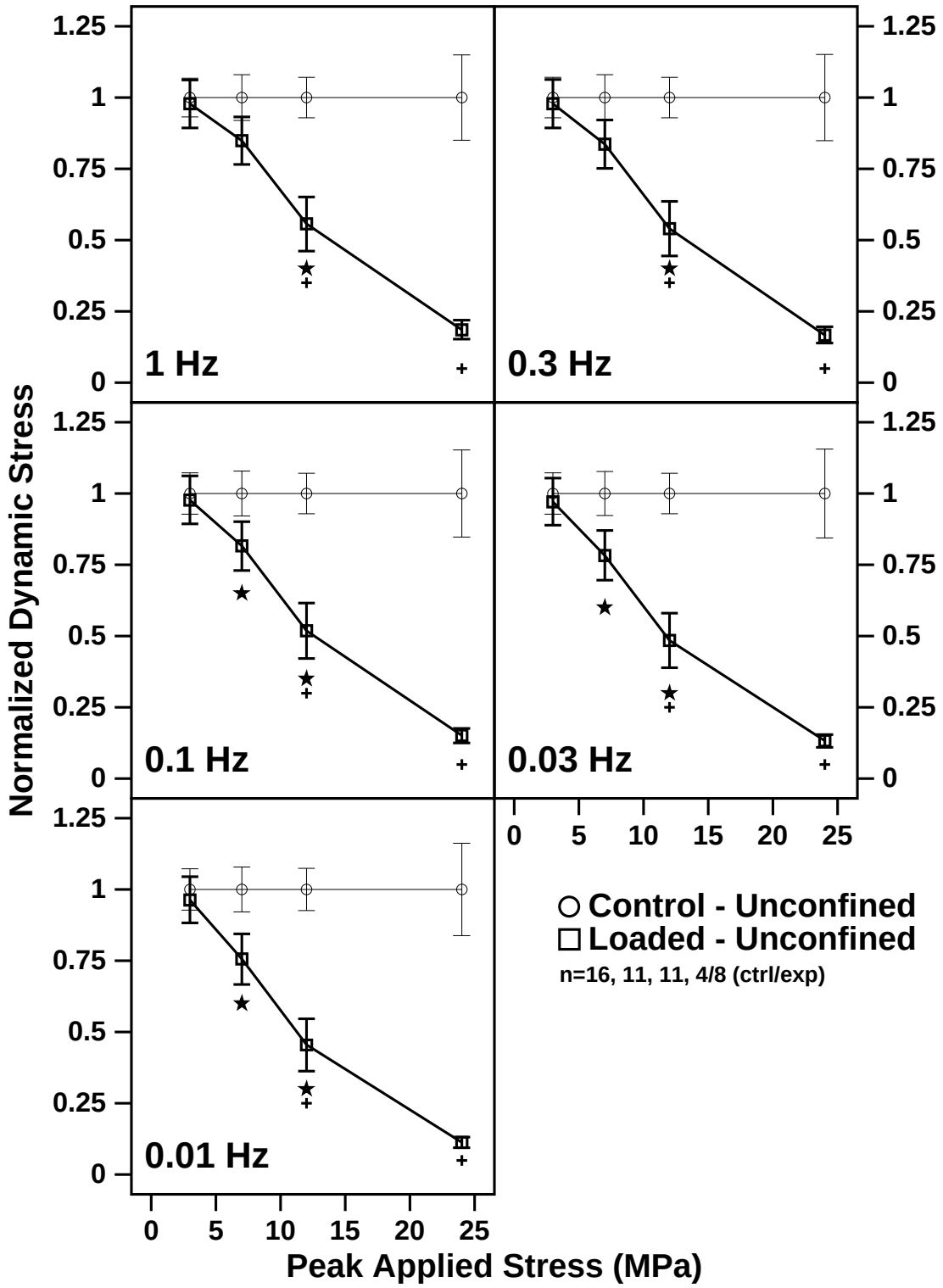

Figure C-5: Normalized unconfined compression mode dynamic stiffness measurements are shown versus peak injury stress at different frequencies. Data are mean±SEM, $\star$ indicates $p < 0.05$ by paired t-test, $+$ indicates $p < 0.05$ by t-test assuming equal variances.

operator and experiment variability. While the raw numbers were difficult to compare, the normalized numbers do show consistent, significant, and interesting trends.

To begin with, these tests show that a dose-dependent range of physical damage can be inflicted on the cartilage in this injurious compression system. Further, these biomechanical measurements show a clear decrease in stiffness for unconfined compression testing of the tissue directly following loading that is not directly paralleled in the confined testing. Since unconfined compression testing is more sensitive to collagen network damage than confined compression testing, the results indicate that the initial damage is primarily to the tissue's collagen network.

It would be interesting to study the change in biomechanical properties with time following an injurious compression. Since the biomechanical testing was done directly after testing, it is reasonable to expect that the proteoglycans may not have had time to diffuse out of the newly weakened collagen matrix, and that the initial damage was seen only in the collagen network. Given the sGAG loss rates in section: 3.2.1.2, one can postulate that significant differences in the confined compression testing values should begin to show up 1-2 days following the injurious compression. Additionally, an experiment using a protein synthesis inhibitor such as cyclohexamide would give information on whether the tissue degradation is due entirely to the mechanical insult or if cell-mediated degradation is occurring.

Appendix D

Preliminary Results: Other Assays for Apoptosis

Nobody wants a Charlie-in-the-Box - Charlie, on the Island of the Misfit Toys, from the movie “Rudolph”

D.1 Flow Cytometry of TUNEL stained cells

D.1.1 Introduction

Flow cytometry (also often called FACS, for fluorescent activated cell sorting) is an often used and often misinterpreted cell analysis method. Even with questionable interpretation, flow cytometry can be fairly useful, but it would be well advised to have someone knowledgeable in flow cytometry interpret results before publication.

In many respects a flow cytometry can be thought of as an automated fluorescent microscope with a computer taking a quantitative assessment of single cells as they pass by the laser. A typical flow cytometer uses a 488 nm laser and measures scatter, side scatter, and fluorescence at 2 or 3 wavelengths. More advanced machines will have different wavelength lasers, particularly UV, and often have cell sorting capabilities. Forward scatter

is the laser light that refracts at a small angle ($5 - 10°$) to the incident beam. Side scatter is the laser light that reflects at a large angle ($90 - 135°$) to the incident beam. Fluorescence is generally measured off of the side scatter and is generally measured at red, yellow, and green wavelengths. For more information on the history and current state of flow cytometry, the interested reader is referred to *Practical Flow Cytometry, 3rd Edition* by Howard M. Shapiro.

Since flow cytometry requires single cell suspensions, it tends to be more useful when working with cell suspension or monolayer cultures, although cells from tissue are sometimes examined by enzymatically isolating them from the tissue. In the chondrocyte apoptosis literature, flow cytometry of freshly isolated, TUNEL labelled cells has been used on several occasions [6, 42, 44, 45] although possible artifacts of the isolation process have been noted [45].

While flow cytometry has detractions due to the loss of spatial information and the possibility of artifacts from the isolation and fixation processes, the advantage of being able to quickly and simply receive a quantitative assessment of apoptosis have made the technique appealing.

D.1.2 Materials and Methods

Dithiothreitol (DTT), sodium nitroprusside (SNP), EDTA, cacodylic acid, protease, paraformaldehyde, terminal transferase (TdT), fluorescein-12-dUTP (F-12-dUTP), and bovine serum albumin (BSA) were obtained from Sigma, St. Louis, MO. Crude collagenase was obtained from Worthington, Lakewood, NJ. Camptothecin was obtained from Oncogene, Cambridge, MA. All other materials were obtained as described in section: 2.1.

D.1.2.1 Tissue Harvesting

Articular cartilage tissue used for chondrocyte isolation was excised from the femoropatellar groove of 1-2 week old calves with a scalpel, washed in explant PBS, and then further processed as described in section: D.1.2.3.

D.1.2.2 Culture

Feed medium for isolated cells consisted of high-glucose, 10% serum-supplemented DMEM with 10 mM HEPES buffer, 110 mg/ml sodium pyruvate, 0.1 mM non-essential amino acids, 0.4 mM proline, 0.1 mM ascorbate acid (20 μg/ml) and gentamicin (50 μg/ml). All media was changed daily.

D.1.2.3 Cell Isolation

Articular cartilage tissue used for chondrocyte isolation was minced, placed into a 20 U/ml protease in feed medium solution (approximately 8 ml of solution per gram of tissue), and placed in a $37\ ^{\circ}C$ incubator. After two hours, the protease solution was aspirated and the tissue was washed once with one volume of PBS. The tissue was then placed into a 200 Mandl U/ml Collagenase in feed media solution and placed on a rotary shaker table in a $37\ ^{\circ}C$ incubator overnight. The following morning, the isolated cells were filtered through 100 μm and 20 μm filters, washed with one volume of PBS, and resuspended in DMEM. Following the determination of cell viability via the red/green assay (section: 2.2.3.5) and cell density using trypan blue and a hemocytometer, the cells were plated on tissue culture plates at the desired densities.

When cells were isolated from cartilage tissue disks for flow cytometry, "overkill" amounts of protease and collagenase solutions were used, the cells were not filtered at the end of the isolation, and the cells were fixed immediately after isolation. In all other respects, cell isolation from cartilage disks was identical to cell isolation from freshly explanted tissue.

D.1.2.4 Red/Green Cell Viability Assay

Viability of cell suspensions was determined by adding ethidium bromide to a final concentration of 18 μM and fluorescein diacetate to a final concentration of 500 μM to a sample of the cell suspension. In cases where the cell suspension was at a high density, the suspension was first diluted with PBS.

D.1.2.5 Paraformaldehyde/Ethanol Fixation of Cells

Cells were either first isolated from cartilage tissue disks as described in section: D.1.2.3 or removed from monolayer culture with the use of 0.25% trypsin in an EDTA solution. The cells were then pelleted, washed with 1% BSA in PBS $\overline{s}\, Ca^{++} + Mg^{++}$, resuspended in 0.2 ml PBS $\overline{s}\, Ca^{++} + Mg^{++}$, added drop-wise to 1 ml 4% Paraformaldehyde (methanol free) in PBS $\overline{s}\, Ca^{++} + Mg^{++}$for prefixation, and placed on ice for 20 minutes. The cells were then washed again in 1% BSA in PBS $\overline{s}\, Ca^{++} + Mg^{++}$and resuspended in 0.5 ml PBS $\overline{s}\, Ca^{++} + Mg^{++}$. For fixation, the cell solution was brought to a final concentration of 70% ethanol by the addition of ice-cold 100% ethanol while vortexing and were then stored at $-20°C$ for at least an hour before use. All centrifugation steps were done for 15 minutes at 300 g. At times, 5 ml 1% Paraformaldehyde was used for the prefixation step and 2% FBS in PBS $\overline{s}\, Ca^{++} + Mg^{++}$was used in place of the 1% BSA in PBS $\overline{s}\, Ca^{++} + Mg^{++}$.

D.1.2.6 TUNEL Staining of Fixed Cells

In most instances, fixed cells were shipped on wet ice to SmithKline Beecham, where they were analyzed using a commercially available TUNEL kit according to the manufacturer's directions (ApopTag, Oncor, Gaithersburg, MD). Occasionally the assay was performed in this lab using a protocol based upon information from the literature [42]. Fixed cells were washed twice with PBS $\overline{s}\, Ca^{++} + Mg^{++}$(centrifugation was for 10 minutes at 3000 g), re-suspended in 50 μl labeling buffer (100 mM cacodylic acid, 1 mM $CaCl_2$, 0.1 mM dithiothreitol, 0.1 mg/ml BSA, 0.1 nmol F-12-dUTP, pH'd to 6.7 with KOH), and incubated on ice for 10 minutes. TdT (10 U) was then added, and the solution was incubated for 60 minutes at $37°C$. The reaction was terminated by the addition of 2 μl 0.5 M EDTA. The cells were then washed with PBS $\overline{s}\, Ca^{++} + Mg^{++}$and resuspended in PBS $\overline{s}\, Ca^{++} + Mg^{++}$in preparation for flow cytometry. Flow cytometry was done immediately using a TUNEL setup page for the flow cytometer (FACScan, Becton Dickinson, Franklin Lakes, NJ).

D.1.3 Results and Discussion

Results on fixed chondrocytes that had been isolated from injuriously compressed tissue 4 days post injury and sent to SmithKline Beecham for flow cytometry have so far been disappointing. A large decrease in cellularity for the more severely loaded conditions has been observed directly after the cell isolation process, and it is currently believed that in the overnight cell isolation process the apoptotic cells are being preferentially lost. Treatments with 1 mM of the nitric oxide donor SNP for 12-24 hours on cartilage tissue, a condition shown to induce chondrocyte apoptosis in monolayer [7], has also shown negative results and low cellularity following digestion indicative of apoptotic cell loss during isolation. There are a large number of protocols for isolating chondrocytes from cartilage, and some should be assessed as possible replacements for the pronase/collagenase digestion protocol when injuriously compressed tissue work is being done.

Monolayer experiments sent to SmithKline Beecham have also been mostly disappointing. The problem here stems from the lack of a good positive control for apoptosis. Chondrocytes have shown themselves to be unresponsive to many standard inducers of apoptosis, including camptothecin and TNF-α with and without cyclohexamide. One positive result has been achieved by treatment with 1 mM of SNP for 12 hours, but this has not been reproducible in tissue as noted above. Retinoic acid has been used successfully in the literature to induce apoptosis in chondrocytes [1] and should be looked into for both monolayer cultures and a possible apoptosis positive control for tissue work.

TUNEL assays performed in this lab on isolated cells have been completely unsuccessful. Due to a complete lack of F-12-dUTP incorporation in control and treated cells, the batch of TdT being used is suspect. For anyone interested in doing the TUNEL assay in this lab, it would be pertinent to eliminate uncertainties by starting with a commercial kit.

D.2 Flow Cytometry of PI stained cells

D.2.1 Introduction

Propidium iodide (PI) staining is often used to detect apoptosis via flow cytometry because of the simplicity and ease of the method. The method is, however, not very sensitive and prone to misinterpretation due to artifactual signal from cellular debris, and data from PI staining should generally be regarded with suspicion. The PI method has been used before for monolayers of articular cartilage chondrocytes [7, 6], but it apparently has never been used correctly (explained below).

Flow cytometry using PI is usually used to determine how much DNA is in a cell and is useful when looking at cell cycle distribution (i.e. how many in G1/G0 phase vs. G2 and S Phase). The basic theory of PI staining for apoptosis is that apoptotic cells will lose their oligonucleosomal DNA fragments following fixation, and when the cells are run on a flow cytometry using a dye that stains for nuclear content (i.e. PI, ethidium bromide), the apoptotic cells will appear as a hypodiploid peak. This hypodiploid peak should appear at somewhere in the range of 50% of the diploid peak. The problem with the peak measured in the articular chondrocyte literature is that the peak is usually situated an order of magnitude below the diploid peak (i.e. at 10% of it's value). Most likely cellular debris is being measured. Even if these peaks arose from an apoptotic process, the apoptotic population would be greatly overestimated, as each apoptotic cell would be divided up into multiple fragments.

D.2.2 Materials and Methods

PI was obtained from Sigma, St. Louis, MO. RNAse (DNAse free) was obtained from Boehringer Mannheim, Indianapolis, IN. For all other materials please see sections: 2.1 & D.1.2.

D.2.2.1 Ethanol Fixation of Cells

Cells were either first isolated from cartilage tissue as described in section: D.1.2.3 or separated from monolayer culture with the use of 0.25% trypsin in an EDTA solution. Cells were then pelleted, washed with PBS $\overline{s}\, Ca^{++} + Mg^{++}$(centrifugation was 10 minutes at 300 g), resuspended in 70% EtOH, and stored at $-20°C$ for at least an hour before use.

D.2.2.2 Nuclear Content Measurements

Ethanol fixed cells were then pelleted by centrifuging at 2000 g for 15 minutes, washed once, and then resuspended in PBS $\overline{s}\, Ca^{++} + Mg^{++}$. RNAse (DNAse free) was added to 2.5 μg/ml, and the solution was incubated for 30 minutes at $37°C$. Following the RNAse treatment, propidium iodide was added to a final concentration of 50 μg/ml and allowed to equilibrate for 10 minutes before flow cytometry. Flow cytometry was performed using a nuclear-content setup page on a FACScan flow cytometer (Becton Dickinson, Franklin Lakes, NJ) measuring channel 2 fluorescence.

D.2.2.3 Results and Discussion

Flow cytometry of PI stained cells did not produce any signs of apoptotic cells in injuriously compressed tissue and SNP treated monolayer cells. While these experiments did confirm that articular cartilage chondrocytes are non-dividing due to the total absence of a G2 peak, this protocol has been completely unsuccessful in terms of finding a subpopulation of cells with hypo-diploid peaks. The PI staining procedure is most likely having the same problems as the TUNEL method, namely the selective loss of subpopulations of cells during isolation.

D.3 Agarose Gel Electrophoresis of Apoptotic DNA

D.3.1 Introduction

The use of agarose gel electrophoresis for the detection of apoptotic DNA is one of the older and more conclusive methods of apoptotic detection. The general theory behind this technique is discussed in section: 1.4.2.6.2. Gel electrophoresis has been used to detect apoptotic DNA from chondrocytes in growth plate cartilage [108] and in monolayer [7, 26, 1]. To date, gel electrophoresis has not been used to identify apoptotic DNA from chondrocytes in articular cartilage.

D.3.2 Materials and Methods

Proteinase K and glycogen were obtained from Boehringer Mannheim, Indianapolis, IN. Gel loading solution (Type I), sodium acetate, Tris·cl, N-methyl arginine (NMA), and phenol/choloroform/isoamyl alchohol (25:24:1) were obtained from Sigma, St. Louis, MO. Sodium dodecyl sulfate (SDS) was obtained from BRL, Gaithersburg, MD. All other materials were obtained as mentioned in sections: 2.1, D.1.2, and D.2.2.

D.3.2.1 Harvest, Culture, and Compression

Harvesting, feeding, injurious compression of tissue, and isolation of cells were conducted as described in sections: D.1.2.2, D.1.2.1, D.1.2.3, 2.2.1.1, 2.2.1.2, and 2.2.2.

D.3.2.2 DNA Isolation

Cell pellets or cartilage tissue disks were incubated in a digestion buffer containing 100 mM NaCl, 10 mM Tris·Cl at pH 8, 25 mM EDTA at pH 8, 0.5% SDS, and 0.1 mg/ml proteinase K in a hot water bath at 60°C overnight. The samples were then thoroughly extracted twice with an equal volume of phenol/chloroform/isoamyl alcohol (25:24:1) (centrifugation was 10 minutes at 1700 g). The aqueous layer was taken, 1/2 volume of 3 M sodium acetate (pH

5.2), 2 (original) volumes of 100% ethanol, and 5 μl of 20 mg/ml glycogen were added, and DNA was recovered by centrifugation for 10 minutes at 1700 g. The pellet was then washed with 85% ethanol, allowed to dry, and dissolved in 50 μl TE buffer (10 mM Tris·Cl, 1 mM EDTA). 5 μL of 500μg/ml RNAse (DNAse free) were added, and the samples were incubated at 37°C for 30 minutes. Gel loading solution (type 1) was added to the samples, and the samples were run on a 2% agarose gel containing 1 μg/ml ethidium bromide at 50 Volts.

D.3.3 Results and Discussion

To date, all attempts at visualizing apoptotic chondrocyte DNA from injuriously compressed tissue and treated cells using agarose gels have been unsuccessful. Injuriously compressed and SNP treated cartilage tissue, along with SNP, IL-1β, IL-1β and DMSO, TNF-α, camptothecin, and actinomycin D treated chondrocytes have all shown no evidence of low molecular weight DNA. Use of F9 ATCC CRL-1720 cells, a murine mouse embryonal carcinoma testicular teratocarcinoma cell line, treated with 10 μM of cisplatin has produced positive results (Fig: D-1, lanes 6 & 7).

The biggest problem with gel electrophoresis is that a relatively large percentage of apoptotic cells are required for resolvable bands to appear. Since chondrocytes are non-dividing, many of the more usual treatments used for inducing apoptosis in other cell types will have no effect and producing a sufficient number of apoptotic chondrocytes even in monolayer may be difficult. In cartilage tissue, extracting the DNA is made even more difficult by the low percentage of the tissue that is cellular. Although gel electrophoresis would not be appropriate for normal experimental use, successful imaging of apoptotic DNA from injurious compressed cartilage would serve as confirmatory evidence that chondrocytes in injuriously compressed tissue are truly undergoing apoptosis.

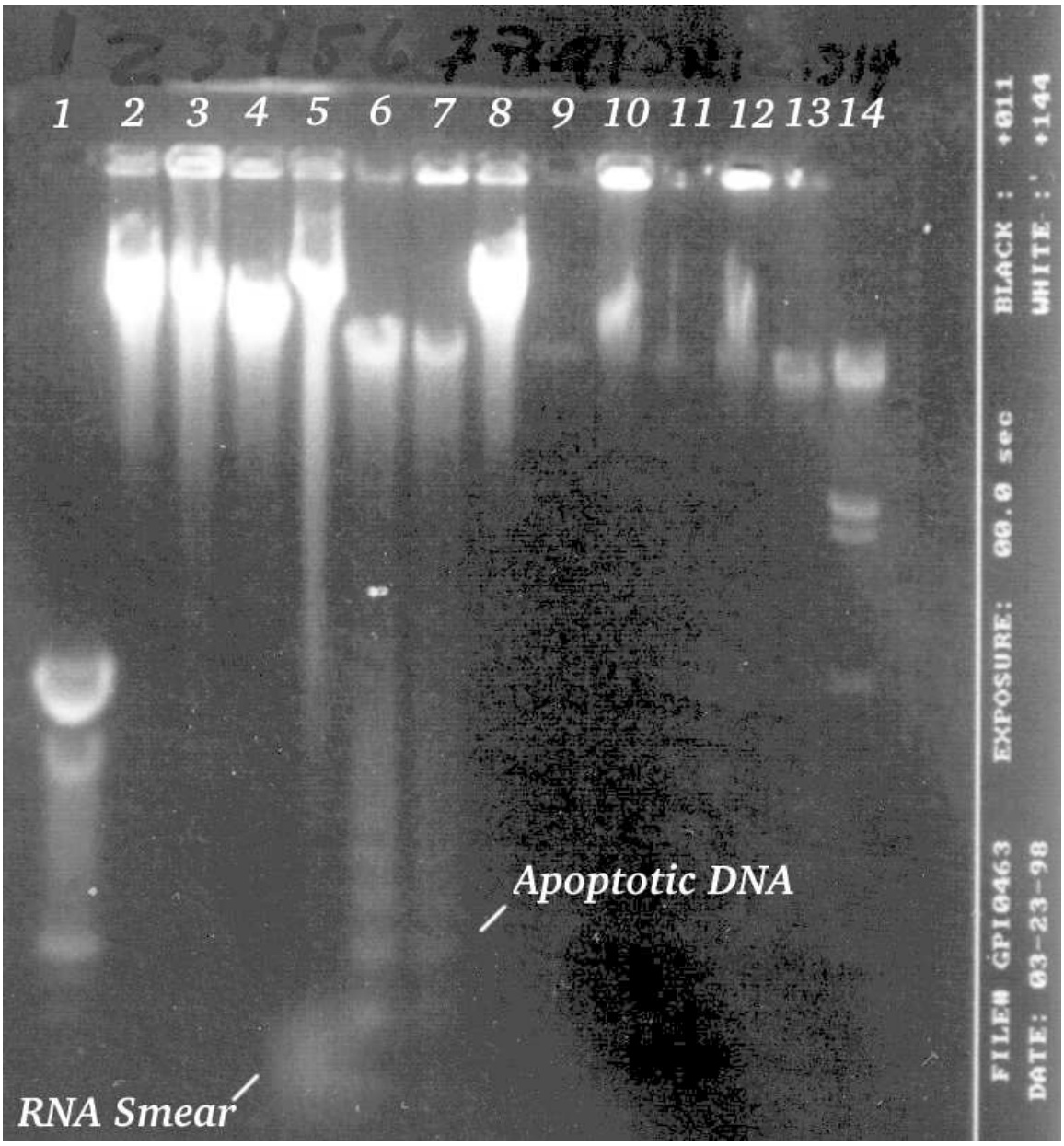

Figure D-1: Agarose gel containing DNA from several different conditions. Note that the picture was taken 12 hours after running the gel, and the DNA has diffused a little smearing the bands. Lane (1) 100 bp DNA marker (2) (3,4,8) Chondrocytes, 2 mM SNP treatment of 1E7 Cells (4) F9 Cells, Control (5) F9 Cells, Control, no RNAse treatment (6) F9 Cells, 10 mM Cisplatin treatment for 24 hours (7) F9 Cells, 10 mM Cisplatin treatment for 24 hours, no RNAse treatment, (9) Chondrocytes, Control (10) Chondrocytes, 5 ng/ml IL-1β treatment for 24 hours (11) Chondrocytes, 5 ng/ml IL-1β and 500 mM DMSO for 24 hours (12) Chondrocytes, 5 ng/ml IL-1β, 500 mM DMSO, and 1 mM NMA (13) Chondrocytes, 2 mM SNP treatment for 24 hours (14) kbp DNA marker

Bibliography

[1] Adams CS, Horton WE: Chondrocyte apoptosis increases with age in the articular cartilage of adult animals. *Anat Rec*, 250:418–425, 1998

[2] Allen RG: Mechanical properties of selectively degraded cartilage explants: correlation to the spatiotemporal distribution of glycosaminoglycans. Master's thesis, Massachusetts Institute of Technology, Cambridge, MA, 1996

[3] Ashkenazi A, Dixit VM: Death receptors: Signaling and modulation. *Science*, 281:1305–1308, 1998

[4] Barinaga M: Death by dozens of cuts. *Science*, 280:32–34, 1998

[5] Beg AA, Baltimore D: An essential role for nf-κb in preventing tnf-α-induced cell death. *Science*, 274:782–784, 1996

[6] Blanco FJ, Guitian R, Vazquez-Martul E, de Toro FJ, Galdo F: Osteoarthritis chondrocytes die by apoptosis: a possible pathway for osteoarthritis pathology. *Arthritis Rheum*, 41:284–289, 1998

[7] Blanco FJ, Ochs RL, Schwarz H, Lotz M: Chondrocyte apoptosis induced by nitric oxide. *Am J Pathol*, 146:75–85, 1995

[8] Boise LH, Thompson CB: Hierarchical control of lymphocyte survival. *Science*, 274:67–68, 1996

[9] Boldin MP, Goncharov TM, Goltsev YV, D W: Involvement of mach, a novel mort1/fadd-interacting protease, in fas/apo-1- and tnf receptor-induced cell death. *Cell*, 85:803–815, 1996

[10] Bonassar LJ, Frank EH, Murray JC, Paguio CG, Moore VL, Lark MW, Sandy JD, Wu JJ, Eyre DR, Grodzinsky AJ: Changes in cartilage composition and physical properties due to stromelysin degradation. *Arthritis Rheum*, 38:173–183, 1995

[11] Bratton DL, Fadok VA, Richter DA, Kailey JM, Guthrie LA, Henson PM: Appearance of phosphatidylserine on apoptotic cells requires calcium-mediated nonspecific flip-flop and is enhanced by loss of the aminophospholipid translocase. *J Biol Chem*, 272:26159–26165, 1997

[12] Brighton CT, Happenstall RB: Oxygen tensions in zones of epiphyseal plate metaphysis and diaphysis. *J Bone Joint Surg*, 53A:719–728, 1971

[13] Bullough PG: The pathology of osteoarthritis. In RW Moskowitz, DS Howell, VM Goldberg, HJ Mankin, editors, *Osteoarthritis*, pp 39–70. WB Saunders, Philadelphia, 1992

[14] Caterson B, Lowther DA: Changes in the metabolism of the proteoglycans from sheep articular cartilage in response to mechanical stress. *Biochim Biophys Acta*, 540:412–422, 1978

[15] Cheng W, Li B, Kajstura J, Li P, Wolin MS, Sonnenblick EH, Hintze TH, Olivetti G, Anversa P: Stretch-induced programmed myocyte cell death. *J Clin Investig*, 96:2247–2259, 1995

[16] Chicheportiche Y, Bourdon PR, Xu H, Hsu YM, Scott H, Hession C, Garcia I, Browning JL: Tweak, a new secreted ligand in the tumor necrosis factor family that weakly induces apoptosis. *J Biol Chem*, 272:32401–32410, 1997

[17] Chinnaiyan AM, O'Rourke K, Tewari M, Dixit VM: Fadd, a novel death domain-containing protein, interacts with the death domain of fas and initiates apoptosis. *Cell*, 81:505–512, 1995

[18] Cotman CW, J AA: A potential role for apoptosis in neurodegeneration and alzheimer's disease. *Mol Neurobio*, 10:19–45, 1995

[19] Davis MA, Ettinger WH, Neuhaus JM, Cho SA, Hauck WW: The association of knee injury and obesity with unilateral and bilateral osteoarthritis of the knee. *Am J Epidemiol*, 130:278–288, 1989

[20] D'Lima DD, Hashimoto S, Chen PC, Colwell CW, Lotz MK: Mechnical load induced cartilage injury. In *Trans 2nd Symposium of the ICRS*, 1998

[21] Donohue JM, Buss D, Oegema TR, Thompson RC: The effects of indirect blunt trauma on adult canine articular cartilage. *J Bone Joint Surg*, 65A:948–957, 1983

[22] Emery E, Aldana P, Bunge MB, Puckett W, Srinivasan A, Keane RW, Bethea J, Levi AD: Apoptosis after traumatic human spinal cord injury. *J Neurosurg*, 89:911–920, 1998

[23] Erlacher L, Maier R, Ullrich R, Kiener H, Aringer M, Menschik M, Graninger W: Differential expression of the protooncogene bcl-2 in normal and osteoarthritic human articular cartilage. *J Rheumatol*, 22:926–931, 1995

[24] Fadok VA, Voelker DR, Campbell PA, Cohen JJ, Bratton DL, Henson PM: Exposure of phosphatidylserine on the surface of apoptotic lymphocytes triggers specific recognition and removal by macrophages. *J Immunol*, 148:2207–2216, 1992

[25] Farndale RW, Buttle DJ, Barrett AJ: Improved quantitation and discrimination of sulphated glycosaminoglycans by use of dimethylmethylene blue. *Biochim Biophys Acta*, 883:173–177, 1986

[26] Feng L, Precht P, Balakir R, Horton WEJ: Evidence of a direct role for bcl-2 in the regulation of articular chondrocyte apoptosis under the conditions of serum withdrawal and retinoic acid treatment. *J Cell Biol*, 71:302–309, 1998

[27] Frank EH, Grodzinsky AJ, Koob TJ, Eyre DR: Streaming potentials: a sensitive index of enzymatic degradation in articular cartilage. *J Orthop Res*, 5:497–508, 1987

[28] Frank EH, Jin M, Loening AM, Levenston ME, Grodzinsky AJ: A versatile shear and compression apparatus for mechanical stimulation of tissue culture explants. In Submission

[29] Garcia AM, Frank EH, Grimshaw PE, Grodzinsky AJ: Contributions of fluid convection and electrical migration to transport in cartilage: Relevance to loading. *Arch Biochem Biophys*, 333:317–325, 1996

[30] Gavrieli Y, Sherman Y, A BSS: Identification of programmed cell death *in situ* via specific labelling of nuclear dna fragmentation. *J Cell Biol*, 119:493–501, 1992

[31] Gibson GJ, Kohler WJ, Schaffler MB: Chondrocyte apoptosis in endochondral ossification of chick sterna. *Dev Dyn*, 203:468–476, 1995

[32] Gong J, Traganos F, Darzynkiewicz Z: A selective procedure for dna extraction from apoptotic cells applicable for gel electrophoresis and flow cytometry. *Anal Biochem*, 218:314–319, 1994

[33] Grasl-Kraupp B, Ruttkay-Nedecky B, Koudelka H, Bukowska K, Bursch W, Schulte-Hermann R: In situ detection of fragmented dna (tunel assay) fails to discriminate among apoptosis, necrosis, and autolytic cell death: a cautionary note. *Hepatology*, 21:1465–1468, 1995

[34] Gray ML, Pizzanelli AM, Lee RC, Grodzinsky AJ, Swann DA: Kinetics of the chondrocyte biosynthetic response to compressive load and release. *Biochim Biophys Acta*, 991:415–425, 1989

[35] Green DR, Reed JC: Mitochondria and apoptosis. *Science*, 281:1309–1312, 1998

[36] Green LC, Wagner DA, Glogowski J, Skipper PL, Wishnok JS, Tannenbaum SR: Analysis of nitrate, nitrite, and [15n]nitrate in biological fluids. *Anal Biochem*, 126:131–138, 1982

[37] Griess JP. *Phil Trans R Soc London*, 154:667–731, 1864

[38] Griess P. *Ber Dtsch Chem Ges*, 12:426–428, 1879

[39] Grodzinsky AJ: Electromechanical and physicochemical properties of connective tissue. *CRC Crit Rev Bioeng*, 9:133–199, 1983

[40] Grodzinsky AJ, Kim YJ, Buschmann MD, Quinn TM, Garcia AM, Huziker EB: Response of the chondrocyte to mechanical stimuli. In KD Brandt, M Doherty, LS Lohmander, editors, *Osteoarthritis*, pp 123–136. Oxford University Press, 1998

[41] Guilak F, Ratcliffe A, Mow VC: Chondrocyte deformation and local tissue strain in articular cartilage: A confocal microscopy study. *J Orthop Res*, 13:410–421, 1995

[42] Hashimoto S, Ochs RL, Komiya S, Lotz M: Linkage of chondrocyte apoptosis and cartilage degradation in human osteoarthritis. *Arthritis Rheum*, 41:1632–1638, 1998

[43] Hashimoto S, Ochs RL, Rosen F, Quach F, McCabe G, Solan J, Seegmiller JE, Terkeltaub R, Lotz M: Chondrocyte-derived apoptotic bodies and calcification of articular cartilage. *Proc Natl Acad Sci*, 95:3094–3099, 1998

[44] Hashimoto S, Setareh M, Ochs R, Lotz M: Fas/fas ligand expression and induction of apoptosis in chondrocytes. *Arthritis Rheum*, 40:1749–1755, 1997

[45] Hasimoto S, Takahashi K, Amiel D, Coutts RD, Lotz M: Chondrocyte apoptosis and nitric oxide production during experimentally induced osteoarthritis. *Trans Orthop Res Soc*, 23:466, 1998

[46] Heinegard D, Oldberg A: Structure and biology of cartilage and bone matrix noncollagenous macromolecules. *FASEB*, 3:2042–2051, 1989

[47] Hockenbery D: Defining apoptosis. *Am J Pathol*, 146:16–19, 1995

[48] Hodge WA, Fijan RS, Carlson KL, Burgess RG, Harris WH, Mann RW: Contact pressures in the human hip joint measured in vivo. *Proc Natl Acad Sci*, 83:2879–2883, 1986

[49] Howell DS, Treadwell BV, Trippel SB: Etiopathogenesis of osteoarthritis. In RW Moskowitz, DS Howell, VM Goldberg, HJ Mankin, editors, *Osteoarthritis: Diagnosis and Medical/Surgical Management*, pp 233–252. W. B. Saunders Co., Philadelphia PA, second edition, 1992

[50] Huang B, Eberstadt M, Olejniczak ET, Meadows RP, Fesik SW: Nmr structure and mutagenesis of the fas (apo-1/cd95) death domain. *Nature*, 384:638–641, 1996

[51] I WC, Atkins RM, Dieppe PA, Elson CJ: Tumor necrosis factor-alpha receptor expression on chondrocytes isolated from human articular cartilage. *J Rheumatol*, 21:1710–1715, 1994

[52] Ishizaki Y, Burne JF, Raff MC: Autocrine signals enable chondrocytes to survive in culture. *J Cell Biol*, 126:1069–1077, 1994

[53] Iwasaki K, Izawa M, Mihara M: Uv-induced apoptosis in rat skin. *J Dermatol Sci*, 12:31–35, 1996

[54] Jeffrey JE, Gregory DW, Aspden RM: Matrix damage and chondrocyte viability following a single impact load on articular cartilage. *Arch Biochem Biophys*, 322(1):87–96, 1995

[55] Jeffrey JE, Thomson LA, Aspden RM: Matrix loss and synthesis following a single impact load on articular cartilage in vitro. *Biochim Biophys Acta*, 1334:223–232, 1997

[56] Jurvelin J, Kiviranta I, Saamanen AM, Tammi M, Helminen HJ: Partial restoration of immobilization-induced softening of canine articular cartilage after remobilization of the knee (stifle) joint. *J Orthop Res*, 7:352–358, 1989

[57] Kenyon C: The nematode *caenorhabditis elegans*. *Science*, 240:1448–1453, 1988

[58] Kluck RM, Bossy-Wetzel E, Green DR, Newmeyer DD: The release of cytochrome c from mitochondria: a primary site for bcl-2 regulation of apoptosis. *Science*, 275:1132–1136, 1997

[59] Kouri JB, Rosales-Encine JL, Chaudhuri PP, Luna J, Mena R: Apoptosis in human osteoarthritic cartilage: a microscopy report. *Med Sci Res*, 25:245–248, 1997

[60] Li P, Nijhawan D, Budihardjo I, Srinivasula SM, Ahmad M, Alnemri ES, Wang X: Cytochrome c and datp-dependent formation of apaf-1/caspase-9 complex initiates an apoptotic protease cascade. *Cell*, 91:479–489, 1997

[61] Majno G, Joris I: Apoptosis, oncosis and necrosis: an overview of cell death. *Am J Pathol*, 146:3–15, 1995

[62] Mankin HJ, Dorman H, Lippiello L, Zarins A: Biochemical and metabolic abnormalities in articular cartilage from osteoarthritic human hips. II. Correlation of morphology with biochemical and metabolic data. *J Bone Joint Surg*, 52:523–537, 1971

[63] Maroudas A: Physical chemistry of articular cartilage and the intervertebral disc. In L Sokoloff, editor, *The Joints and Synovial Fluid*, volume 2, pp 239–291. Academic Press, New York, 1980

[64] Maroudas A, Venn MF: Chemical composition and swelling of normal and osteoarthritic tissues II: swelling. *Ann Rheum Dis*, 36:399–406, 1977

[65] Marsters SA, Sheridan JP, Pitti RM, Brush J, Goddard A, Ashkenazi A: Identification of a ligand for the death-domain-containing receptor apo3. *Curr Biol*, 8:525–528, 1998

[66] Marzinzig M, Nussler AK, Stadler J, Marzinzig E, Barthlen W, Nussler NC, Beger HG, Morris SMJ, Brueckner UB: Improved methods to measure end products of nitric oxide in biological fluids: Nitrite, nitrate, and s-nitrosothiols. *Nitric Oxide*, 1:177–189, 1997

[67] McCutchen CW: Lubrication of joints. In L Sokoloff, editor, *The Joints and Synovial Fluid*, volume 1, pp 437–483. Academic Press, New York, NY, 1980

[68] Meachim G, Collins DH: Cell counts of normal and osteoarthritic articular cartilage in relation to the uptake of sulfate ($^{35}s0_4$) in vitro. *Ann Rheum Dis*, 21:45–50, 1962

[69] Mooney A, Jobson T, Bacon R, Kitamura M, Savill J: Cytokines promote glomerular mesangial cell survival *in vitro* by stimulus-dependent inhibition of apoptosis. *J Immunol*, 159:3949–3960, 1997

[70] Moskowitz RW, Howell DS, Goldberg VM, Mankin HJ, editors: *Osteoarthritis: Diagnosis and Medical/Surgical Management*. W.B. Saunders, Philadelphia, 2nd edition, 1992

[71] Mudle SD, Gao XZ, Khan S, Gregory SA, Preisler HD, Raza A: Two *in situ* labeling techniques reveal different patterns of dna fragmentation during spontaneous apoptosis *in vivo* and induced apoptosis *in vitro*. *Anticancer Res*, 15:1895–1904, 1995

[72] Muzio M, Chinnaiyan AM, Kischkel FC, O'Rourke K, Shevchenko A, Ni J, Scaffidi C, Bretz JD, Zhang M, Gentz R, Mann M, Krammer PH, Peter ME, Dixit VM: Flice, a novel fadd-homologous ice/ced-3-like protease, is recruited to the cd95 (fas/apo-1) death–inducing signaling complex. *Cell*, 85:817–827, 1996

[73] Muzio M, Stockwell BR, Stennicke HR, Salvesen GS, Dixit VM: An induced proximity model for caspase-8 activation. *J Biol Chem*, 273:2926–2930, 1998

[74] Myers ER, Mow VC: Biomechanics of cartilage and its response to biomechanical stimuli. In BK Hall, editor, *Cartilage: Structure, function, and biochemistry*, volume 1, pp 313–341. Academic Press, New York, NY, 1983

[75] Nicholson DW, Thornberry NA: Caspases: killer proteases. *Trends Biochem Sci*, 22:299–306, 1997

[76] Olson RL, Everett MA: Epidermal apoptosis: cell deletion by phagocytosis. *J Cutan Pathol*, 2:53–57, 1975

[77] Onishi Y, Azuma Y, Sato Y, Mizuno Y, Tadakuma T, Kizaki H: Topoisomerase inhibitors induce apoptosis in thymocytes. *Biochim Biophys Acta*, 1175:147–154, 1993

[78] Palmoski MJ, Brandt KD: Effects of static and cyclic compressive loading on articular cartilage plugs *in vitro*. *Arthritis Rheum*, 27:675–681, 1984

[79] Poole CA: The structure and function of articular cartilage matrices. In JF Woessner Jr, DS Howell, editors, *Joint Cartilage Degradation*, chapter 1, pp 1–35. Dekker, New York, 1993

[80] Quinn TM: *Articular Cartilage: Matrix Assembly, Mediation of Chondrocyte Metabolism, and Response to Compression*. PhD thesis, Massachusetts Institute of Technology, Cambridge, MA, 1996

[81] Quinn TM, Grodzinsky AJ, Hunziker EB, Sandy JD: Effects of injurious compression on matrix turnover around individual cells in calf articular cartilage explants. *J Orthop Res*, 16:490–499, 1998

[82] Rao L, Perez D, White E: Lamin proteolysis facilitates nuclear events during apoptosis. *J Biol Chem*, 135:1441–1455, 1996

[83] Repo RU, Finlay JB: Survival of articular cartilage after controlled impact. *J Bone Joint Surg*, 59A:1068–1076, 1977

[84] Rudel T, Bokoch GM: Membrane and morphological changes in apoptotic cells regulated by caspase-mediated activation of pak2. *Science*, 276:1571–1574, 1997

[85] Sah RL, Kim YJ, Doong JH, Grodzinsky AJ, Plaas AHK, Sandy JD: Biosynthetic response of cartilage explants to dynamic compression. *J Orthop Res*, 7:619–636, 1989

[86] Sakahira H, Enari M, Nagata S: Cleavage of cad inhibitor in cad activation and dna degradation during apoptosis. *Nature*, 391:96–99, 1998

[87] Smith A, Smith H: A comparison of fluorescein diacetate and propidium iodide staining and in vitro excystation for determining giardia intestinalis cyst viability. *Parasitology*, 99:329–331, 1989

[88] Smith CA, Farrah T, Goodwin RG: The tnf receptor superfamily of cellular and viral proteins: activation, costimulation, and death. *Cell*, 76:959–962, 1994

[89] Srinivasula SM, Ahmad M, Fernandes-Alnemri T, Alnemri ES: Autoactivation of procaspase-9 by apaf-1-mediated oligomerization. *Mol Cell*, 1:949–957, 1998

[90] Stockwell RA: The cell density of human articular and costal cartilage. *J Anat*, 101:753–763, 1967

[91] Stockwell RA, Meachim G: The chondrocytes. In MAR Freeman, editor, *Adult Articular Cartilage, 2nd ed.*, pp 69–144. Pitman, Tunbridge Wells, England, 1979

[92] Tartaglia LA, Ayres TM, Wong GH, Goeddel DV: A novel domain within the 55 kd tnf receptor signals cell death. *Cell*, 74:845–853, 1993

[93] Tartaglia LA, Goeddel DV: Two tnf receptors. *Immunol Today*, 13:151–153, 1992

[94] Tew SR, Kwan APL, Hann AC, Poole AR, Thomson B, Archer CW: The reactions of chondrocytes and their extracellular matrix to experimental wounding. In *Trans 2nd Symposium of the ICRS*, 1998

[95] Thompson RC, Oegema TR, Lewis JL, Wallace L: Osteoarthrotic changes after acute transarticular load: an animal model. *J Bone Joint Surg*, 73A:990–1001, 1991

[96] Upholt WB, Olsen BR: The active genes of cartilage. In B Hall, S Newman, editors, *Cartilage: Molecular Aspects*, pp 43–79. CRC, Boca Raton, Fl., 1991

[97] Verhoven B, Schlegel RA, Williamson P: Mechanisms of phosphatidylserine exposure, a phagocyte recognition signal, on apoptotic t lymphocytes. *J Exp Med*, 182:1597–1601, 1995

[98] Vermes I, Haanen C, Steffens-Nakken H, Reutelingsperger C: A novel assay for apoptosis. flow cytometric detection of phosphatidylserine expression on early apoptotic cells using fluorescein labelled annexin v. *J Immunol Methods*, 184:39–51, 1995

[99] Walker EA, Archer CW: The cellular response of embryonic chick hyaline cartilage to experimental wounding. *Trans Orthop Res Soc*, 23:502, 1998

[100] Walker PR, Kokileva L, LeBlanc J, Sikorska M: Detection of the initial stages of dna fragmentation in apoptosis. *Biotechniques*, 15:1032–40, 1993

[101] Webb GR, Westacott CI, Elson CJ: Chondrocyte tumor necrosis factor receptors and focal loss of cartilage in osteoarthritis. *Osteoarthritis and Cartilage*, 5:427–437, 1997

[102] Weil M, Jacobson MD, Coles HS, Davies TJ, Gardner RL, Raff KD, Raff MC: Constitutive expression of the machinery for programmed cell death. *jcb*, 133:1053–1059, 1996

[103] Wijsman JH, Jonker RR, Keijzer R, van de Velde CJ, Cornelisse CJ, van Dierendonck JH: A new method to detect apoptosis in paraffin sections: in situ end-labeling of fragmented dna. *J Histochem Cytochem*, 41:7–12, 1993

[104] Wiley SR, Schooley K, Smolak PJ, Din WS, Huang CP, Nicholl JK, Sutherland GR, Smith TD, Rauch C, Smith ea C A: Identification and characterization of a new member of the tnf family that induces apoptosis. *Immunity*, 3:673–682, 1995

[105] Wyllie AH, Morris RG, Smith AL, Dunlop D: Chromatin cleavage in apoptosis: association with condensed chromatin morphology and dependence on macromolecular synthesis. *J Physiol*, 142:67–77, 1984

[106] Xiang J, Chao DT, Korsmeyer SJ: Bax-induced cell death may not require interleukin 1 beta-converting enzyme-like proteases. *Proc Natl Acad Sci*, 93:14559–14563, 1996

[107] Yeh WC, Pompa JL, McCurrach ME, Shu HB, Elia AJ, Shahinian A, Ng M, Wakeham A, Khoo W, Mitchell K, El-Deiry WS, Lowe SW, Goeddel DV, Mak TW: Fadd: essential for embryo development and signaling from some, but not all, inducers of apoptosis. *Science*, 279:1954–1958, 1998

[108] Zenmyo M, Komiya S, Kawabata R, Sasaguri Y, Inoue A, Morimatsu M: Morphological and biochemical evidence for apoptosis in the terminal hypertrophic chondrocytes of the growth plate. *J Physiol*, 180:430–433, 1996

[109] Zhang G, Gurtu V, Kain S, Yan G: Early detection of apoptosis using a fluorescent conjugate of annexin v. *Biotechniques*, 23:525–531, 1997